TURBULENCE PREDICTION AND MEASUREMENT IN A TURBULENT TRAILING VORTEX.

by

W. R. PHILLIPS.

REPORT No. 74-5

A thesis submitted to the Faculty of Graduate Studies and Research in partial fulfilment of the requirements for the degree of Master of Engineering.

Department of Mechanical Engineering

McGill University

Montreal, P.Q.

CANADA

June, 1974

SUMMARY.

The flow in a single turbulent trailing vortex with superimposed jet or wake is considered. This is a means of increasing the turbulence level in the vortex and hence the diffusion of mean axial vorticity. In this way the rotational velocities in the vortex are reduced and it provides a method for reducing delay between the operation of aircraft at airports.

Measurements have been made on a vortex generated in the centre of a circular wind tunnel on five cases, two jets, two wakes, and a flow for which the excess longitudinal momentum is nearly zero. The measurements include the three mean velocity components, and the six components of Reynolds stress, all made using a hot wire anemometer. The second order closure theory of Launder, Reece and Rodi has been applied to model the Reynolds stress equations, and these plus the momentum equations are then solved numerically using the upstream results as starting conditions. The results at the remaining two downstream stations are predicted well by the theory. The numerical results are then carried far downstream.

The above results are used to show that the rotational velocities in the trailing vortic es from a Boeing 747 Jumbo jet in the take-off mode are reduced by less than 5%, (two and one half kilometers downstream), if 10% of the total engine thrust is used to modify them.

RESUME

CALCULS DE PREDICTION ET MESURES DE LA TURBULENCE DANS UN TOURBILLON DE BORD DE FUITE.

Dans ce mémoire on se propose d'étudier l'effet d'un jet aval surimposé au tourbillon qui se crée dans le sillage d'un profil d'aile sectionné. L'addition du jet a pour but d'augmenter la turbulence dans le tourbillon et ainsi d'accroître la diffusion de la composante axiale moyenne du vecteur tourbillon. Cela réduit les vitesses de rotation dans le tourbillon diminuant ainsi le laps de temps qu'il est nécessaire de maintenir entre le passage de deux avions dans un aéroport.

Au cours des expériences on a effectué des mesures sur un tourbillon créé au centre d'une soufflerie circulaire dans les cinq cas suivants : deux jets différents, deux sillages différents et un écoulement dans lequel la quantité de mouvement longitudinale excédentaire était pratiquement nulle. Les mesures prises comprennent les trois composantes du vecteur vitesse moyen et les six composantes du tenseur de Reynolds. Elles ont toutes été effectuées à l'aide d'un anémomètre à fil chaud. Les équations des contraintes de Reynolds sont basées sur le modèle mathématique du deuxième ordre de Launder, Reece et Rodi. La solution numérique de ces équations et des équations de quantité de mouvement utilise comme conditions initiales les données expérimentales prises en amont. Cette théorie permet une bonne prédiction des résultats obtenus aux deux stations de mesures avales.

Le calcul numérique des paramètres de l'écoulement, poussé assez loin vers l'aval, indique qu'un supplément de quantité de mouvement d'environ 10% de la poussée totale du moteur induit une vitesse rotationnelle dans eviron 75% de la distance du tourbillon naturel.

ACKNOWLEDGEMENTS

This work was supported by grants held by Dr B.G. Newman from the Defense Research Board (9551-12) and the National Research Council of Canada (A7096). The project was initiated by Professor Newman who I wish to thank for his support and helpful advice. The experiments described were initiated by Dr J.A.H. Graham and executed with him. Mr. H.P.A.H. Irwin introduced me to the turbulence modelling method and deserves special thanks for useful and helpful discussions.

Valuable technical support was provided by Louis Vroomen of the DATAC Computer Laboratory and Joe Dubic of the Aerodynamics Laboratory.

CONTENTS.

LIST OF FIGURES.

NOTATION.

A	Characteristic constant of vortex during overcirculation.
$a_1, a_2 \ldots a_{10}$	Constants in second order closure equations.
B	General constant.
C^{ijkn}	Tensor representing part of the redistribution term.
C	General constant.
c	Wing Area/Span = Average Wing Chord. (= 5.08 cms.)
g^{ij}, g_{ij}	Metric tensor (Appendix A).
h	$= rq.\overline{v_r'^2}/\varepsilon$.
h	Scale factor (Appendix A).
J	Axial momentum increment. $= 2\pi\rho\int_0^\infty v_z[v_z - 1].rdr$
$J(z)$	Angular momentum decrement.
L_o	Radial width at half maximum axial velocity perturbation.
L_ε	Dissipation length scale.
ℓ	Characteristic length.
p	Pressure.
q	Turbulence Kinetic Energy $(= 1/2(\overline{v_z'^2} + \overline{v_r'^2} + \overline{v_\theta'^2}))$
Q_E	Effective cooling velocity (Appendix A).
Q_I	Instantaneous velocity (Appendix A).
q_s, q_t, q_n	Instantaneous velocities in s, t, n directions (Appendix A).
Re	Vortex Reynolds number $= \Gamma_\infty/\nu$.
Re_λ	Turbulence Reynolds number $= \overline{v_z'^2}[15/\nu\varepsilon]^{1/2}$
Re_D	Pipe flow Reynolds number.
r	Radius.
r_1	Radius of maximum circumferential velocity.

S^{ij}	Summation of Dissipation, Production and Redistribution terms in the Reynolds Stress Equations.
t	Time.
U	Mean velocity.
U_o	Maximum axial velocity perturbation
U_∞	Free Stream velocity.
u	Fluctuating velocity.
v_r, v_z, v_θ	Mean velocities in the r,z and θdirections.
v_1	Maximum velocity in θ direction.
x	Lateral coordinate of vortex.
y	Transverse coordinate of vortex.
z	Longitudinal coordinate of vortex.
α	Eddy viscosity coefficient.
α^{ij}	Diffusion coefficient.
α	Angle of inclined hot wire.
β_3	Angle between instantaneous hot wire and velocity vector.
Γ	Circulation (= $2\pi v_\theta r$)
Γ_∞	Free stream circulation.
Γ_1	Circulation at maximum tangential velocity (= $2\pi v_1 r_1$)
δ^{ij}	Kronecker delta
ε	Dissipation rate of turbulence energy.

ϕ Azimuthal angle of hot wire.

ϕ^{ij} Component of redistribution term.

SUBSCRIPTS AND SUPERSCRIPTS.

i,j,k,l,m,n. Tensor indices.

$|^{i}$, $|_{j}$ Contravariant and covariant derivatives in the i and j directions.

$'$ Instantaneous fluctuations.

OTHER SYMBOLS.

$\overline{\quad}$ Conventional time average.

$\{\ \}$ Christoffel symbol of the second kind.

1. INTRODUCTION

1.1 GENERAL.

When lift is generated by a three dimensional wing, the vortex sheet shed by it is unstable and rolls up into two discrete vortices which trail behind the wing. The strength of the vortices is directly related to the lift generated by the wing and inversely to the span and the free stream velocity approaching it, and hence those trailing behind a large aircraft can cause considerable danger to following aircraft. The danger is enhanced by the fact that the vortices persist for some time (about ten minutes for a Jumbo jet) before decaying or breaking down. With the high frequency throughput of aircraft at large airports, the trailing vortex problem is of considerable importance and has recently stimulated much research into its origin and nature.

From a high aspect ratio wing the vortex has three stages, (1) the rollup stage as the vortex sheet leaves the wing and rolls up, (2) the intermediate stage when it is completely rolled up and begins to decay, and (3) the final stage when the two trailing vortices induce a mutual instability between themselves, and develop into vortex rings.

1.2 PREVIOUS WORK

The concept of roll-up was first discovered by Prandtl and the equations governing the motion (for the finite case) remain unsolved; they are steady three dimensional. Betz (1932) approached the problem by considering an inviscid semi-infinite vortex sheet of known initial circulation, and postulated that the angular impulse of vorticity remained constant during roll-up, this allows an estimate of the final roll-up state to be found. However the approximation cannot be used for the finite case because it fails to conserve energy. Westwater (1935), Takami (1964), Moore (1971, 1974), Clements and Maul (1973) and others have reframed the problem to an unsteady one in two dimensions and simulated the vortex sheet by a finite number of line vortices. Takami (1964) and Moore (1971) found that an accurate numerical approach lead to a chaotic mess, and only after careful simulation of the region of maximum vorticity could consistent results be obtained, Moore (1974). Another approach was by Kaden (1931) who solved the problem for a semi-infinite wing; he assumed a two dimensional hydrodynamically self similar flow and a limiting form for the circulation as a function of radius. He found the self similar shape of the deforming vortex sheet to be given by a spiral. Moore and Saffman (1973) have since

extended this to the case of a finite wing. It remains to include the axial velocity perturbation inherent in the vortex during roll up.

Once the vortex sheet has rolled up and the turns in the spiral have merged together, the vortex may be considered as one having developed from an infinite line vortex. For the laminar case with no axial velocity perturbation, the governing equations were first solved by Oseen (1911), and subsequently by Hamel (1916), Lamb (1932) and others; Hilton (1938) however noticed that axial velocities existed in the vortex. Newman (1959) then considered this property, and by linearizing the equations of motion (the linearization requires that the axial velocity perturbation be small compared to the free stream velocity),solved them. His equations were uncoupled. Kirde (1962) considered the two dimensional case with a power law swirl distribution and solved the equations numerically, Batchelor (1964) used coupled equations and a similarity technique and proved that axial flow was dynamically necessary. Moore and Saffman (1973) have since solved for the more general case with axial flow which recovers the solutions of both Kirde and Batchelor. They have also extended the analysis to include the wake deficit due to the laminar boundary layer developed on the generating wing surface. They also used linearized equations.

For the turbulent case Squire (1954) utilized the solution of Lamb(1932) and instituted an eddy viscosity, a similar approach was proposed by Newman (1959). Hoffman and Joubert (1963) discovered a log law region similar in form to that near the wall in a turbulent boundary layer and Govindaraju and Saffman (1971) found that the equations of motion evoked a phenomenon called overcirculation. That is the vortex would produce a circulation greater than that generated by a wing. Owen (1970) proposed a model for a turbulent vortex and developed a formula for the decay in maximum tangential velocity with time.

In the late nineteen sixties and early seventies, much experimental work was done on the turbulent vortex, all with the object of increasing the diffusion rate of the mean vorticity contained within it. McCormick et al (1968), Mason and Marchman (1972), Kantha et-al (1972) and Poppleton (1970) all performed experiments with varying levels of axial momentum, all finding that vorticity diffusion was related to the axial momentum and/or turbulence level in the vortex core. In an effort to determine the underlying mechanism involved, Poppleton (1970) attempted to measure the Reynolds stresses; his results however contained much scatter. Graham et-al (1974) hypothesized that the vortex is initially jet (or wake) dominated, and by using small increment theory evoked a relationship between the axial momentum increment, the circulation and the maximum tangential velocity. At a

given strain rate ratio they proposed that the jet would cease to dominate; this lead to a series of curves relating the three variables. Snedeker (1972) incorporated Donaldson et-al's two dimensional model of invariant scales to numerically solve the equations of motion. Starting with Poppelton's results at his z/c = 78 station, they predicted the situation at his z/c = 109 station, their findings indicated that a two dimensional model of turbulence was not adequate to simulate the flow.

Work was also proceeding in the areas of mutual instability between two trailing vortices and vortex breakdown,(the abrupt change of a swirling flow in the axial direction which results in a pronounced retardation of the flow). Crow (1970) presented the first analysis of mutual instability between two inviscid infinite vortices, and this was later improved and generalized by Moore and Saffman (1972). Vortex breakdown has also received lively attention, and several postulates have been put forward regarding the phenomenon; these are well described in Hall (1972). The most promising appears to be that breakdown is a consequence of a critical state. Randel and Leibovich (1972) have extensively analysed this concept and their results predict much of that measured experimentally by Sarpkaya (1972).

1.3 PRESENT WORK.

The area of this dissertation lies in the second stage of the trailing vortex development, that of a fully rolled up turbulent vortex. Its aim was to conduct an experiment in a turbulent vortex and measure the downstream change in Reynolds stresses and mean velocities,and then numerically solve the equations governing the vortex motion and to compare the results with the downstream measurements. Measurements were made for five cases of axial momentum using hot wire anemometers, and readings were taken at three downstream stations.

To derive a tractable set of equations, the second order closure procedure of Launder et-al was utilized. This procedure had not previously been used in an axisymmetric coordinate system and thus the project became as much a test of it, as to explore the downstream behaviour of the vortex. The closure procedure worked very well and so predictions of the far downstream situation were possible with reasonable confidence. The Reynolds number dependence of vortex decay, apparent from many experimental and flight measurements is clearly seen and so is the effect of enhancing the turbulence level in the vortex core.

2. THEORY.

2.1 THE EQUATIONS OF MOTION.

The motion of a steady, incompressible , fully rolled up turbulent vortex is defined by the three momentum equations,* (in tensor notation).

$$U^j U^i|_j + \frac{p}{\rho}|^i = \nu U^i|^k_k \qquad 2.1.1$$

the six Reynolds stress equations,*

$$U^k \overline{u^i u^j}|_k = -(\overline{u^j u^k} U^i|_k + \overline{u^i u^k} U^j|_k) - (2\nu \overline{u^i|^k u^j|_k})$$
$$\overbrace{-\left[\overline{u^i u^j u^k} - \nu(\overline{u^i u^j})|^k\right.}^{\text{PRODUCTION}} \overbrace{\left. + \frac{p}{\rho}(u^i g^{jk} + u^j g^{ik})\right]|_k\Big\}}^{\text{DISSIPATION}}$$
$$\overbrace{+ \frac{p}{\rho}(u^i|^j + u^j|^i)}^{\text{DIFFUSION}} \qquad 2.1.2$$
$$\text{REDISTRIBUTION}$$

and the continuity equation*

$$U^i|_i = 0 \qquad 2.1.3$$

In the cylindrical polar coordinate system (fig. 2A) and taking the vortex axis to lie in the z direction, the vortex has the boundary conditions;

$$\left.\begin{aligned} v_r &= v_\theta = 0 \\ \overline{v_r^2} &= \overline{v_\theta^2} \geq 0 \\ \overline{v_z^2} &\geq 0 \end{aligned}\right\} \quad r = 0 \qquad 2.1.4$$

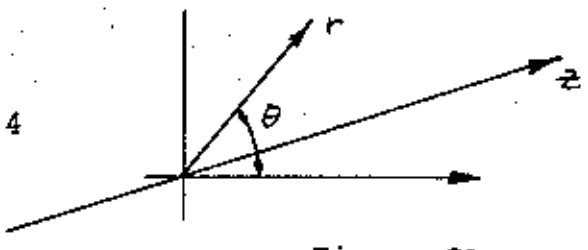

Figure 2A.

* The relevant covariant derivatives to transpose these tensorial equations into cylindrical polar coordinates are given in Appendix B.

$$\left.\begin{aligned} v_\theta &= \Gamma_\infty/2\pi r \\ v_r &= 0 \\ \overline{v_z'^2} &= \overline{v_r'^2} = \overline{v_\theta'^2} = 0 \\ \frac{\partial v_\theta}{\partial r} &= -\frac{\Gamma_\infty}{2\pi r^2} \end{aligned}\right\} \quad r \to \infty \qquad 2.1.5$$

all other first derivatives equal zero at $r = 0$ and $r \to \infty$.

2.2 SIMPLE SOLUTIONS.

Squire (1954) used the laminar solution of Lamb (1932) which assumed that the mean motion was independent of θ and z and replaced the kinematic viscosity ν with an eddy viscosity $\nu + \alpha\Gamma_\infty$, giving the expression for the tangential velocity.

$$v_\theta = \frac{\Gamma_\infty}{2\pi r}\left[1 - \exp\left(-\frac{r^2}{4(\nu+\alpha\Gamma_\infty)t}\right)\right] \qquad 2.2.1$$

Hoffman and Joubert (1963) assumed an equilibrium layer (i.e. one in which production equals dissipation ε) to exist in the vortex. From equation 2.1.2 in the θ or 3 direction (see Appendix B), if terms of small magnitude are neglected, the equation reduces to,

$$-\overline{v'_r v'_\theta}\cdot\frac{1}{r}\cdot\frac{\partial(rv_\theta)}{\partial r} = \varepsilon \qquad 2.2.2$$

Utilizing the similarity expressions of Townsend (1961) viz,

$$\varepsilon = q^{3/2}/L_\varepsilon \qquad \text{and} \qquad \overline{v'_r v'_\theta} = \text{const.}q \qquad 2.2.3$$

leads to (where $\ell = (\text{const})^{3/2}.L_\varepsilon$)

$$\frac{\ell}{r}\cdot\frac{\partial\Gamma}{\partial r} = -(\overline{v'_r v'_\theta})^{1/2} = \frac{C^{1/2}}{r} \qquad 2.2.4$$

now as the streamlines are circular, the flow processes are likely to depend only upon the local curvature, hence $\ell = f(r)$, and since no other characteristic lengths are involved, $\ell = Br$. Substituting into equation 2.2.4 then and

integrating gives;

$$\Gamma = \frac{C^{1/2}}{B} \ln(r) + \text{const.} \qquad 2.2.5$$

Hence it is plausible that a logarithmic region with constant slope will exist in the vortex.

Govindaraju and Saffman (1971) considered the steady theta-wise momentum equation (3 direction in equation 2.1.1), and knowing that

$$v_\theta = \Gamma/2\pi r \qquad 2.2.6$$

substituted into equation 2.1.1 and used the boundary layer assumption $(\partial/\partial z << \partial/\partial r)$, this lead to;

$$U_\infty \frac{\partial(\Gamma - \Gamma_\infty)}{\partial z\, 2\pi r} = \frac{\nu}{r^2}\frac{\partial}{\partial r}\left[r^3 \frac{\partial}{\partial r}\left(\frac{\Gamma}{2\pi r^2}\right)\right] - \frac{1}{r^2}\frac{\partial}{\partial r}(r^2\overline{v'_r v'_\theta}) \qquad 2.2.7$$

multiplying by r and integrating with respect to r gives;

$$U_\infty \frac{\partial}{\partial z}\int_o^\infty (\Gamma - \Gamma_\infty) r dr = \nu r^3 \frac{\partial}{\partial r}\left(\frac{\Gamma}{r^2}\right)\Bigg|_o^\infty + 2\pi r^2 \overline{v'_r v'_\theta}\Bigg|_o^\infty \qquad 2.2.8$$

For the case that $\overline{v'_\theta v'_r}$ approaches zero faster than $1/r^2$, the second term of the right hand side of equation 2.2.8 equals zero, then;

$$\frac{\partial}{\partial z}\int_0^\infty \left(\frac{\Gamma_\infty - \Gamma}{\Gamma_\infty}\right) r dr = \frac{2\nu}{U_\infty} \qquad 2.2.9$$

integrating with respect to z and taking $\xi = r/r_1$ where r_1 is the radius at which the maximum circumferential velocity occurs, then gives;

$$J(z) = \int_0^{\infty} \left(\frac{\Gamma_\infty - \Gamma}{\Gamma_\infty} \right) \xi d\xi \qquad 2.2.10$$

which is the angular momentum defect, and for the case cited above this equals;

$$J(z) = \frac{A}{r_1^2} + \frac{2(z - z_o)\nu}{r_1^2 U_\infty} \qquad 2.2.11$$

where A is a constant whose value is defined by the initial conditions. If r_1 increases faster than $\sqrt{\nu(z - z_0)/U_\infty}$ then J(z) must decrease, and small J(z) implies that $\Gamma/\Gamma_\infty > 1$ for some value or r, i.e. the vortex is over-circulating. For a Rankine vortex J(z) = .25 and for a plane laminar one J(z) ≈ .45.

Graham, Newman and Phillips (1974) hypothesized that when the axial velocity perturbation is enhanced by a jet or wake that this initially dominates the vortex. By using small increment theory for the axial contribution, and equation 2.2.1 to describe the circumferential motion, they found that

$$\left[\frac{U_\infty}{v_1} \right]^3 \propto \left[\frac{U_\infty z}{\Gamma_\infty} \right] \left[\frac{|J|}{\rho \Gamma_\infty^2} \right] \qquad 2.2.12$$

where the constant of proportionality is directly related to the eddy viscosity Reynolds number. When the strain rate ratio between the axial and circumferential velocity components fell below a given value (chosen as 1.0), the jet or wake was considered to no longer have an effect

and the decay was then solely defined by equation 2.2.1 with the eddy viscosity given to it by the jet.

2.3 SECOND ORDER CLOSURE PROCEDURE.

The numerical solution of equations 2.1.1, 2.1.2, and 2.1.3 is possible providing the terms on the right hand side of the Reynolds Stress equations (2.1.2) are modelled. Hanjalic and Launder (1972) presented a model which permits this and it has since been improved by Launder Reece and Rodi (1973). The model is based upon the assumption that the turbulence is locally isotropic. The dissipation term;

$$\overline{[2\nu u^i|^k u^j|_k]}$$

is then equal to $2/3.g^{ij}.\varepsilon$ 2.3.1

And following Chou (1945), the redistribution term is

$$\overline{\frac{p}{\rho}(u^i|^j + u^j|^i)} = \phi_1^{ij} + \phi_2^{ij} \qquad 2.3.2$$

where $\phi_1^{ij} = -a_1\varepsilon/q.(\overline{u^iu^j} - 2/3.g^{ij}.q)$ 2.3.3 (Rotta 1951)

and $\phi_2^{ij} = U_n|_m\,(C^{nmij} + C^{nmji})$ 2.3.4

$$C^{mnij} = a_{10}g^{nj}\overline{u^mu^i} + a_7(g^{mn}\overline{u^iu^j} + g^{mj}\overline{u^iu^n} + g^{ij}\overline{u^mu^n} + g^{in}\overline{u^mu^j})$$

$$+ a_2g^{mi}\overline{u^nu^j} + q[a_8g^{mi}g^{nj} + a_9(g^{mn}g^{ij} + g^{mj}g^{in})] \qquad 2.3.5$$

here $a_{1,2,\cdots}$, are constants, (see Appendix B).
In the diffusion term the viscous dependent term is neglected and the pressure velocity diffusion term is assumed to be incorporated into the redistribution term. The triple velocity correlation $\overline{u^iu^ju^k}$ is found by approximating the triple velocity correlation transport equation, leaving;

$$-\overline{u^i u^j u^k} = a_6 q/\varepsilon \left[\overline{u^i u^n}\left(\overline{u^j u^k}\right)\big|_n + \overline{u^j u^n}\left(\overline{u^k u^i}\right)\big|_n + \overline{u^k u^n}\left(\overline{u^i u^j}\right)\big|_n\right] \quad 2.3.6$$

The modelled form of equation 2.1.2 may now be written as;

$$U^k \overline{u^i u^j}\big|_k = -\left[\overline{u^j u^k} U^i\big|_k + \overline{u^i u^k} U^j\big|_k\right] - 2/3.g^{ij}.\varepsilon$$

$$- a_1 \varepsilon/q.\left[\overline{u^i u^j} - 2/3.g^{ij}.q\right] + U_n\big|_m \left[C^{nmij} + C^{nmji}\right] \quad 2.3.7$$

$$+ a_6 \left[q/\varepsilon\left[\overline{u^i u^n}\left(\overline{u^j u^k}\right)\big|_n + \overline{u^j u^n}\left(\overline{u^k u^i}\right)\big|_n + \overline{u^k u^n}\left(\overline{u^i u^j}\right)\big|_n\right]\big|_k\right]$$

Another equation must be introduced to determine the dissipation ε, this results from the approximated transport energy equation yielding;

$$U^k \varepsilon\big|_k = a_3\left[\overline{u^k u^n}\varepsilon\big|_n . q/\varepsilon\right]\big|_k - a_4 \varepsilon \overline{u^i u^k}/q.g_{ij}U^i\big|_k - a_5 \varepsilon^2/q \quad 2.3.8$$

2.4 THE MODELLED EQUATIONS.

With these assumptions it is now possible to derive a numerically tractable set of equations describing the motion of a turbulent vortex. Incorporating the relevant covariant derivatives given in Appendix B for a cylindrical polar coordinate system, the complete equations in modelled form were derived. Two assumptions were then made, namely that the boundary layer approximation is valid ($\partial/\partial z << \partial/\partial r$) and that the flow is independent of θ. The resulting equations then are;

the continuity equation,

$$\frac{\partial v_z}{\partial z} + \frac{1}{r}\frac{\partial r v_r}{\partial r} = 0 \qquad 2.4.1$$

The momentum equations;

in the z direction

$$v_z\frac{\partial v_z}{\partial z} + v_r\frac{\partial v_z}{\partial r} = -\frac{1}{\rho}\frac{\partial p}{\partial z} + \frac{1}{r}\frac{\partial}{\partial r}\left(r\nu\frac{\partial v_z}{\partial r}\right) - \frac{1}{r}\frac{\partial}{\partial r}\left(r\overline{v'_z v'_r}\right) - \frac{\partial \overline{v'^2_z}}{\partial z} \qquad 2.4.2$$

in the r direction (neglecting the $v_z\frac{\partial v_r}{\partial z}$ term)

$$v_r\frac{\partial v_r}{\partial r} - \frac{v_\theta^2}{r} = -\frac{1}{\rho}\frac{\partial p}{\partial r} + \frac{\nu}{r}\frac{\partial}{\partial r}\left(r\frac{\partial v_r}{\partial r}\right) - \frac{\nu v_r}{r^2} - \frac{1}{r}\frac{\partial r\overline{v'^2_r}}{\partial r} + \frac{\overline{v'^2_\theta}}{r} \qquad 2.4.3$$

As this equation is a function of r only we may integrate it with respect to r. Integrating then and neglecting terms of

small order gives,

$$\frac{p_o}{\rho} = \frac{p_r}{\rho} - \int_o^r \frac{v_\theta^2}{r}\,dr \qquad 2.4.4$$

In the θ direction , expressed as an angular momentum,

$$v_z\frac{\partial rv_\theta}{\partial z} + v_r\frac{\partial rv_\theta}{\partial r} = \frac{1}{r\partial r}\left(\nu r\frac{\partial rv_\theta}{\partial r}\right) - \frac{2\nu\partial rv_\theta}{r\partial r} - \frac{\partial r\overline{v_r'v_\theta'}}{\partial r} - \overline{v_r'v_\theta'} - \frac{\partial r\overline{v_z'v_\theta'}}{\partial z} \qquad 2.4.5$$

The Reynolds stress equations are;

$\overline{v_z'^2}$ equation,

$$v_z\frac{\partial\overline{v_z'^2}}{\partial z} + v_r\frac{\partial\overline{v_z'^2}}{\partial r} = \frac{1}{r}\frac{\partial}{\partial r}\left(\alpha^{11}h\,\frac{\partial\overline{v_z'^2}}{\partial r^z}\right) + S^{11} \qquad 2.4.6$$

$\overline{v_r'^2}$ equation,

$$v_z\frac{\partial\overline{v_r'^2}}{\partial z} + v_r\frac{\partial\overline{v_r'^2}}{\partial r} = \frac{1}{r}\frac{\partial}{\partial r}\left(\alpha^{22}h\,\frac{\partial\overline{v_r'^2}}{\partial r^r}\right) + S^{22} \qquad 2.4.7$$

$\overline{v_\theta'^2}$ equation,

$$v_z\frac{\partial\overline{v_\theta'^2}}{\partial z} + v_r\frac{\partial\overline{v_\theta'^2}}{\partial r} = \frac{1}{r}\frac{\partial}{\partial r}\left(\alpha^{33}h\,\frac{\partial\overline{v_\theta'^2}}{\partial r^\theta}\right) + S^{33} \qquad 2.4.8$$

$\overline{v_z'v_r'}$ equation,

$$v_z\frac{\partial\overline{v_z'v_r'}}{\partial z} + v_r\frac{\partial\overline{v_z'v_r'}}{\partial r} = \frac{1}{r}\frac{\partial}{\partial r}\left(\alpha^{12}h\,\frac{\partial\overline{v_z'v_r'}}{\partial r^{zr}}\right) + S^{12} \qquad 2.4.9$$

$\overline{v_r'v_\theta'}$ equation,

$$v_z\frac{\partial\overline{v_r'v_\theta'}}{\partial z} + v_r\frac{\partial\overline{v_r'v_\theta'}}{\partial r} = \frac{1}{r}\frac{\partial}{\partial r}\left(\alpha^{23}h\,\frac{\partial\overline{v_r'v_\theta'}}{\partial r^{r\theta}}\right) + S^{23} \qquad 2.4.10$$

$\overline{v_z'v_\theta'}$ equation,

$$v_z\frac{\partial\overline{v_z'v_\theta'}}{\partial z} + v_r\frac{\partial\overline{v_z'v_\theta'}}{\partial r} = \frac{1}{r}\frac{\partial}{\partial r}\left(\alpha^{13}h\,\frac{\partial\overline{v_z'v_\theta'}}{\partial r^{z\theta}}\right) + S^{13} \qquad 2.4.11$$

where

$$h = r.q.\overline{v_r'^2}/\varepsilon \qquad 2.4.12$$

and

$$S^{11} = -2/3\varepsilon + \phi_1^{11} + \phi_2^{11} + 2\overline{v_z'^2}\frac{\partial(rv_r)}{r\partial r} - 2\overline{v_z'v_r'}\frac{\partial v_z}{\partial r} \qquad 2.4.13$$

$$S^{22} = -2/3\varepsilon + \phi_1^{22} + \phi_2^{22} - 2\overline{v_r'^2}\frac{\partial v_r}{\partial r} + 4\frac{v_\theta}{r}\overline{v_r'v_\theta'} \qquad 2.4.14$$

$$S^{33} = -2/3\varepsilon + \phi_1^{33} + \phi_2^{33} - 2\overline{v_r'v_\theta'}\frac{\partial v_\theta}{\partial r} - 2\frac{v_\theta}{r}\overline{v_r'v_\theta'} - 2\frac{v_r}{r}\overline{v_\theta'^2} \qquad 2.4.15$$

$$S^{12} = \phi_1^{12} + \phi_2^{12} - \overline{v_r'^2}\frac{\partial v_z}{\partial r} + 2\frac{v_\theta}{r}\overline{v_z'v_\theta'} + \frac{\overline{v_z'v_r'}v_r}{r} \qquad 2.4.16$$

$$S^{23} = \phi_1^{23} + \phi_2^{23} - \overline{v_r'^2}\frac{\partial v_\theta}{\partial r} + \frac{v_\theta}{r}(2\overline{v_\theta'^2} - \overline{v_r'^2}) - \frac{\overline{v_r'v_\theta'}}{r}\frac{\partial(rv_r)}{\partial r} \qquad 2.4.17$$

$$S^{13} = \phi_1^{13} + \phi_2^{13} - \overline{v_r'v_\theta'}\frac{\partial v_z}{\partial r} - \overline{v_z'v_r'}\frac{\partial v_\theta}{\partial r} - \frac{v_\theta}{r}\overline{v_z'v_r'} + \frac{\overline{v_z'v_\theta'}}{r}\frac{\partial v_r}{\partial r}$$

and the α^{ij}'s are given in Appendix B. 2.4.18

Equation 2.3.8 for the dissipation ε becomes;

$$v_z\frac{\partial\varepsilon}{\partial z} + v_r\frac{\partial\varepsilon}{\partial r} = \frac{1}{r}\frac{\partial}{\partial r}\left(h.a_3.\frac{\partial\varepsilon}{\partial r}\right) - a_3.q/\varepsilon.\frac{\partial\varepsilon}{\partial r}.\frac{\overline{v_\theta'^2}}{r} - a_5.\varepsilon^2/q \qquad 2.4.19$$

$$- a_4\varepsilon/q\left[-\frac{\overline{v_z'^2}}{r}\frac{\partial rv_r}{\partial r} + \overline{v_z'v_r'}\frac{\partial v_z}{\partial r} + \overline{v_r'v_\theta'}\frac{\partial v_\theta}{\partial r} + \frac{v_r}{r}\overline{v_\theta'^2} - \frac{v_\theta}{r}\overline{v_r'v_\theta'}\right]$$

With the boundary conditions 2.1.4 and 2.1.5, these equations may now be solved numerically. This was done using the finite difference procedure proposed by Spalding and Patankar (1967). The problem is of the initial value type and hence a complete solution must be known at one time in order to predict solutions at another later time.

The only initial condition not available from the results of Graham and Phillips is the dissipation ε, and for the first step this was approximated by

$$\varepsilon = q^{3/2}/L_\varepsilon \qquad 2.4.20$$

where the dissipation length scale L_ε was taken to equal L_0 the radial width at which the axial velocity reaches half of its maximum perturbation. For case (c), the initial guess for L_ε was taken to be $1/c$.

2.5 CHECK ON THE NUMERICAL PROCEDURE.

As there are no analytical solutions to the motion of a turbulent vortex a direct check of the numerical solution to the eleven partial differential equations is not possible. Checks against laminar solutions both with and without (initial) axial velocity check only parts of the axial and tangential momentum equations, but as nothing else (apart for the experimental results) was available this was done. Two cases were considered, the first with simply a two-dimensional vortex, the second with the same initial conditions as the first but here the axial equation was also solved downstream. Over a downstream distance of one hundred chord lengths* the numerical solution predicted a maximum tangential velocity that was 1½ % lower than the analytical; in the second case the axial profile developed a very small deficit, but this had a negligible effect on v_1 over the distance considered.

The second check was done with an axisymmetric jet in streaming flow with a zero pressure gradient, this checked parts of the turbulence model and the axial momentum equation. The results were compared with the measurments of Graham and Phillips. The numerical results predicted an axial velocity decay rate slower than that measured by 5%. This is in qualitative agreement with the prediction

* c was used to nondimensionalize z because at this stage Γ_∞ was not known accurately, thus excluding the group $U_\infty z/\Gamma_\infty$.

of the decay of a plane jet in streaming flow done by Launder et-al (1973) and appears to be indicative of what they call weak shear flows or flows in which the importance of the production term diminishes downstream, and leads to a relatively large convective term. They suggest that this is partly relieved by including the normal stress terms which are generally important in this type of flow, and this was done. It is also possible to improve the decay rate by changing the diffusion constant a_4 (= 1.45) to 1.35, this increases the axial shear stress $\overline{v'_z v'_r}$ and the turbulence level $\overline{v'^2_z}$, and the predicted axial profile then agrees well (within 2%) with that measured. From the point of view of a general turbulence model however it was not possible to substantiate this change and so in spite of the slower decay rate $a_4 = 1.45$ was used throughout the investigation.

3. EXPERIMENT.

3.1. AIM OF THE EXPERIMENT.

The aim of the experiment was to generate a turbulent vortex and to measure the change in velocity components and Reynolds stresses of the vortex with distance downstream. This was done for five different values of axial momentum. In two cases there would be an axial velocity increment (jet) and in two a deficit (wake) about the free stream velocity profile. The remaining case would have zero increment or deficit. In the vortex generated, a small deficit existed in the axial velocity profile; hence the zero and increment cases were achieved by blowing a jet of air along the vortex axis. To increase the axial velocity deficit, a bluff body was placed along the vortex axis. Readings were taken at three downstream stations, $z/c = 45, 78, 109$, where c (=5.08cm.) is the average chord of the wing.

3.2 EXPERIMENTAL APPARATUS.

The experiment was conducted in the McGill circular blower tunnel previously used by Vogel (1968) and Poppleton (1970). The tunnel has a 6.4 metre working section and is .76 m. in diameter, it is constructed from seven, .915 m. long modules, each of perforated sheet metal, thus enabling the free stream pressure gradient to be adjusted by blanking off the perforations with tape.

The vortex was generated by two half wings mounted at equal and opposite incidence to the free stream. They were designed (by Poppleton(1970)) to develop constant circulation along each span with a sinusoidal variation of circulation between them, hence producing an area of high vorticity between the wing halves. Separating the two wings was a nacelle enclosing a 7.75 mm. internal diameter pipe; this was used to supply the jet and also hold the bluff body (fig.2). The circulation developed by the wings with a free stream velocity of 21.33 m/s and an incidence angle of 9° was 0.794 m^2/s, (see Section 4.4).

The pressure gradient along the tunnel was adjusted (by trial) to be close (within 0.4% on dynamic pressure) to zero.

The mean and fluctuating velocity components were measured with a constant temperature hot wire probe, this was mounted in a traversing mechanism capable of motion in

the x and y directions (fig. 1A). The probe holder was also capable of azimuthal rotation (ϕ in fig. 1A). To ensure accurate alignment of the probe with the streaming flow the traverse gear was moved to the four extremities of its travel ($\pm$ 17.8, $\pm$ 17.8 cm), and with the wings set at zero incidence an inclined hot wire was rotated azimuthally. If the probe is parallel to the streaming flow the reading from it is independent of ϕ, fine adjustments on the traverse gear allow this to be approached and the probe was always brought within $\pm$ 1/4° of the axial velocity vector.

Traverse movement in the x direction was manual and position was indicated by a graduated marker ;this could be attained within 1 mm. Movement in the y direction was similar although here position was indicated by a counter. The azimuthal rotation of the probe was in increments of 45° by a small servo motor.

The hot wire probes used were DISA type 55A22 normal and DISA type 55A25 inclined, connected with 1mm. of five micron tungsten wire. The probe was connected to a DISA type 55D01 constant temperature anemometer and then to a DISA type 55D10 linearizer.

3.3 HOT WIRE CALIBRATION.

Calibration of the wires (normal and inclined) were done initially at the beginning of each experiment, however due to the cleanliness of the air in the tunnel (filtered to about 1 micron) and almost constant temperature of the airconditioned laboratory, very little change (< 1%) in calibration occurred; as a result the wires were only recalibrated after several experiments.

Calibration was done in the tunnel at (17.8,17.8 cm) with the wings at zero incidence; at least nine points were taken and to these a least squares straight line was fitted. The calibration coefficients for pitch and yaw were done in the Aerodynamic Laboratories calibration drum (Arnot Smith (1973)), and the angle of the inclined wires were measured with a 50X Nikkor profile projector. Each wire (i.e. normal and inclined) had its own anemometer and linearizer and were normalized to an output of 5.0 volts at a free stream velocity of 21.33 m/s.

3.4 VELOCITY AND TURBULENCE MEASUREMENTS.

The signal from the linearizer fed via a DISA type 55D25 filter to a DISA type 55D35 R.M.S. meter; the filter removed all frequencies above 20K Hz. A schematic diagram is given in figure 1. To deduce the three velocity components and six Reynolds stresses, mean and fluctuating readings were required at six different azimuthal ϕ positions with an inclined hot wire, and one ϕ position with a normal hot wire at each point in the flow. The velocity components and Reynolds stresses were then derived from these: the analysis substantiating this reduction is given in Appendix A. In the analysis the mean velocity readings are taken to second order, and the fluctuating to third. Readings were taken at azimuthal ϕ angles of 0°, 45°, 90°, 135°, 180°, and 270°; from these $\overline{v_z'^2}$ was derived using a normal wire at ϕ = 90°, $\overline{v_r'^2}$ from the sum of two readings from an inclined wire at ϕ = 90° and 270°, $\overline{v_\theta'^2}$ from the sum of two inclined readings at ϕ = 0° and 180°. The cross coupled values were all found from the difference between two readings, for $\overline{v_z'v_r'}$ they were ϕ = 90° and 270°, for $\overline{v_r'v_\theta'}$, ϕ = 45° and 135° and for $\overline{v_z'v_\theta'}$, ϕ = 0° and 180°. The axial velocity was found both from a normal wire at ϕ = 90° and also from the sum of two readings from an inclined wire at ϕ = 0° and 180°. The radial and tangential velocities were found from the difference between two readings

from an inclined wire; for v_θ, $\phi = 90°$ and $270°$ and for v_r, $\phi = 0°$ and $180°$.

The free stream velocity was determined from the pressure drop across the throat of the wind tunnel and was measured with a Statham pressure transducer.

3.5 DATA ACQUISITION.

The readings from the linearizer, R.M.S. meter and pressure transducer were linked via high quality triple shielded cable to a VIDAR integrating digital volt meter, interfacing to a GEPAC 4020 computer. The VIDAR integrated readings over 166, 16.6, or 1.66 milliseconds and then summed the result over any period ranging from 1.66 milliseconds to 30 minutes. Those chosen for the experiment were 16.6 ms and ten seconds. The summed reading from the VIDAR was then placed in core storage and when 1000_8 words of information had been collected in core, the information was automatically transferred to a predetermined area on disc. This information was later recorded on magnetic tape. The program used to record these events was developed by Vroomen and Graham(1973) and was based upon an earlier version by Poppleton (1970).

3.6 DATA REDUCTION.

Data reduction was also performed using the GEPAC 4020 and was generally done at the completion of an experiment. The information had first to be retrieved from disc and transferred into core (this section of the program was written by Vroomen and Graham), the information was then processed and the results were printed and plotted out.

3.7 CHECK ON EXPERIMENTAL PROCEDURE.

To check the experimental procedure and data reduction, the traverse gear was removed from the blower tunnel and aligned at the exit of the Aerodynamics Laboratory 7.62 cm. diameter 11m. long pipe. An experiment was than performed using fully developed pipe flow with a Reynolds number of $Re_D = 3.48 \times 10^5$. The wall shear stress was measured via the pressure drop along the pipe and compared with that measured by the hot wire, and the normal stresses were compared with those of Laufer (1953) at an $Re_D = 5 \times 10^5$, and Guitton at $Re_D = 3.50 \times 10^5$.

The shear stress agrees well with those predicted (fig. 4), the normal stress in the axial direction is slightly higher than Laufer's and the transverse and lateral stresses are lower, (fig. 3). They are in very close agreement with those of Guitton (1968) however, who who made his measurements in the same pipe.

3.8 STABILITY OF THE VORTEX.

Experimenters generating vortices in rectangular wind tunnels e.g. Mason and Marchman (1972), have found the downstream trajectory of the vortex to be affected by the introduction and motion of the measuring probe. This problem was not apparent in the present experiment. To check this , a pitot tube was attached parallel to and 2.5 cms from the hot wire probe; the pitot tube was 2 mm. in diameter. Both instruments were then successively used to find the center of the vortex; they agreed upon the position within 1.5 mm.

The stability was further exemplified by taking both a vertical and horizontal traverse through the vortex and checking the axial symmetry; the results revealed no abnormal effects. It was important that the vortex trajectory should be stable because then, providing the probe traverse passed through its center, the hot wire readings relative to the coordinate system x',y',z' (fig. 1A) were exactly equivalent to those relative to the vortex coordinate system x,0,z (fig. 1A). Consequently considerable care was taken to find the vortex center prior to each experiment.

3.9 CASES MEASURED.

Five cases were measured, each at three downstream stations z/c = 45,78,109. At the z/c = 45 station these cases were:

Case.		$\frac{U_\Omega}{U_\infty}$	$\frac{J}{\rho\Gamma_\infty^2}$	$\frac{L_o}{c}$	J(z)
(a)	High Jet	0.26	5.17	1.55	0.228
(b)	Low Jet	0.077	0.33	0.77	0.44
(c)	Zero Jet	~ 0	-0.025	-	
(d)	Natural Wake	-0.08	-0.235	0.56	0.892
(e)	Deep Wake	-0.13	-0.736	0.94	0.446

The vortex Reynolds number ($\frac{\Gamma}{\nu}_\infty$) was constant throughout the experiments and was approximately 5.7×10^4.

$U = 21.33$ m/s.

$\Gamma_\infty = 0.7938$ m^2/s

$c = 5.08$ cm.

$J = 2\pi\rho \int_0^\infty v_z[1 - v_z]\, r dr$

$$J(z) = \int_0^\infty \frac{[\Gamma_\infty - \Gamma]}{\Gamma_\infty} \xi d\xi$$

4. DISCUSSION.

4.1 EXPERIMENTAL RESULTS.

The results in general contained much less scatter than those of Poppleton (1970) and gave a reasonable quantitative indication of the effect of turbulence enhancement in the core region of a vortex. The tangential velocity measurements figures 5-7, all exhibited a central core region of close to solid body rotation, and in the outer part collapsed about the circulation value Γ_∞ estimated for the wings, (see Sect. 4.4) thus demonstrating that the outer part of the vortex is potential. The two regions were separated by one of high strain and shear stress. With the exception of the high jet (case(a)), all had the highest tangential velocity gradient $\partial v_\theta/\partial x$ at the centre. This case had an inner core region of lower angular velocity than the outer which slowly merged into the more highly sheared section of the vortex as the flow developed downstream. The inner region grew downstream and by z/c = 109 completely occupied the rotational part of the vortex (fig. 7) exhibiting a tangential velocity profile very similar to that of a Rankine vortex. This case also exhibited over-circulation relative to the value of Γ_∞ predicted for the wings. It is possible that Γ_∞ is greater for this case because of the local increase in velocity over the wings due to entrainment of air by the jet. However it is difficult to know by how much because at z/c = 45 (fig.5) the

points at large x/c fall well within the scatter of the other results, and for this reason Γ_∞ was taken to be the same for all cases.

The increase of turbulence level in the core due to the insertion of a jet or wake had a significant effect upon the radial diffusion of vorticity and consequent decrease in magnitude of v_1, the maximum circumferential velocity. This is clearly seen in figures 5-7. In case (d), (fig.5) that of the natural wake, a definite kink appears in the tangential velocity profile (this was first noticed by Poppleton (1970)). Checks of axial symmetry for this case and for case (a), (by taking both vertical and horizontal traverses), indicated that v_1 varied by only ± 2%, thus implying that the roll up process was almost complete at z/c = 45. A similar kink also appears in the corresponding z/c = 20 and 30 profiles of Mason and Marchman*(1972), (their figures 26 and 28) but does not appear in their z/c = 10 profile. In case (c) a kink appeared on one side and not on the other, it is probable that for this case roll up is not complete.

The stress level increased markedly with $|J|$, for example the normal stresses $\overline{v_z^2}$ of cases(a) remain approximately one order of magnitude higher than for case (d) over the range z/c = 45 to 109. Going downstream the turbulence intensity level decays rapidly, and by z/c = 109 (for case (a)), is only 20% of its z/c = 45 value. The normal stresses for cases (b),(c), and (d) all exhibit a

*These correspond to $U_\infty z/\Gamma_\infty$ values of 74 & 111 compared to 61.5 in this report.

region of highest turbulence in the core (due perhaps to the wake caused by the nacelle between the wing halves) which rapidly decays, merging into an area of almost constant stress in the rotational region of the vortex. For all cases the radial turbulence quantity $\overline{v_r'^2}$ is greater than both the axial and tangential; this is typical of flows in which the production term is significantly smaller than the diffusion term; for example the central region of an axisymmetric wake.

The shear stresses $\overline{v_z'v_r'}$ and $\overline{v_z'v_\theta'}$ for the two extreme cases (a) and (e) are clearly defined (figs. 15 and 18). For the inner cases (b), (c), and (d) the $\overline{v_z'v_r'}$ and $\overline{v_z'v_\theta'}$ stresses are an order of magnitude lower than cases (a) and (e), but the form of the profile is visible. The results are effectively anti-symmetrical but only one side is drawn. The stress of most interest in controlling the tangential motion however is $\overline{v_r'v_\theta'}$ and as this is the most difficult to measure the results are not as clearly defined (fig. 27). Profiles for most $\overline{v_r'v_\theta'}$ stresses were found by fitting smooth profiles to the original hot wire readings $\overline{e_{45}^2}$ - $\overline{e_{135}^2}$ (equation 31A in Appendix A), and all other measurements required for its calculation, and then rederiving it.

The log law region predicted by Hoffman and Joubert is evident from the experimental results (fig. 10), which were plotted as a function of Γ/Γ_∞ against r/r_1; the respective

values of r_1 and v_1 being taken from figures 5 to 7. The region is very definite and within the experimental scatter can accomadate a line of slope = $\log_e(10)$, (as predicted by Govindaraju and Saffman) for cases (b),(c),(d) and (e), but in case (a) the slope is higher and not as well defined. In the derivation of the log law in Section 2.2, an assumption was made that an equilibrium layer (i.e. one in which production equals dissipation) was present. A study of the predicted terms in the energy equation indicate that this is not the case.

4.2 NUMERICAL RESULTS

Using the upstream (z/c = 45) experimental results as initial conditions, the momentum and modelled Reynolds stress equations given in Section 2.4 were solved numerically to predict the results at the remaining downstream stations. This was a severe test for the turbulence model of Launder et al, firstly because it had not previously been used in an axisymmetric coordinate system and secondly the constants (a_1- a_{10}) in the model were chosen from comparisons with strong shear flows, that is flows in which the average production and dissipation levels are almost equal across the flow. The present flow is a weak shear flow (i.e. one in which the importance of the production term decreases downstream leading to a relatively large convective term) and so trying to predict it probed the generality of the turbulence model. The model fared very well, and although some disagreement occurs between the measured and predicted results, the variance is not catastrophic.

The axial velocity profiles exhibit a slower rate of decay than the experimental and this is most noticeable in the two extreme cases (a) and (e) which are both about 10% high on the vortex axis at z/c = 109 (fig. 8-9). This is not unexpected as the same effect is noticeable in the prediction of the axisymmetric jet in streaming flow without a vortex (Sect. 2.5), consequently the downstream growth (which as affected considerably by the presence of the vortex) is also slower. Due to the

rotational motion of the vortex a radial pressure gradient is generated across it and as the vortex decays downstream this causes an axial pressure gradient. The axial gradient is small $\sim$ O(.1) $N/m^2/m$, and this caused the momentum increment of cases (a) and (b) to decrease , and the momentum decrement of cases (c), (d) and (e) to increase slowly downstream. With zero pressure gradient, $|J|$ must remain constant and this property was used to check the accuracy with which the numerical scheme conserved momentum. Over the experimental range (with $\partial p/\partial z$ set to zero) $|J|$ varied by only 0.01% ; this was felt to be acceptable.

The tangential velocity profiles are predicted well for the extreme cases (a) and (e), although the numerical scheme tends to predict a slightly greater overcirculation than that measured (figs. 11 and 14). The spread of the core region of case (a) is predicted very well (fig. 14) although by z/c = 109 both r_1 and v_1 are about 10% high. In case (e), r_1 and v_1 agree almost exactly with the measurements. In the intermediate cases (b), (c) and (d) a slow downstream decay in v_1 is predicted while the measurements indicate a slight increase, thus by z/c = 109 the predictions of v_1 are about 10% low and the predicted value of r_1 is slightly high. This downstream increase in v_1 is possible (see Sect. 4.5) but unlikely for the present low Reynolds number and is taken to be experimental error.

The turbulence levels are low in the core region of all flows, case (a) being the worst ($\overline{v_z'^2}$, $\overline{v_r'^2}$, $\overline{v_\theta'^2}$ are all $\simeq$ 40% low), followed by case (e) where $\overline{v_\theta'^2}$ and $\overline{v_r'^2}$ are 30% low, ($\overline{v_z'^2}$ surprisingly

is in close agreement with the measurements in this case). In cases (b), (c) and (d) the central peak which is prominent in the measurements at all stations, is not predicted. Outside the core region, the predicted levels are in good agreement with the measurements in all cases except (a); here they remain 25-30% low.

The predicted shear stresses for cases (a) and (e) follow the general form of the measured stresses but some deviate in magnitude. In case (e) the $\overline{v'_z v'_\theta}$ stress is 25% low and peaks at about r_1, (the experimental points peak at about $2/3 r_1$), $\overline{v'_z v'_r}$ is also about 25% low. The predicted $\overline{v'_r v'_\theta}$ stresses approximately divide the scatter in the measured results at z/c = 78,& 109, (fig. 15) and as the v_θ profile is well predicted for this case (and $\overline{v'_r v'_\theta}$ is the dominating shear stress in the tangential momentum equation), this is a good cross check for both the measurements and predictions. In case (a) $\overline{v'_r v'_z}$ is about 12% low at z/c = 78 but almost correct at z/c = 109 although its peak value occurs at a larger radius than the experimental. At both downstream stations $\overline{v'_z v'_\theta}$ is about 30% high. The $\overline{v'_r v'_\theta}$ stress again divides the experimental points at z/c = 78, but the negative region present in the z/c = 45 and 109 measurements is not predicted.

In the remaining cases (b), (c) and (d) both the measured and predicted stresses are an order of magnitude lower than for cases (a) and (e), and the predicted profiles vary from the measured as follows. In case (d) (fig. 16) the predicted $\overline{v'_z v'_\theta}$ follows the measured profile well but spreads over a larger

radius and is 25% low at z/c = 109 (the peak values are almost equal at z/c = 78). The $\overline{v'_z v'_r}$ profiles are predicted very badly being only about 10% of that measured. The predicted and measured $\overline{v'_r v'_\theta}$ are about the same magnitude (NB. the experimental points are given in fig. 27) but the predicted profile has two peaks at z/c = 78; the measured has only one. In case (b) the $\overline{v'_z v'_\theta}$ predictions again follow the measured profile well with magnitudes almost equal at z/c = 78 and 30% low at z/c = 109, and very badly predicted $\overline{v'_z v'_r}$ profiles. The predicted $\overline{v'_r v'_\theta}$ profiles are also much lower (60%) than those measured. Case (c) follows the same pattern as both case (b) and (d), however here the $\overline{v'_r v'_\theta}$ profiles, although being lower than the experimental, do follow the same profile.

4.3 VALIDITY OF TURBULENCE MODEL ASSUMPTIONS.

All of the assumptions in the turbulence model are dependent upon local isotropy existing in the shear flow and confidence in the downstream predictions is reasonable only if this assumption is valid. Bradshaw (1967) has shown that the turbulence Reynolds number $Re_\lambda = \overline{v_z^{'2}}[15/\nu\varepsilon]^{1/2}$ can be as small as 100 for an inertial subrange to exist in a plane shear flow. However it is feasible that the criterion for an inertial subrange would be different for a highly curvilinear shear flow such as the present one; but no experimental work exists to support or reject this. For the experiments ($Re = 5.7 \times 10^4$) the turbulence Reynolds number Re_λ fell around 100, the actual value depending very much upon r/c. This variation is given in figures 24 and 25 which gives two downstream situations (z/c = 109 and 140) for cases (d) and (a). For both cases Re_λ is seen to have a maximum in the core region ≃ 200-250 (z/c = 109) and then decreases rapidly as the vortex becomes potential at larger radii. For case (d) the microscale $\lambda = (15\nu\overline{v_z^{'2}}/\varepsilon)^{1/2}$ also has a maximum in the core region and decreases to remain almost constant ($\lambda/r_1 \simeq 0.05$) once the core region has passed; case (a) remains almost constant across the flow ($\lambda/r_1 \simeq 0.007$). Both Re_λ and λ increase slowly downstream.

For local isotropy $u/\lambda > 10u/\ell$ (Tennekes and Lumley 1972) and taking the characteristic length scale of the flow to

be r_1, then $\ell = r_1$ and so r_1 is at least > 10λ and should probably be > 100λ. For the experimental cases b and d this condition is barely satisfied $r_1 \simeq 50\lambda$ and going downstream λ increases until $\lambda \simeq r_1$ at $\frac{U_\infty z}{\Gamma_\infty} \simeq 1000$. For case e this occurs at approximately 2000; the problem was not experienced in case a.

By this definition of local isotropy then it is doubtful whether the far downstream predictions for Re $\sim O(10^4)$ in cases b and d are valid. In figure 23 an arrow is used to indicate where $r_1 \simeq 10\lambda$ (at $r = r_1$) occurs for these cases. As the Reynolds number increases however the local isotropy assumption becomes much easier to satisfy and for Re $\sim O(10^6)$ for case d, $r_1 \simeq 10\lambda$ does not occur until $\frac{U_\infty z}{\Gamma_\infty} \simeq 1000$.

4.4 DETERMINATION OF THE FREE STREAM CIRCULATION.

The free stream circulation Γ_∞ was initially estimated from lifting line theory using a lift slope coefficient of $2\pi k$ ($k = 0.7$) as suggested by Poppleton (1970). For a wing incidence angle of 9° and a free stream velocity of 21.33 m/s, this gave Γ_∞ as 0.749 m^2/s. The experimental results fell close to this value but in general slightly above it; $k = 0.75$ ($\Gamma_\infty = 0.802$ m^2/s) was therefore tried and this curve appeared to approximate the scatter more convincingly (see figures 5-7). This value was then used as the initial boundary condition for Γ_∞ in the numerical scheme.

A one percent change in Γ_∞ has virtually no effect upon the solution of v_θ but causes the integral $\int_0^\infty (\Gamma_\infty - \Gamma)/\Gamma_\infty) r dr$ to change by as much as ten percent. Hence in the region far downstream where $\overline{v_r' v_\theta'} \to 0$ faster than $1/r^2$ and equation 2.2.11 is valid;

$$A = \int_0^\infty \left[\frac{\Gamma_\infty - \Gamma}{\Gamma_\infty} \right] r dr - \frac{2\nu}{U_\infty} [z - z_0] \qquad 4.4.1$$

and the evaluated value of A can only remain constant if the value of Γ_∞ being used is correct. Over this range the computed value of A did vary slightly and so another estimate of Γ_∞ was found by taking a Γ profile at each end of the range and evaluating A for different values of Γ_∞ (in increments of 0.01%) until they agreed, this lead to a value of

$\Gamma_\infty = 0.793\ m^2/s$ for case (e) and $\Gamma_\infty = 0.7945\ m^2/s$ for case (d). These values are about 1% less than that estimated by lifting line theory.* In all future cases Γ_∞ was taken to be the average of these namely $\Gamma_\infty = 0.7938\ m^2/s$.

4.5 THE THREE DOWNSTREAM REGIONS.

The decay of the tangential velocity in the turbulent vortex passes through three stages with distance downstream. The first is a region of rapid decay which occurs up to about $U_\infty z/\Gamma_\infty \approx 80$, in this region the decay rate is independent of the vortex Reynolds number but closely related to the axial momentum increment or decrement imposed upon the vortex. The second region is a transition region between the first and third and ends at about $U_\infty z/\Gamma_\infty \approx 100$. In the third region the vortex decay is Reynolds number dependent to Reynolds numbers Γ_∞/ν of $\sim O(10^5)$ but virtually independent of Reynolds number above this value. The three regions are visible from the experimental results but are more clearly indicated in the numerical results which are extended much further downstream (figure. 23).

It is interesting to consider the relative magnitudes of the terms in the tangential momentum equation as the vortex passes through the three stages. Equation 2.4.5 may be written in the form 4.5.1 (with $\partial\overline{v_z'v_\theta'}/\partial z$ neglected) with the convection term broken into

$$\underbrace{v_z\frac{\partial v_\theta}{\partial z}}_{\zeta} + \underbrace{\left[\frac{v_r v_\theta}{r} + v_r\frac{\partial v_\theta}{\partial r}\right]}_{\eta} = \underbrace{\nu\left[\frac{\partial^2 v_\theta}{\partial r^2} + \frac{1}{r}\frac{\partial v_\theta}{\partial r} - \frac{v_\theta}{r^2}\right]}_{\beta} - \underbrace{\left[\frac{1}{r}\frac{\partial}{\partial r}\overline{v_r'v_\theta'} + \frac{\overline{v_r'v_\theta'}}{r}\right]}_{\gamma} \qquad 4.5.1$$

two parts $\zeta + \eta$. From an order analysis $\eta/v_r \sim O(\frac{\beta r}{\nu})$ and so if $v_r \sim O(\frac{\nu}{r})$ then $\eta \sim O(\beta)$, where β is the viscous stress term. In stage one $v_r >> O(\frac{\nu}{r})$; this is seen because $v_r = -\int_0^R r\frac{\partial v_z}{\partial z}dr/R$ (continuity) and at small z, $\partial v_z/\partial z$ is larger than at large z (the magnitude being closely related to the decay rate of the jet or wake which is in turn related to the turbulence level present in the jet or wake). Hence $\eta >> O(\beta)$ and so the β term is negligible;

that is in stage one the decay of v_θ with z is independent of Reynolds number, η now is the order of γ (the Reynolds stress term), and so is ζ. It is interesting to note that the sign of v_r is different for a jet and wake and thus an identical decay rate in $|v_z|$ for both will not result in the same decay rate for the tangential velocity v_θ.

Proceeding downstream as $|\partial v_z/\partial z|$ decreases so in turn does v_r, and by stage two $v_r \sim O(\frac{\nu}{r})$, and so $\eta \sim O(\beta)$ but β is still much less than γ. By stage three $v_r < O(\frac{\nu}{r})$ and η soon becomes much less than β and is therefore negligible. The only convective term remaining then is ζ, being controlled by $\beta - \gamma$. For Reynolds numbers $\sim O(10^4)$, $\beta \rightarrow O(\gamma)$ as the vortex proceeds downstream, and as $\beta = f(Re)$ and γ is virtually independent of Reynolds number, for Reynolds numbers less than $O(10^5)$ the decay of v_θ with z will be Reynolds number dependent, (see Sect. 4.6).

The region of validity of equation 2.2.11 occurs after about $U_\infty z/\Gamma_\infty \approx 500$, and in this region the constant A is 8.45×10^{-3}, 1.02×10^{-2} and 1.46×10^{-2} for cases e,d and b respectively, in case a this region was not reached. Overcirculation of the form predicted by Govindaraju and Saffman (1971) became apparent shortly after the region was reached, it began at large r/c and spread slowly inwards with downstream distance, the amount of overcirculation being very small (<5%). This is physically different to the overcirculation occuring at around $U_\infty z/\Gamma_\infty \approx 100$ in cases a and c which was induced by the high radial diffusion of vorticity and in case a continues far downstream.

4.6 REYNOLDS NUMBER DEPENDENCE.

Comparison of flight and laboratory measurements have always suggested that there is a Reynolds number dependence for the decay of a turbulent vortex. The simple theory of of Owen (1970) tried to include this effect and the more sophisticated analysis of Saffman (1973) attempted to explain it. The reason for it is readily seen from figure 26, where the terms in equation 4.5.1 are plotted against radial distance. The example is case d at z/c = 78. Two plots are given; in figure 26a the $\overline{v'_r v'_\theta}$ profile that was used was a smooth profile through the experimental points (fig.27), in figure 26b the $\overline{v'_r v'_\theta}$ profile was as predicted. The v_r and v_θ terms are as predicted in both cases. The point of interest which is eminent in both plots is that the viscous stresses β are only one order of magnitude lower than the Reynolds stresses γ, and by z/c = 109 the margin is considerably less (the z/c = 109 experimental points for $\overline{v'_r v'_\theta}$ are also given in figure 27). Thus as the Reynolds stresses are effectively independent of Reynolds number, as the Reynolds number decreases (or the Reynolds stresses decay going downstream) the viscous stresses become more dominant. Hence in the range where most experiments were carried out [Re $\sim O(10^3-10^4)$] the decay rate (assuming the γ term in equation 4.5.1 to be positive, the β term is always negative) will be much higher than the real flight

situation where Reynolds number is $O(10^7)$. This is seen in figure 28 where the Reynolds number is varied from 5.7×10^2 to 5.7×10^6, (the initial conditions are for case d). Over the small downstream distance indicated the dependence on Reynolds number is clearly seen. It should be noted that in the $Re = 5.7 \times 10^2$ curve Re_λ is only about 25 at $r = r_1$ and it is unlikely that local isotropy exists. Other examples at higher Reynolds numbers are given in figure 23 which also extends further downstream.

In figure 29 the predicted $\overline{v'_r v'_\theta}$ shear stress is plotted for various downstream stations to $z/c = 1146$. Very shortly after $z/c = 109$ the shear stress changes sign for $r < r_1$ and this remains until $z/c \approx 1000$ (a negative shear stress in this region of the $\overline{v'_r v'_\theta}$ profiles is also seen in the starting profiles for cases a,d and e). This means that γ will be negative in this region, and from equation 4.5.1 if $\gamma > O(\beta)$ and z is large enough so that $v_r < O(\frac{\nu}{r})$ making η negligible, then providing $\partial(\overline{v'_z v'_\theta})/\partial z$ is $< \gamma$, $v_z \partial v_\theta/\partial z$ becomes positive (as v_z is always positive). For the experimental results case e $\overline{v'_r v'_\theta}$ is negative in this region (figure 15) and $\gamma >> \partial(\overline{v'_z v'_\theta})/\partial z$. As these stresses are virtually independent of Reynolds number , if we increase it until $\gamma >> \beta$, then $\partial v_\theta/\partial z$ will be positive.

That is the tangential velocity will increase downstream. Angular momentum must be conserved and this is possible by the inward diffusion of vorticity. By $z/c \approx 1150$, $\overline{v'_r v'_\theta}$ is

positive again for all r and $\partial v_z/\partial z$ is then negative and decay once again occurs. In the far downstream examples (fig.23) this occured for a Reynolds number of 5.7×10^6 (case d). At the onset of positive $\partial v_z/\partial z$ the turbulence Reynolds number was 2650 at $r = r_1$ and the microscale was $\lambda/r_1 = 3.5 \times 10^{-2}$ and so the assumptions in the turbulence model are well satisfied (Sect. 4.3). It is probable that this slow pulsation will be damped with downstream distance but no evidence is available to support this. It is also interesting to note that the curve for this case neatly divides the experimental results of Verstynen and Dunham (1973) who measured the decay of trailing vortices downstream of a C5A Jumbo jet transport. They measured cases with flaps both up and down with Reynolds numbers $Re = 2.9 \times 10^7$ and $Re = 4.0 \times 10^7$ respectively.

From this same figure (23), it is possible to estimate the real situation. Consider a Boeing 747 jet in the take off mode travelling at about 65 m/s*; with a wing drag coefficient of 0.05, this gives a $|J|/\rho\Gamma^2$ of about 0.005 which corresponds closely to case (c). If 10% of the total thrust from the Pratt and Whitney JT9D engines is used to modify the vortex, a $|J|/\rho\Gamma^2$ of about 0.08 results, and as the closest jet curve (case (b)) on the figure has a $|J|/\rho\Gamma^2$ of about 0.33, an estimate of the 0.08 case may be found by interpolat ing between the curves of cases (b) and (c)# At about two and one half kilometers downstream (where $U_\infty z/\Gamma_\infty \simeq 200$), the case (b) curve gives a U_∞/v_1

* $Re \simeq 5. \times 10^7$

Remember that these curves are at $Re \simeq 5.7 \times 10^4$ and so give an optimistic decay rate for the higher Reynolds number under consideration.

value of 10.3 and this value occurs at $U_\infty z/\Gamma_\infty \simeq 150$ on the 0.08 interpolated curve, that is the same tangential velocity is reached in about 75% of the distance of the unmodified vortex. By $U_\infty z/\Gamma_\infty = 200$, the modified vortex has decayed to a value of $U_\infty/v_1 = 10.7$, a decrease in tangential velocity of less than 5%. As 10% of the total thrust from the engines is a realistic upperbound that can be used to modify the trailing vortic es, it appears likely that this is <u>not</u> a practical method for reducing the hazard caused by them.

CONCLUSIONS.

(1). An axisymmetric, fully turbulent vortex of Reynolds number $\Gamma_\infty/\nu = 5.7 \times 10^5$ was generated at the exit of the McGill circular blower tunnel. The velocity and turbulence compononts of the Reynolds stress tensor were measured at three downstream stations $z/c = 45,78,109$, for five cases of axial momentum; two jets, two wakes and a case with zero axial momentum increment. The results contain less scatter than those of Poppleton (1970) thus giving a better indication of the velocity and stress distribution throughout the vortex; the two most noteable results being that a circulation greater than the far field value occurred in case (a), and in case (d) the viscous stresses are only one order of magnitude lower than the turbulent stresses at the second and third stations.

(2). Increasing the momentum increment or decrement $|J|$ causes a marked increase in the shear stress and turbulence levels within the vortex and thus a more rapid diffusion of vorticity. This causes a marked increase in radial velocity v_r (related to $\partial v_z/\partial z$, which in turn is related to the turbulence level present). If $v_r \sim O(\frac{\nu}{r})$ the term $\eta = v_r[\frac{\partial v}{\partial r}\theta + \frac{v}{r}\theta]$ in the tangential momentum equation is of $\sim O(\beta)$,

where β is the viscous term. When the turbulence level is increased $v_r >> O(\frac{\nu}{r})$ thus making β negligihle and the decay of v_θ independent of Reynolds number. The Reynolds stress term γ also increases and is the same order as η.

(3). As the turbulence level decays the value of v_r decreases and far downstream v_r becomes less than $O(\frac{\nu}{r})$. The decay of v_θ is then controlled by the combination $\beta - \gamma$, where β is always negative and γ can be either positive or negative or both with r, (all occurred in the measurements but the negative γ was confined to $r < r_1$). As $|\beta| \sim O(|\gamma|)$ at $Re \sim O(10^4)$ and $\beta = f(Re)$, it is seen that the decay of vortic-es for Reynolds numbers less than about 10^5 are Reynolds number dependent. Hence it is plausible that turbulent vortic es generated in the laboratory will decay more rapidly than full scale ones with higher Reynolds numbers.

(4). By using the second order closure theory of Launder ,Reece and Rodi (1973), the Reynolds stress equations were modelled, and these plus the momentum equations and relevant boundary conditions were cast to simulate the motion of a steady, fully rolled up,axisymmetric, turbulent vortex. Using the upstream experimental results as initial conditions

the above equations were solved numerically to predict the experimental results at the remaining two downstream stations. Over the experimental range the assumption of local isotropy used in the closure model is well satisfied for the high jet (a) and deep wake (e) cases but only just satisfied for the remaining cases at Re $\sim O(10^4)$.

(5). The turbulence model predicts a slower axial rate of decay for the axial component of mean velocity than that measured; this discrepancy is evident for jets in streaming flow both with and without a superimposed vortex. The growth and magnitude of the tangential velocity profiles are predicted well, especially in the most extreme cases (a) and (e) with large $|J|$. The turbulence predictions tended to be low in the core region but agreed well outside it for all cases except (a) where they remained low. The shear stresses in cases (a) and (e) were also slightly low. In the remaining cases (b), (c) and (d) the measured shear stresses are an order of magnitude lower than for cases (a) and (e) and the shear stress predictions for cases (b), (c) and (d) do not compare well with their respective experimental results.

(6). The numerical calculations were carried far downstream (to $U_\infty z/\Gamma_\infty \simeq 2000$) but it is doubtful whether the predictions for cases (b) and (d) at Re $\sim O(10^4)$ are valid because the flow is no longer locally isotropic. The turbulence Reynolds number increases slowly with z and relative to r_1 so does the turbulence microscale.

the above equations were solved numerically to predict the experimental results at the remaining two downstream stations. Over the experimental range the assumption of local isotropy used in the closure model is well satisfied for the high jet (a) and deep wake (e) cases but only just satisfied for the remaining cases at Re $\sim O(10^4)$.

(5). The turbulence model predicts a slower axial rate of decay for the axial component of mean velocity than that measured; this discrepancy is evident for jets in streaming flow both with and without a superimposed vortex. The growth and magnitude of the tangential velocity profiles are predicted well, especially in the most extreme cases (a) and (e) with large $|J|$. The turbulence predictions tended to be low in the core region but agreed well outside it for all cases except (a) where they remained low. The shear stresses in cases (a) and (e) were also slightly low. In the remaining cases (b), (c) and (d) the measured shear stresses are an order of magnitude lower than for cases (a) and (e) and the shear stress predictions for cases (b), (c) and (d) do not compare well with their respective experimental results.

(6). The numerical calculations were carried far downstream (to $U_\infty z/\Gamma_\infty \simeq 2000$) but it is doubtful whether the predictions for cases (b) and (d) at Re $\sim O(10^4)$ are valid because the flow is no longer locally isotropic. The turbulence Reynolds number increases slowly with z and relative to r_1 so does the turbulence microscale.

(7). The conditions required for overcirculation of the form predicted by Govindaraju and Saffman (1971) were satisfied at about $U_\infty z/\Gamma_\infty \simeq 500$, giving values of their constant $A = 8.45 \times 10^{-3}$, 1.02×10^{-2} and 1.46×10^{-2} respectively for cases (e), (d) and (b). Overcirculation of this kind was not encountered for case (a).

(8). The numerical results are used to show that the rotational velocities in the trailing vortic es two and one half kilometers downstream ($U_\infty z/\Gamma_\infty \simeq 200$) of a Jumbo 747 in the take-off mode, are reduced by only 5%, if 10% of the total engine thrust is used to modify them. It is deduced therefore, that this is <u>not</u> a practical way of causing trailing vortic es from large aircraft to decay more rapidly.

REFERENCES.

Batchelor G.K. (1964) — Axial Flow in Trailing Line Vortices. J.Fluid Mech. Vol.20. pp645-658

Betz A. (1932) — Verhalten von Wirbelsystem Z. angew. Math Mech. 12, 164

Bradshaw P. (1967) — Conditions for the existence of an Inertial Subrange in a Turbulent Flow. N.P.L. Aero Rpt. 1220. A.R.C. 28 664, F.M. 3798.

Champagne F.H. and Sleicher C.A. (1967). — Turbulence Measurements with Inclined Hot Wires. Part II J.Fluid Mech. Vol.28, pp177-182

Chou P.Y. (1945) — On Velocity Correlations and the solution of the equations of Turbulent Fluctuations. Quart. Appl. Math. Vol.3 p39.

Clements R.R. and Maul D.J. (1973) — The Rolling up of a Trailing Vortex Sheet. J. of A. January 1973

Crow S.C. (1970) — Stability Theory for a pair of Trailing Vorticies. A.I.A.A. J. Vol. 8, No. 12.

Govindaraju S.P. and Saffman P.G. (1971) — Flow in a turbulent trailing vortex. Physics of Fluids. Vol.14, p2074.

Graham J.A.H., Newman B.G. and Phillips W.R. (1974)
Turbulent Trailing Vortex with Central Jet or Wake.
I.C.A.S. Conf. August 1974.

Graham J.A.H. and Phillips W.R. (1974)
Measurements in a Turbulent Vortex.
Mech. Eng. Rpt. McGill Uni.
(to be published)

Hall M.G. (1972)
Vortex Breakdown.
Ann. Rev. of Fluid Mech.
Vol. 4, pp195-217.

Hanjalić K. and Launder B.E. (1972)
A Reynolds Stress Model of Turbulence and its application to thin shear flows.
J.of Fluid Mech. Vol. 52,pp609-638

Hilton W.F. (1938)
Longitudinal flow in a Trailing Vortex.
R.& M. 1858.

Hoffman E.R. and Joubert P.N. (1963)
Turbulent Line Vortices
J.of Fluid Mech. Vol.16,p3.

Irwin H.A.P.H. (1974)
Private Communication.

Kaden H. (1931)
Aufwickling einer unstabilen unstetigkeitsflache.
Ing. Arch. Vol.2 p140.

Kantha H.L, Lewellen W.S. and Durgin F.H. (1972)
Response of a Trailing Vortex to Axial Injection into the Core.
J.of A. Vol. 9 , No. 3.

Kirde K. (1962)
Untersuchengen uber die zeitliche Weiterentwicklung eines Wirbels mit Vorgegebener Anfangsverteilung. Ing. Arch. Vol. 31. p 385.

Lamb H. (1932)
Hydrodynamics. Cambridge Uni. Press.

Laufer J. (1953)
The Structure of Turbulence in Fully Developed Pipe Flow. N.A.C.A. T.N. 2954.

Launder B.E., Reece G. and Rodi W. (1974)
Developement and Application of a Reynolds Stress Turbulence Closure. Imp. Coll. Mech. Eng. Rpt. HTS/73/31

Mason W.H. and Marchman J.F. (1972)
Farfield Structure of an Aircraft Trailing Vortex, Including Effects of Mass Injection. N.A.S.A. C.R. 62078.

McCormick B.W. ,Tangler J.L. and Sherrieb H.E. (1968)
Structure of Trailing Vortices. J. of A. Vol.5, No. 3

Moore D.W. (1971)
The Discrete Vortex approximation of a finite vortex sheet. Cal. Tech. Rpt. AFOSR-TR-72-0034.

Moore D.W. (1974)
A Numerical study of the rollup of a finite Vortex Sheet. J.of Fluid Mech. Vol.63,pt.2

Moore D.W. and Saffman P.G. (1972) — The Motion of a Vortex Filament with axial flow. Phil. Trans. Vol.272.,No.1226. pp403-429.

Moore D.W. and Saffman P.G. (1973) — Axial Flow in Laminar Trailing Vortices. Proc. R. Soc. Lond. A333,pp491-508

Newman B.G. (1959) — Flow in a Viscous Trailing Vortex. Aero. Quat. May 1959,pp149-162.

Oseen C.W. (1911) — Ark. f. Math Astron. och. Fys.7.

Owen P.R. (1970) — The decay of a Turbulent Trailing Vortex. Aero. Quat. Feburary 1970.

Poppleton E.D. (1970) — A Preliminary Experimental Investigation of the Structure of a Turbulent Trailing Vortex. Mech. Eng. Rpt. 71-1. McGill Uni.

Randel J.D. and Leibovich S. (1973) — The Critical State : a trapped wave model of vortex breakdown. J.of Fluid Mech. Vol.58.pp495-515.

Rotta J.C. (1951) — Statistijche Theorie nichthomogener Turbulenz Zeitsch f. Physic Vol. 129 p547.

Saffman P.G. (1973) — Structure of Turbulent line Vortices Physics of Fluids. Vol.16,pp1181-1188.

Saffman P.G. (1974)
The Structure and Decay of Trailing Vortices.
Appld. Math. Dept. Cal. Tech. (unpublished).

Sarpkaya T. (1971)
On Stationary and Travelling Vortex Breakdown.
J. of Fluid Mech. Vol.45.pp545-559.

Snedeker R.S. (1972)
A Comparison of the trailing vortex measurements of Poppleton with Invariant modelling computations
A.R.A.P. T.M. 72-5.

Spalding D.B. and Pa tankar S.J. (1967)
Heat and Mass Transfer in Boundary Layers.
Morgan-Grampian Press.

Squire H.B. (1954)
The Growth of a Vortex in Turbulent Flow.
Aero Quat. August 1965 pp302-306 (reprinted)

Takami H. (1964)
A numerical experiment with discrete vortex approximation with reference to the rolling up of a vortex sheet.
Stanford Rpt. SUDAER 202.

Townsend A.A. (1956)
The Structure of Turbulent Shear Flow.
Cambridge Uni. Press.

Verstynen H.A and Dunham R. (1973)
A Flight investigation of the Trailing Vortices generated by a Jumbo Jet Transport.
N.A.S.A. TN.D 7172.

Vogel W.M. (1968)

General Description and Calibration of the McGill 30 inch diameter Blower Tunnel.
Mech. Eng. TN. 68-1 McGill Uni.

Vroomen L. and Graham J.A.H. (1973)

Private Communication.

Westwater F.L. (1935)

The rolling up of the surface of discontinuity behind an aerofoil of finite span.
A.R.C. R.&.M. No. 1692.

Arnot Smith P. (1973)

A Two Dimensional Jet with Small Curvature.
PhD. Thesis. McGill Uni.

Guitton D.E. (1968)

Correction of Hot wire data for High Intensity Turbulence, Longitudinal Cooling and Probe Interference.
Rpt. 68-6 . Mech. Dept. McGill Uni.

Tennekes H. and Lumley (1972)

A First Course in Turbulence.
M.I.T. Press.

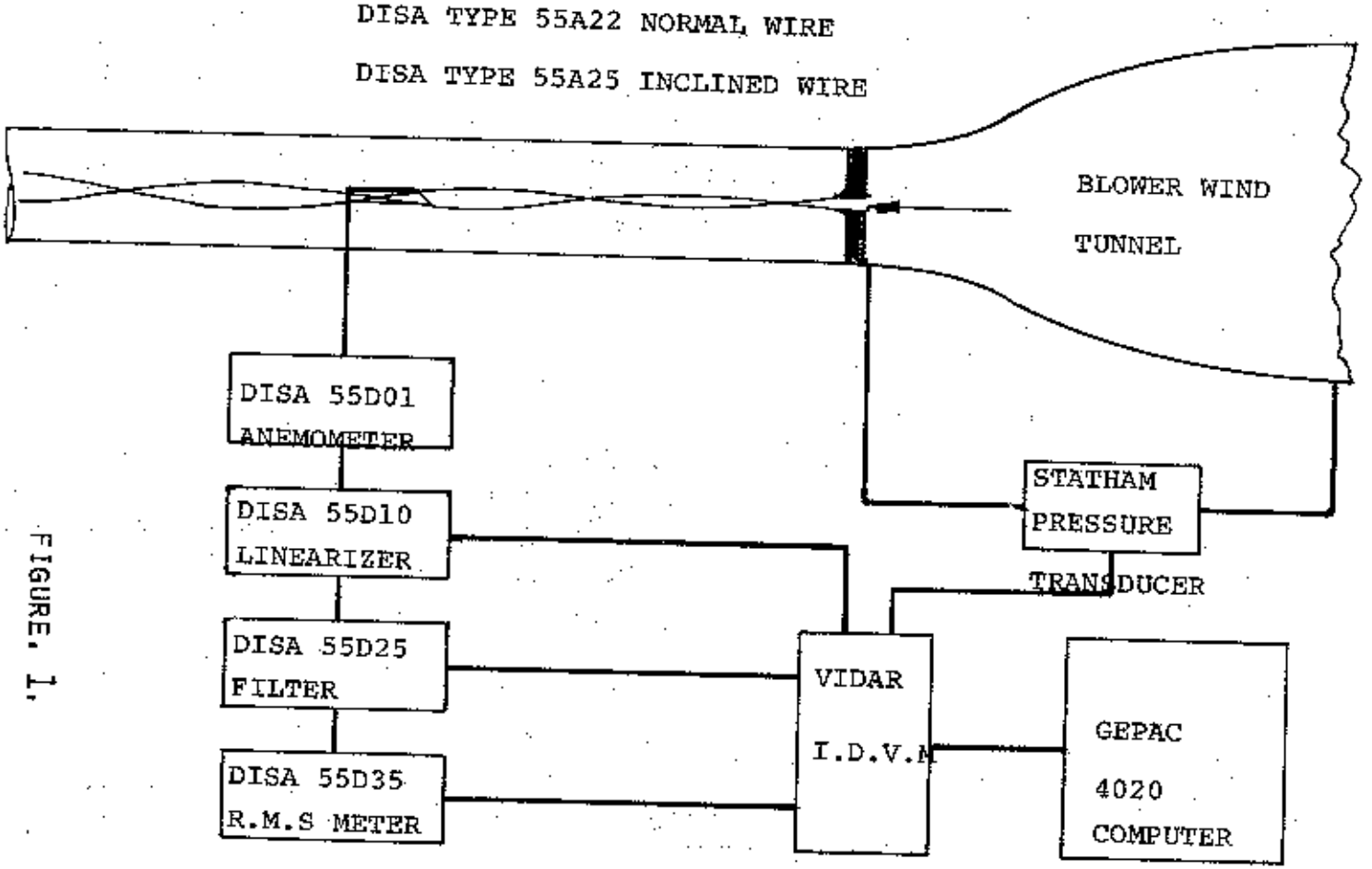

FIGURE. 1. EXPERIMENTAL LAYOUT.

FIGURE. 2.

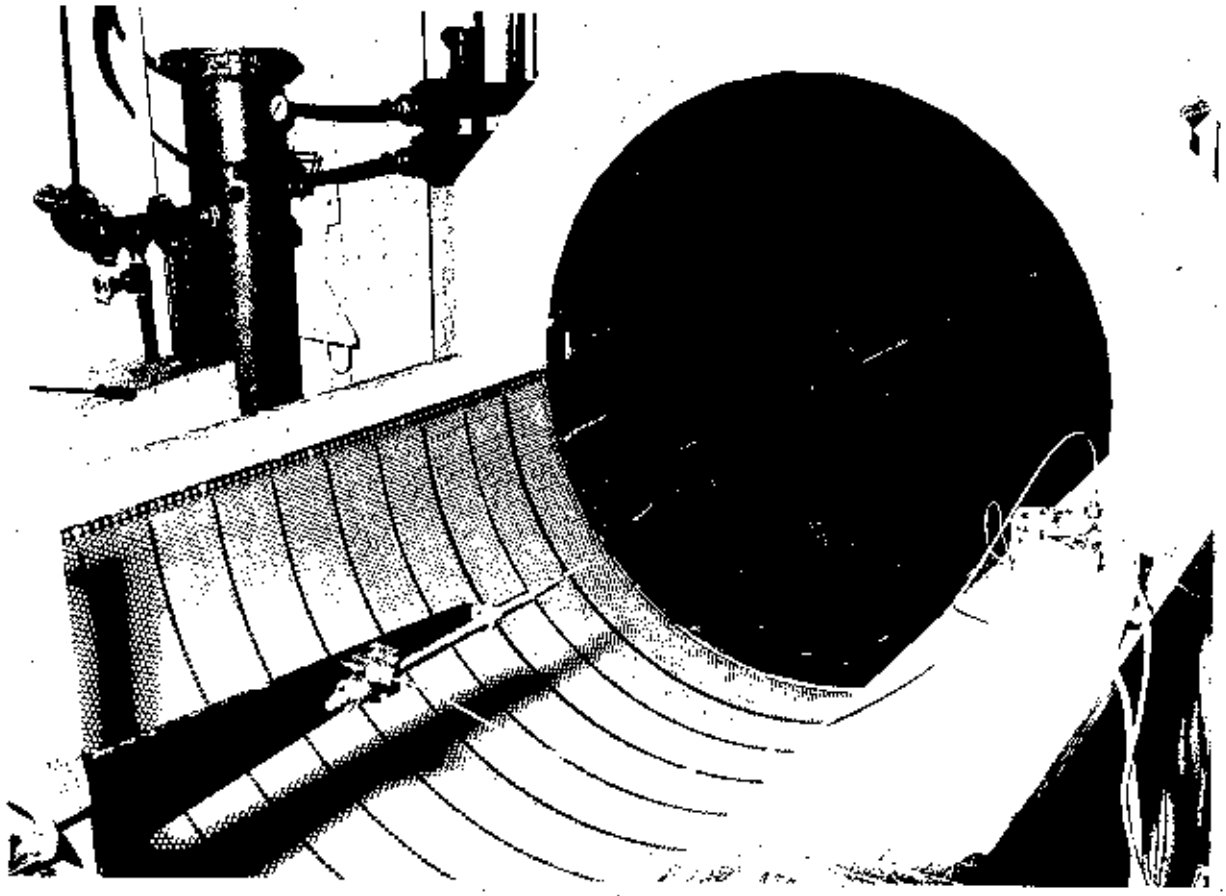

THE VORTEX GENERATOR AND APPARATUS.

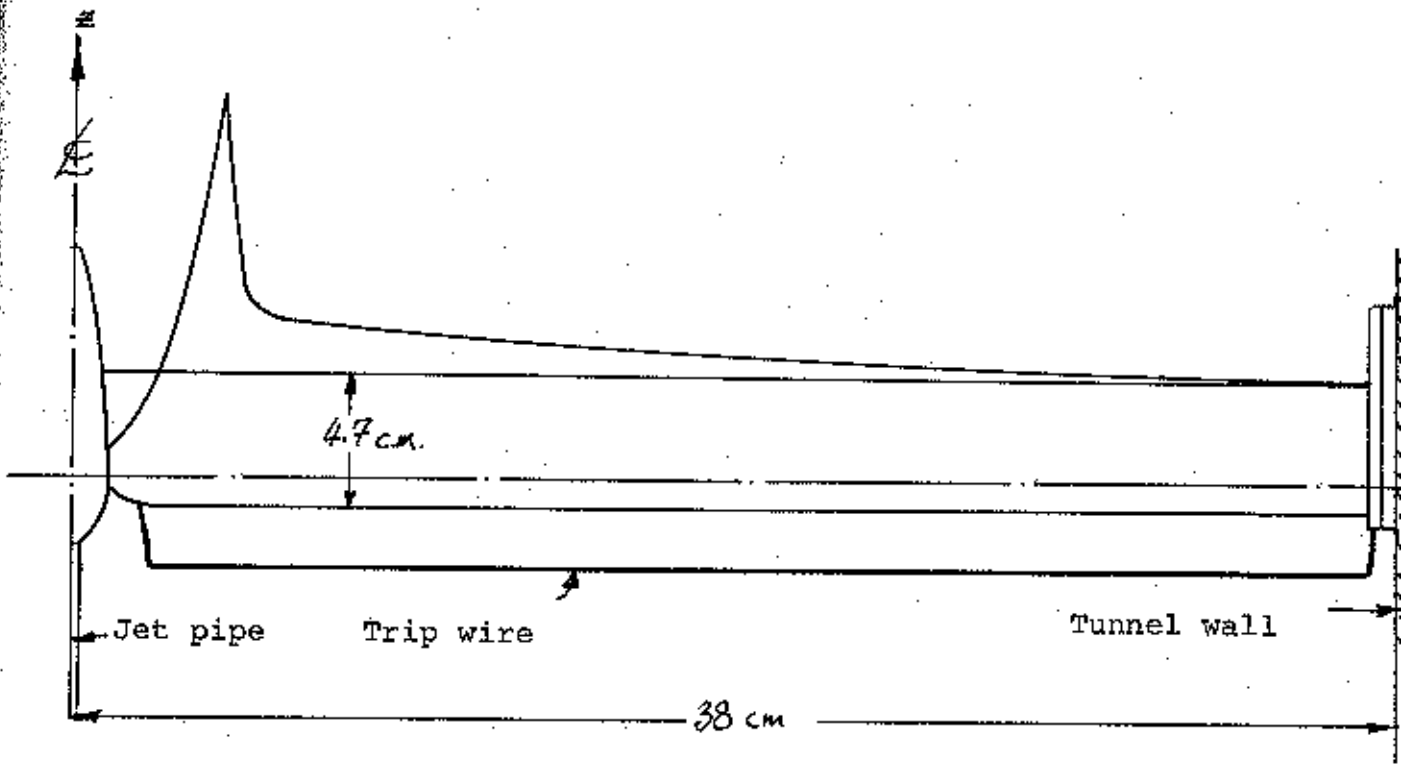

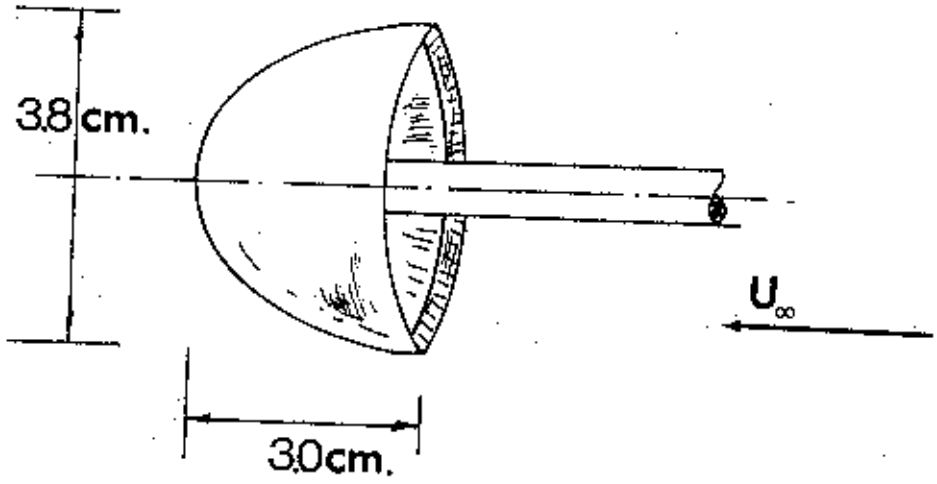

THE BLUFF BODY. FIGURE. 2A

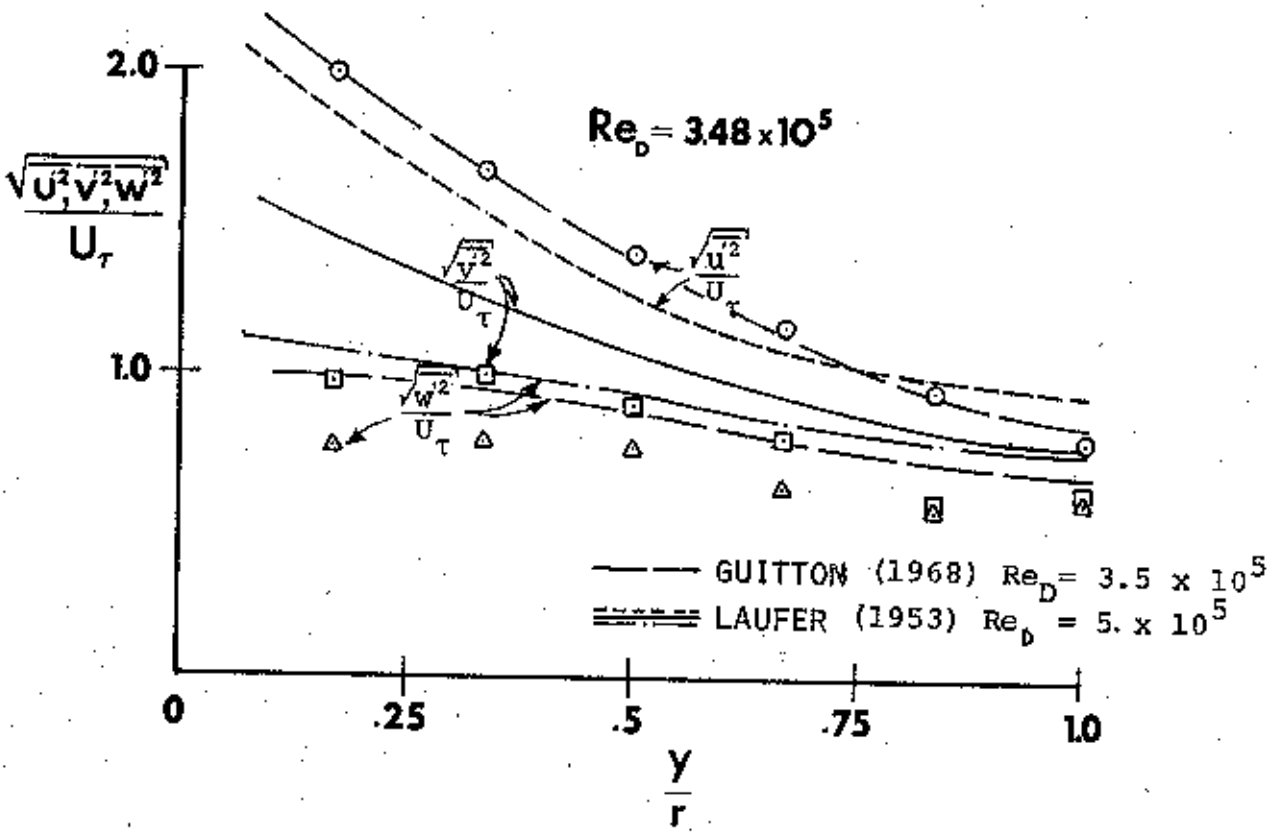

FIGURE. 3.

TURBULENCE LEVELS IN FULLY DEVELOPED PIPE FLOW.

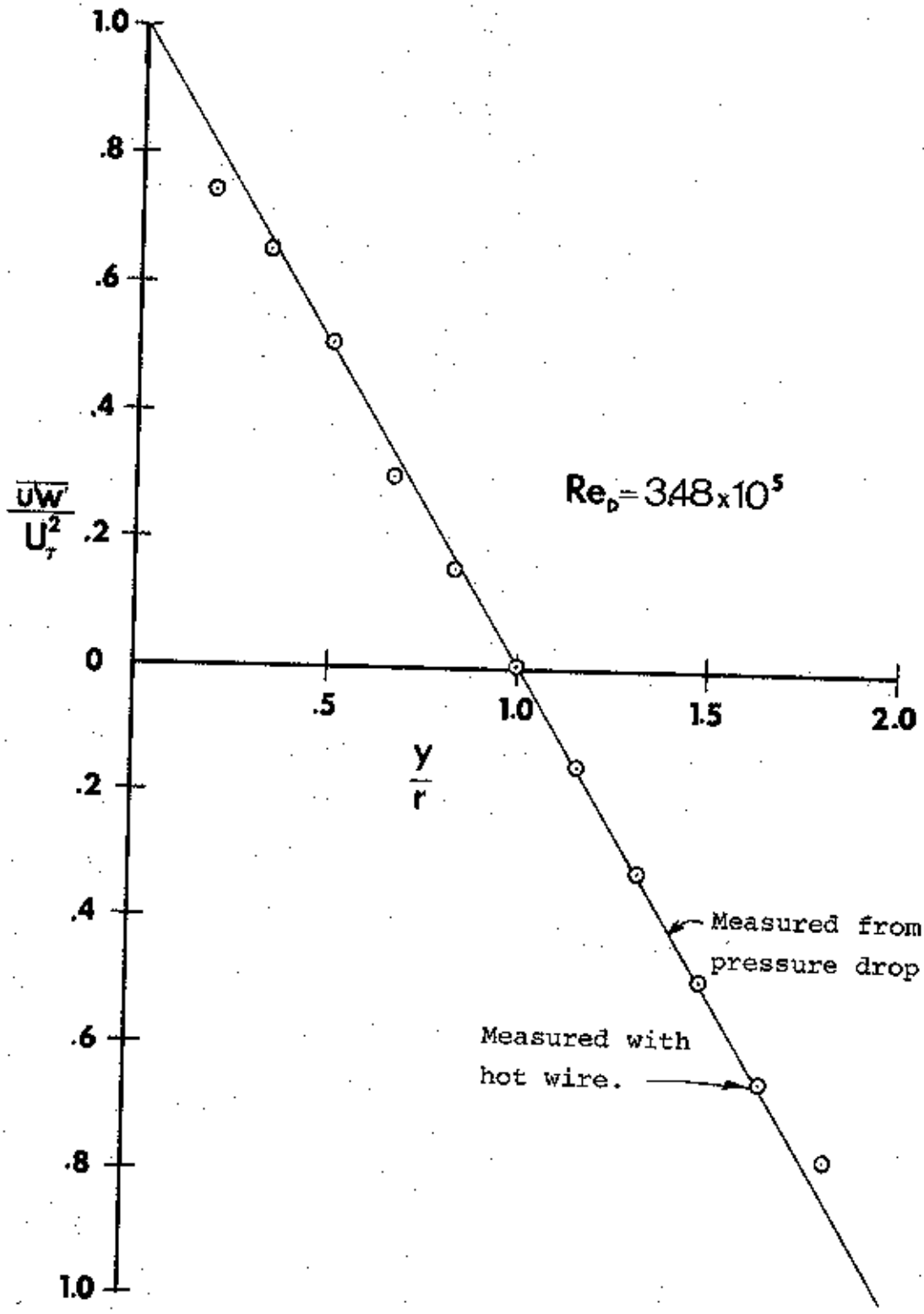

SHEAR STRESS IN TURBULENT PIPE FLOW.

FIGURE. 4.

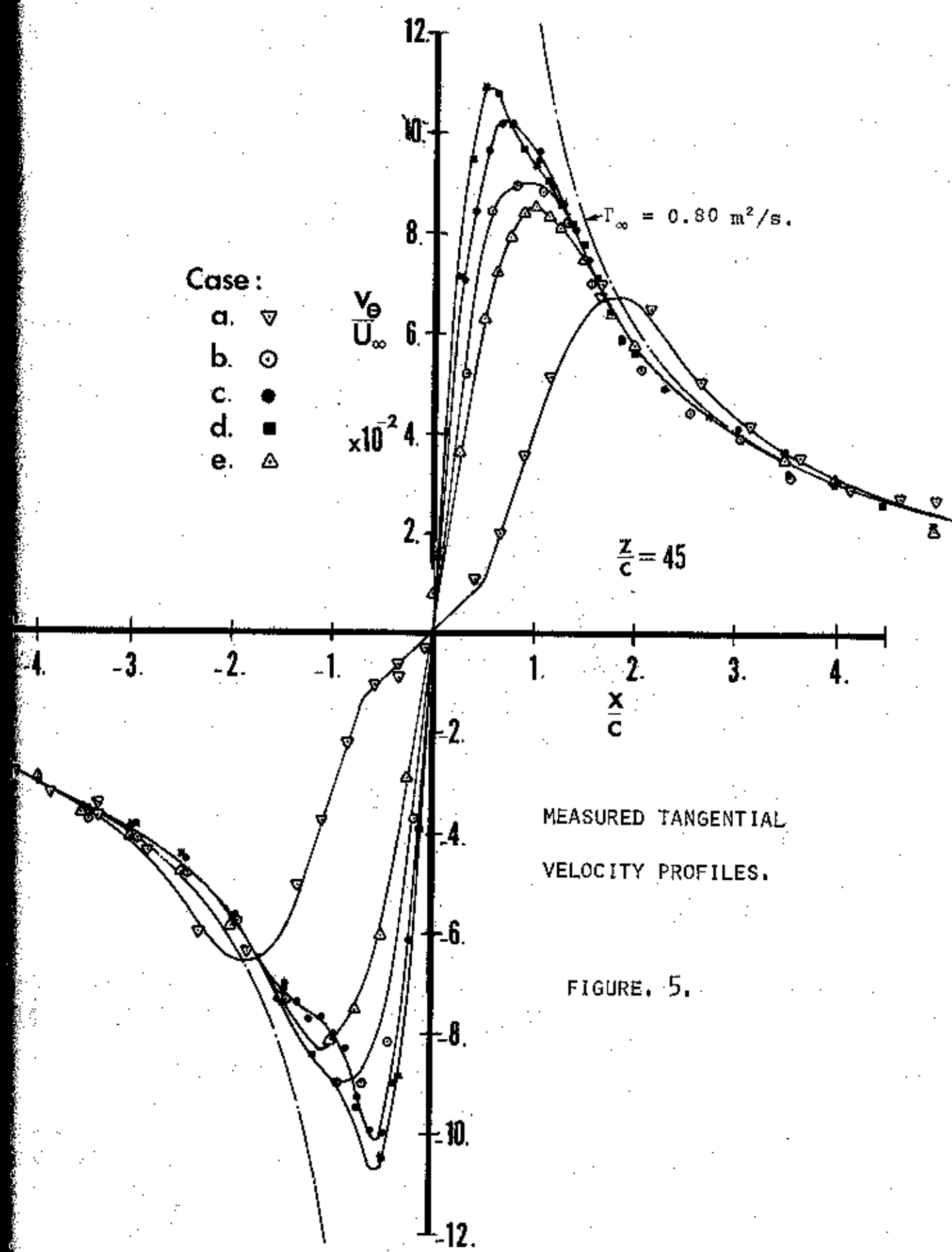

MEASURED TANGENTIAL VELOCITY PROFILES.

FIGURE. 5.

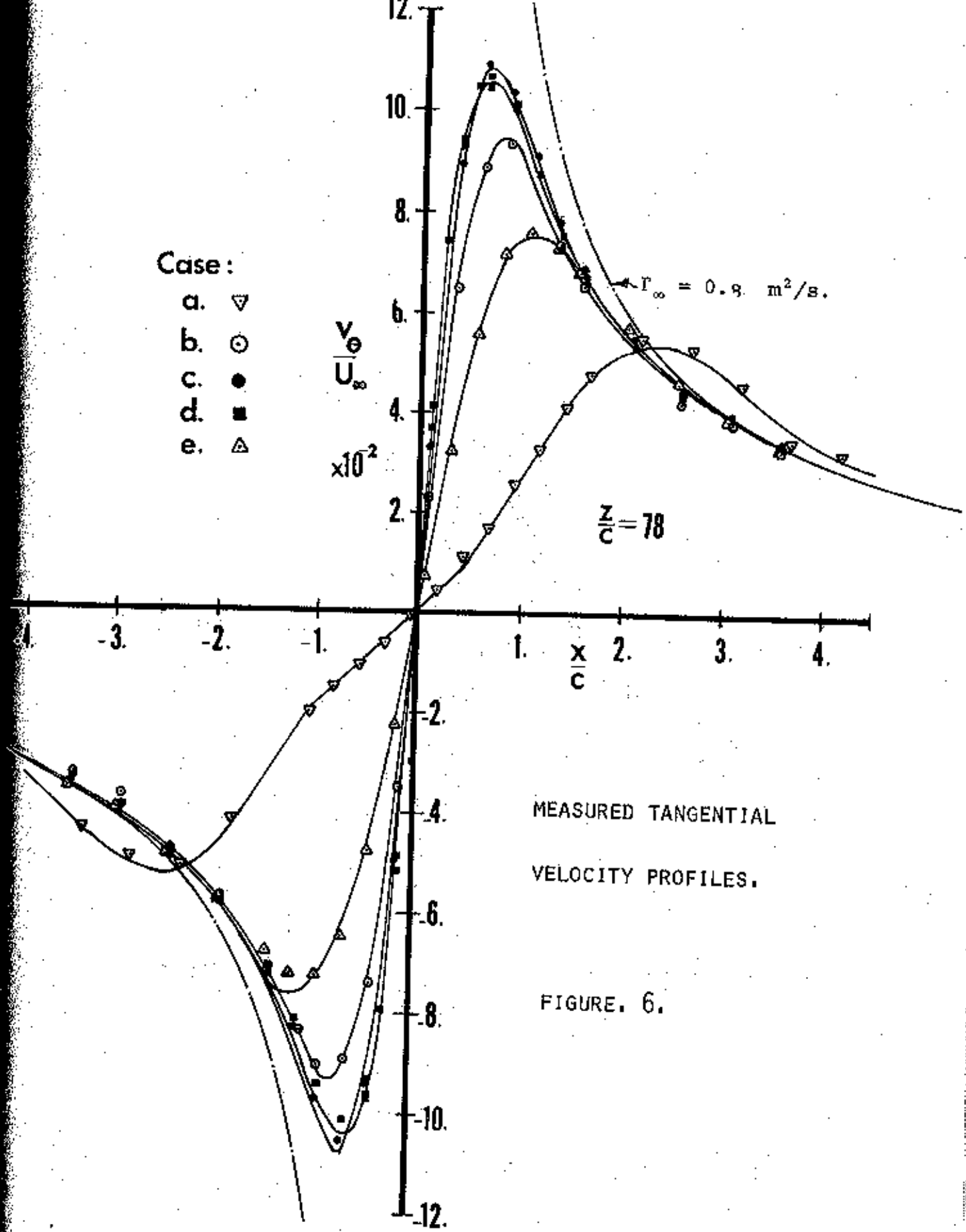

MEASURED TANGENTIAL VELOCITY PROFILES.

FIGURE. 6.

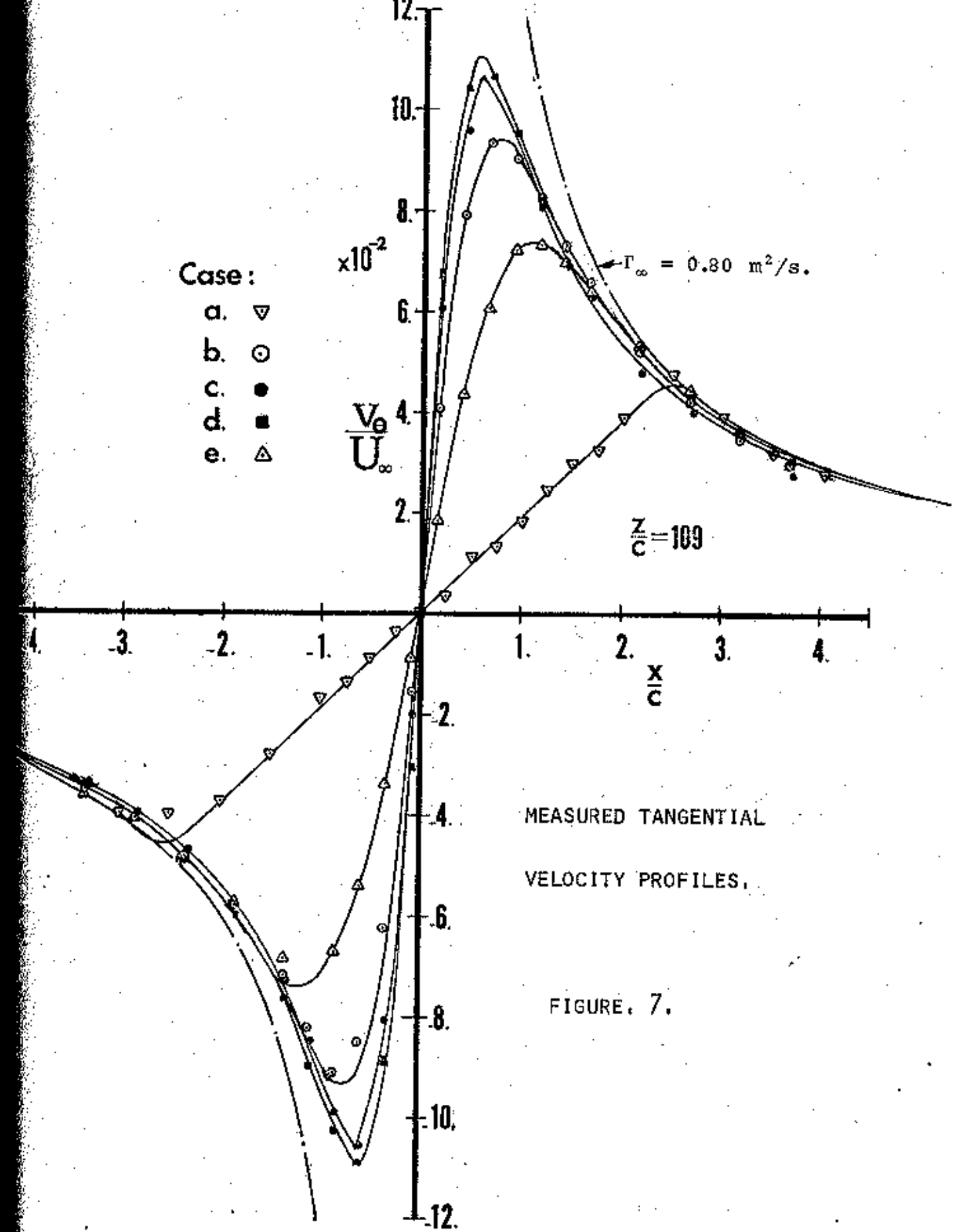

MEASURED TANGENTIAL VELOCITY PROFILES.

FIGURE. 7.

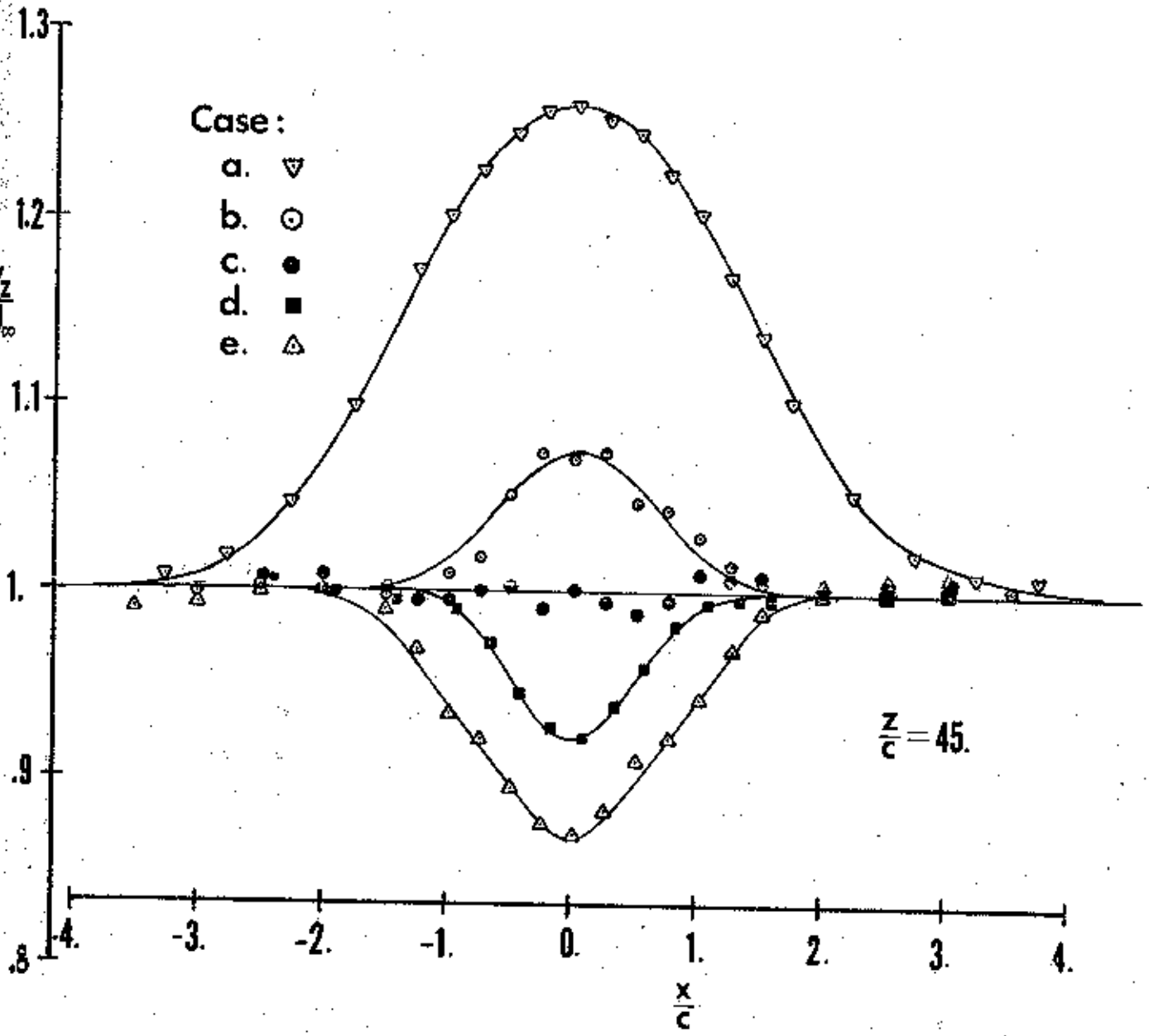

MEASURED AXIAL VELOCITY PROFILES.

FIGURE, 8.

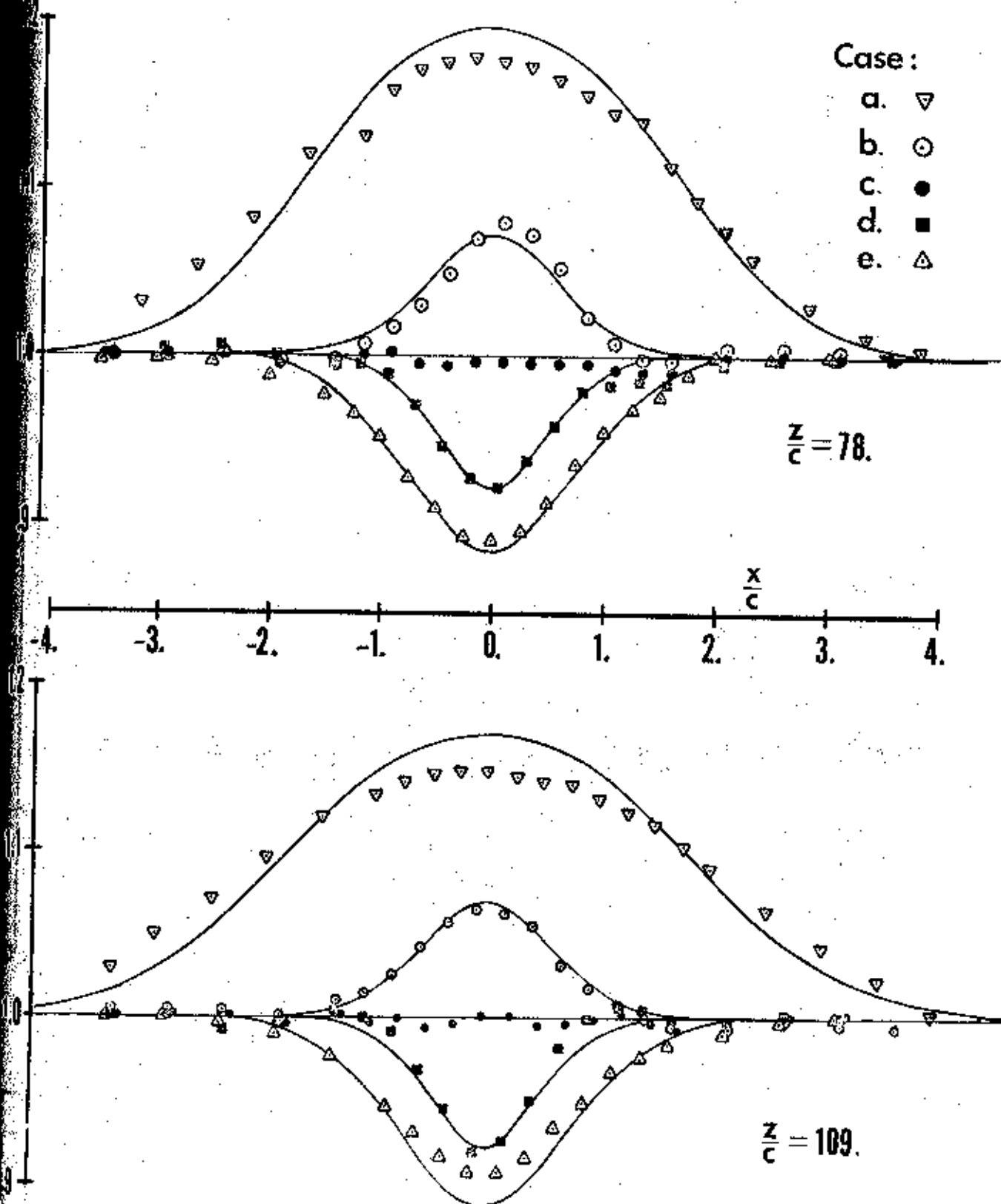

PREDICTED AND MEASURED AXIAL VELOCITY PROFILES.

FIGURE. 9.

LATION DISTRIBUTION IN A TURBULENT VORTEX.

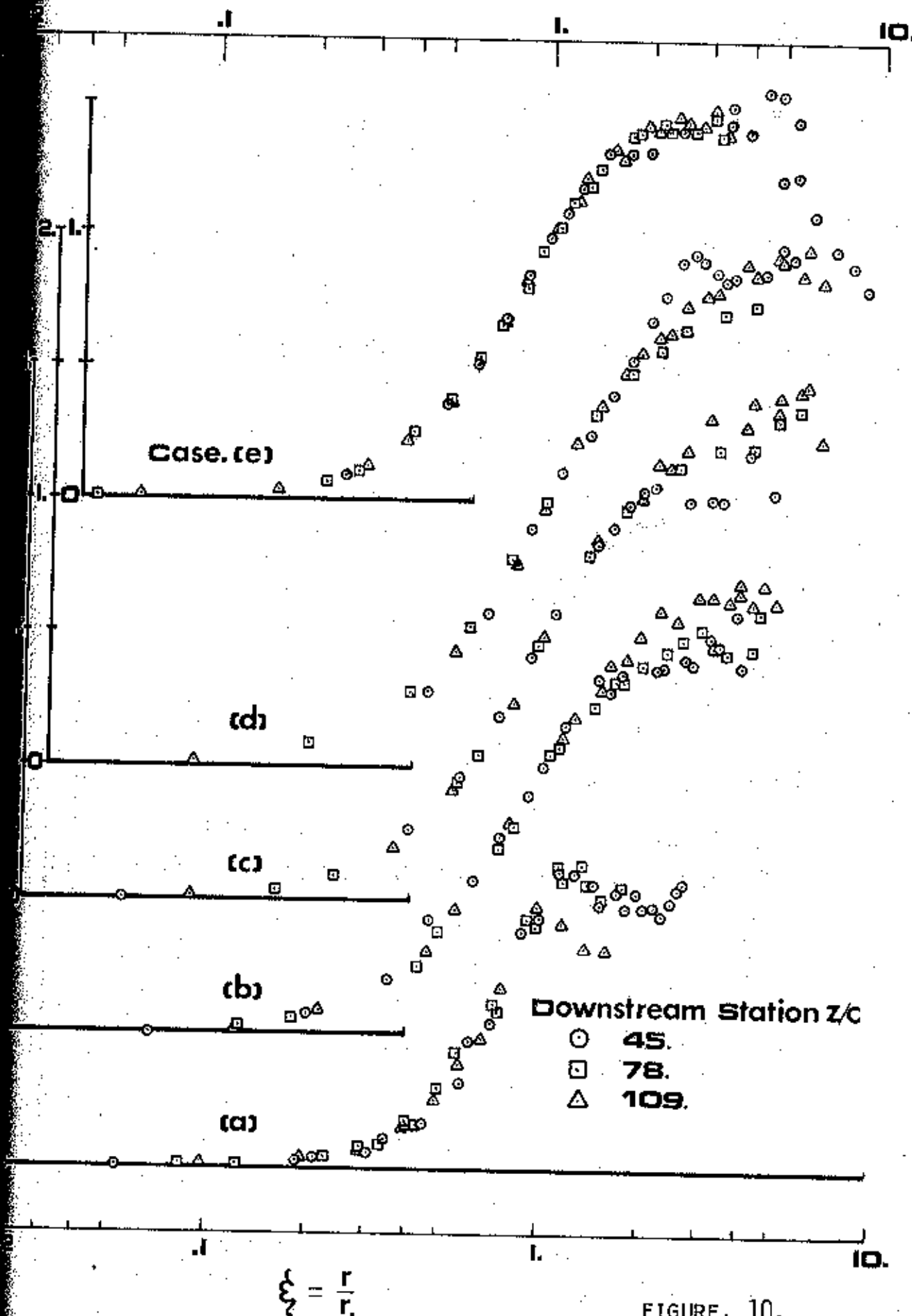

FIGURE. 10.

PREDICTED AND MEASURED CIRCUMFERENTIAL VELOCITY PROFILES.

CASE (e) DEEP WAKE.

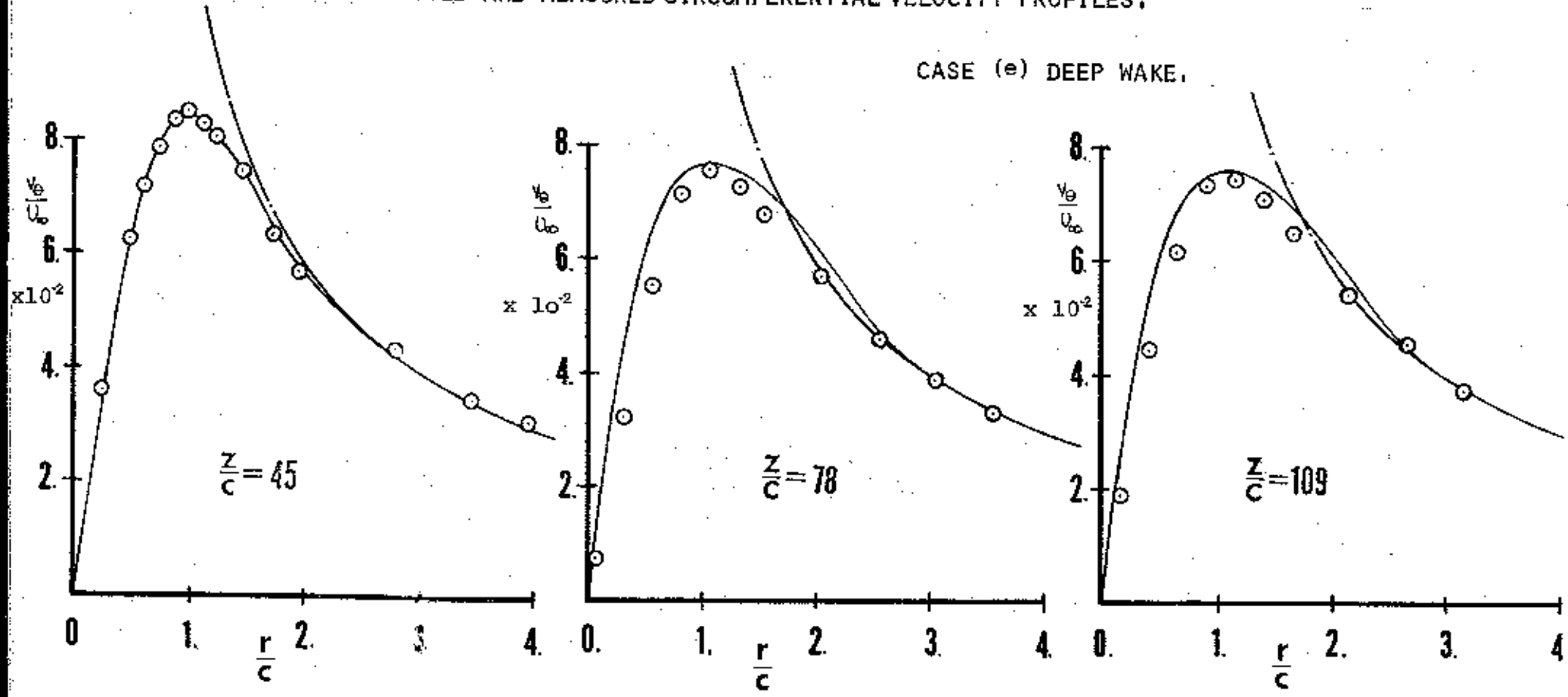

FIGURE. 11.

MEASURED AND PREDICTED CIRCUMFERENTIAL VELOCITY PROFILES.

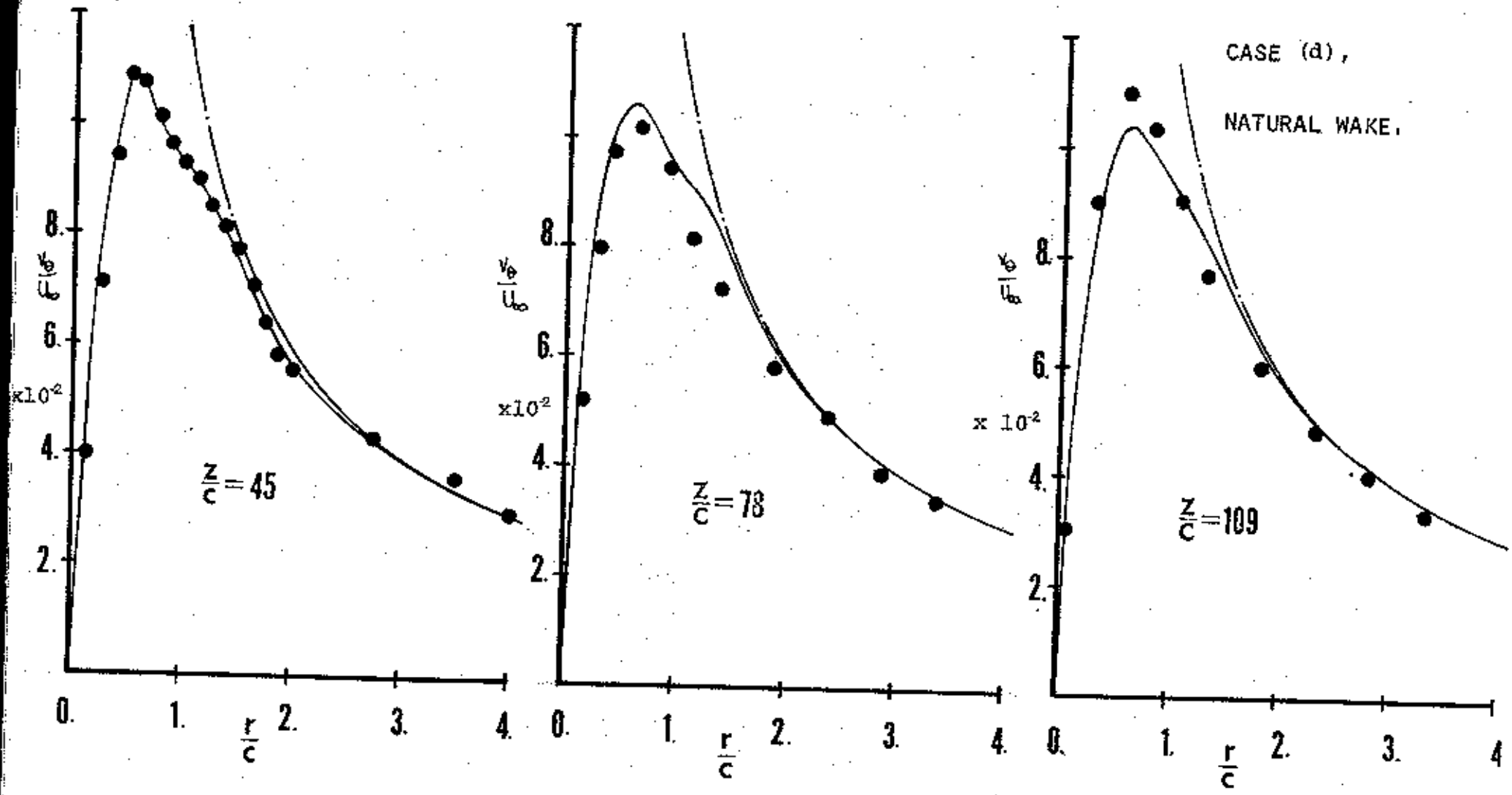

FIGURE. 12.

PREDICTED AND MEASURED CIRCUMFERENTIAL VELOCITY PROFILES,

CASE (b) LOW JET.

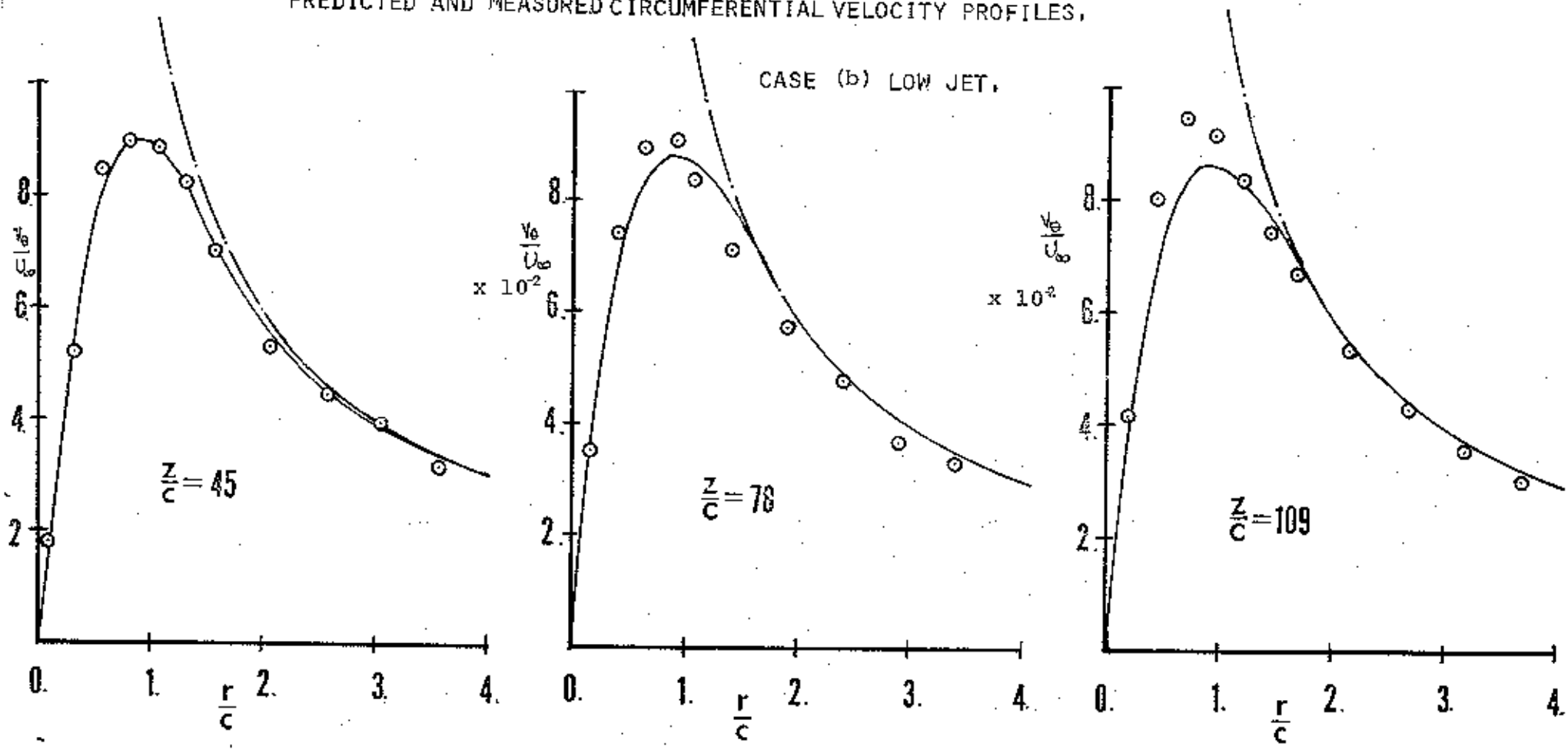

FIGURE. 13.

PREDICTED AND MEASURED CIRCUMFERENTIAL VELOCITY PROFILES.

CASE (a) HIGH JET.

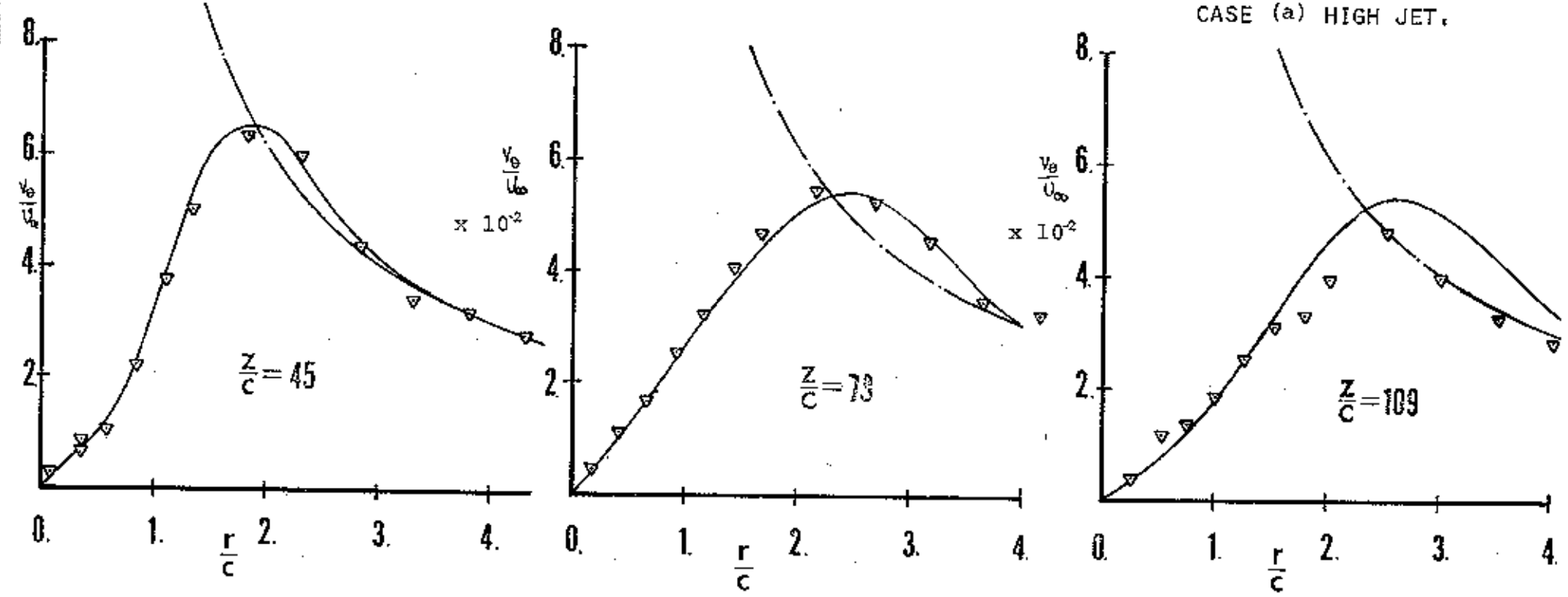

FIGURE. 14.

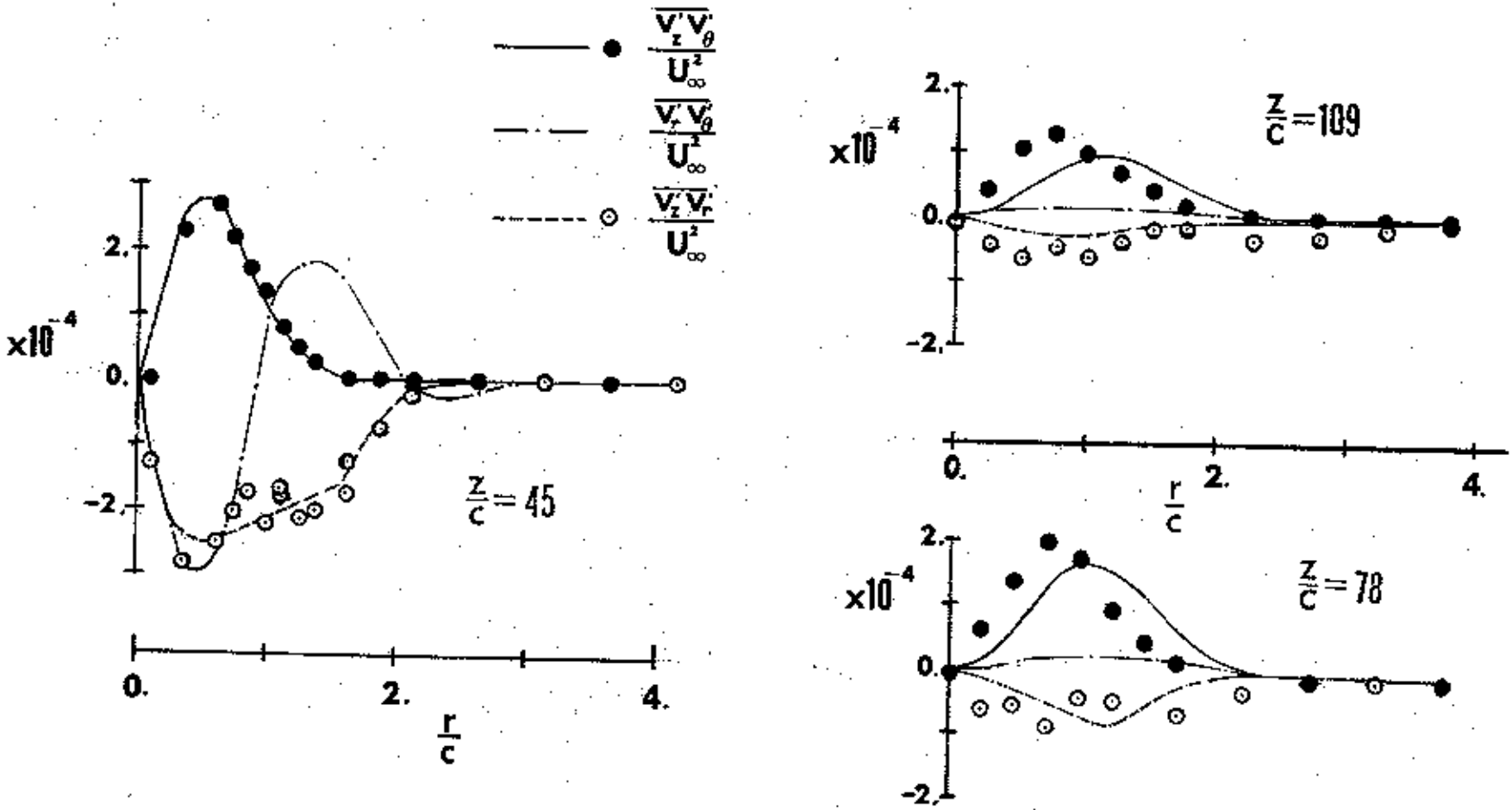

PREDICTED AND MEASURED SHEAR STRESSES, CASE (e). FIGURE. 15.

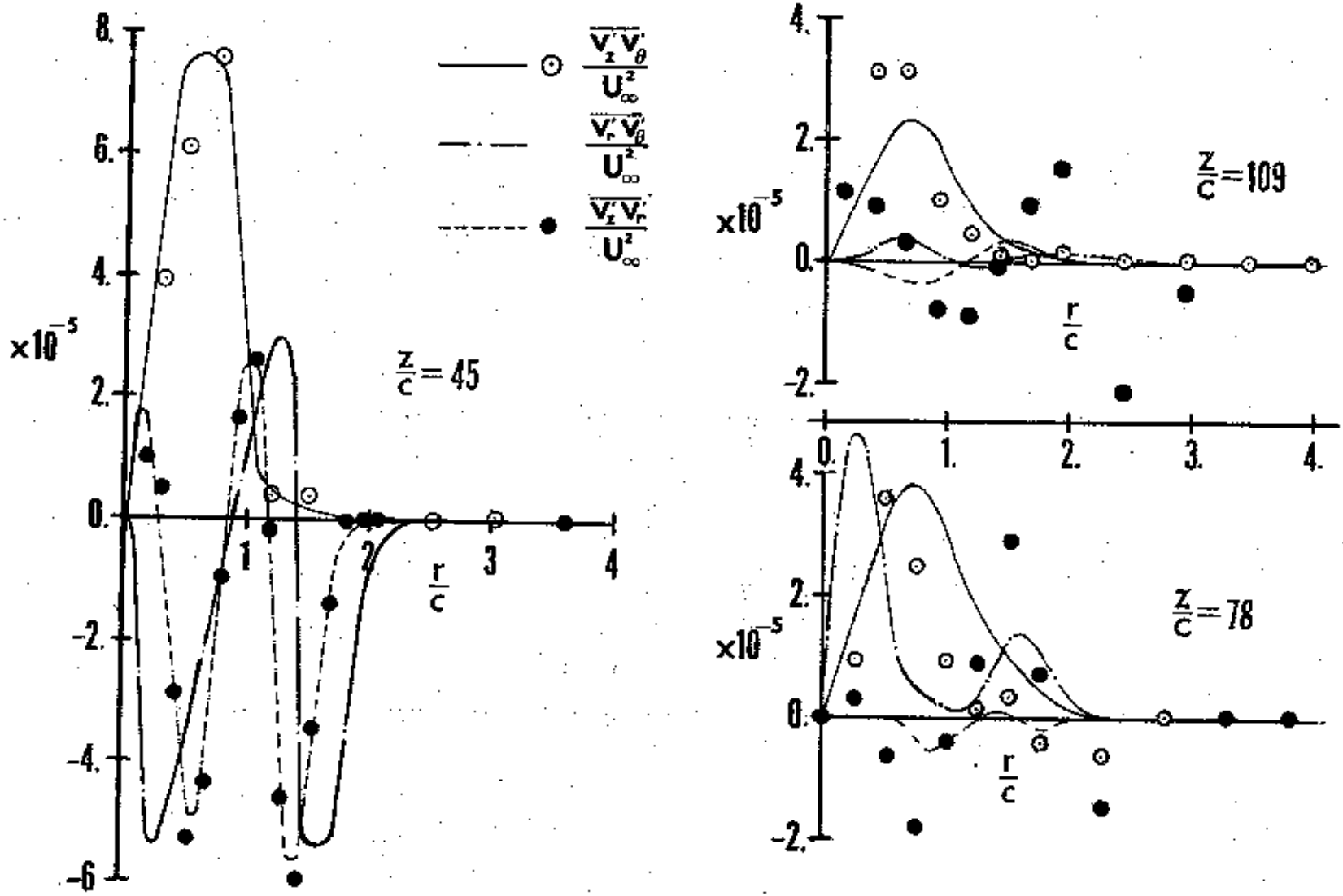

PREDICTED AND MEASURED SHEAR STRESSES, CASE (d) FIGURE, 16.

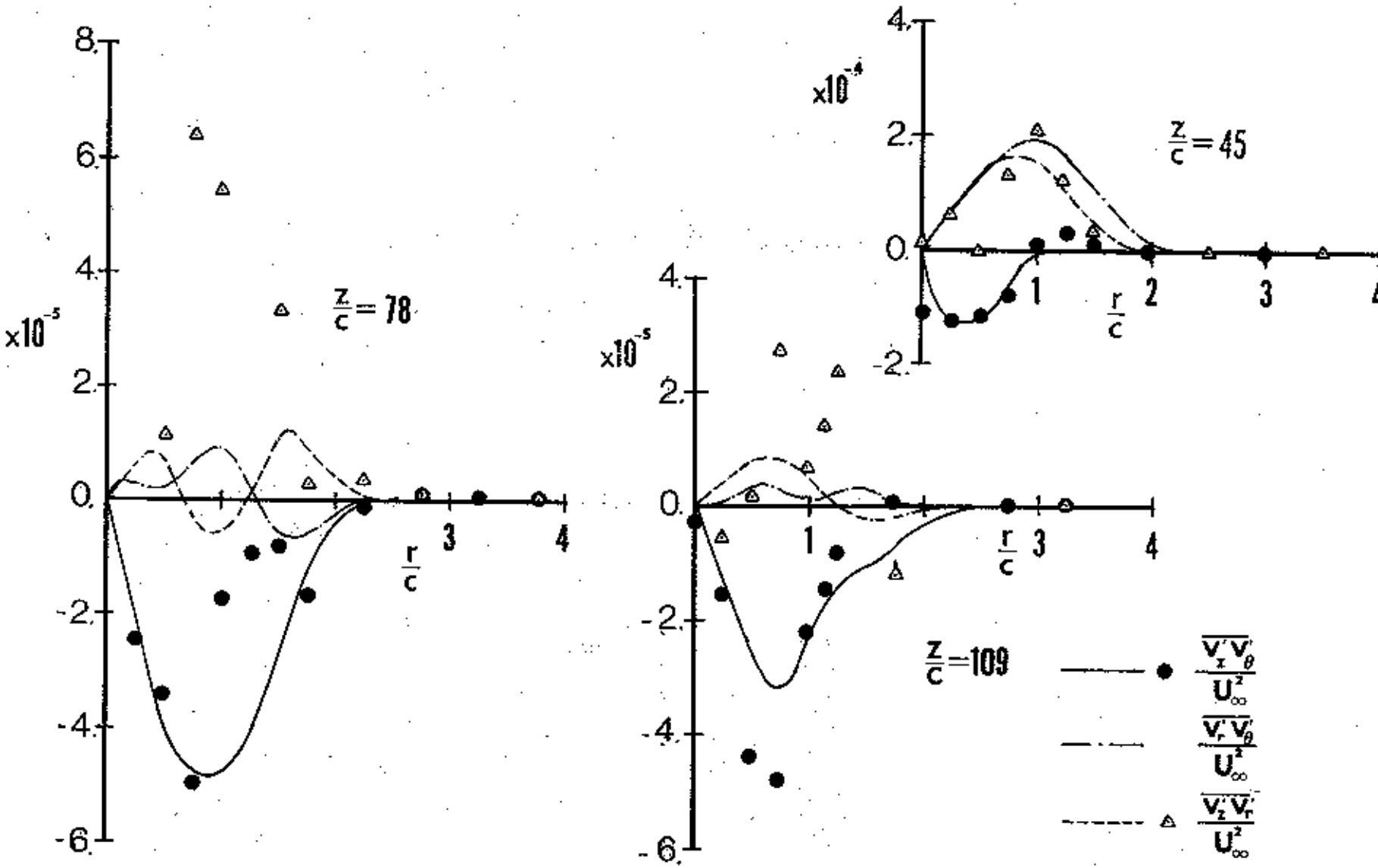

PREDICTED AND MEASURED SHEAR STRESSES. CASE (b) FIGURE. 17.

PREDICTED AND MEASURED SHEAR STRESSES

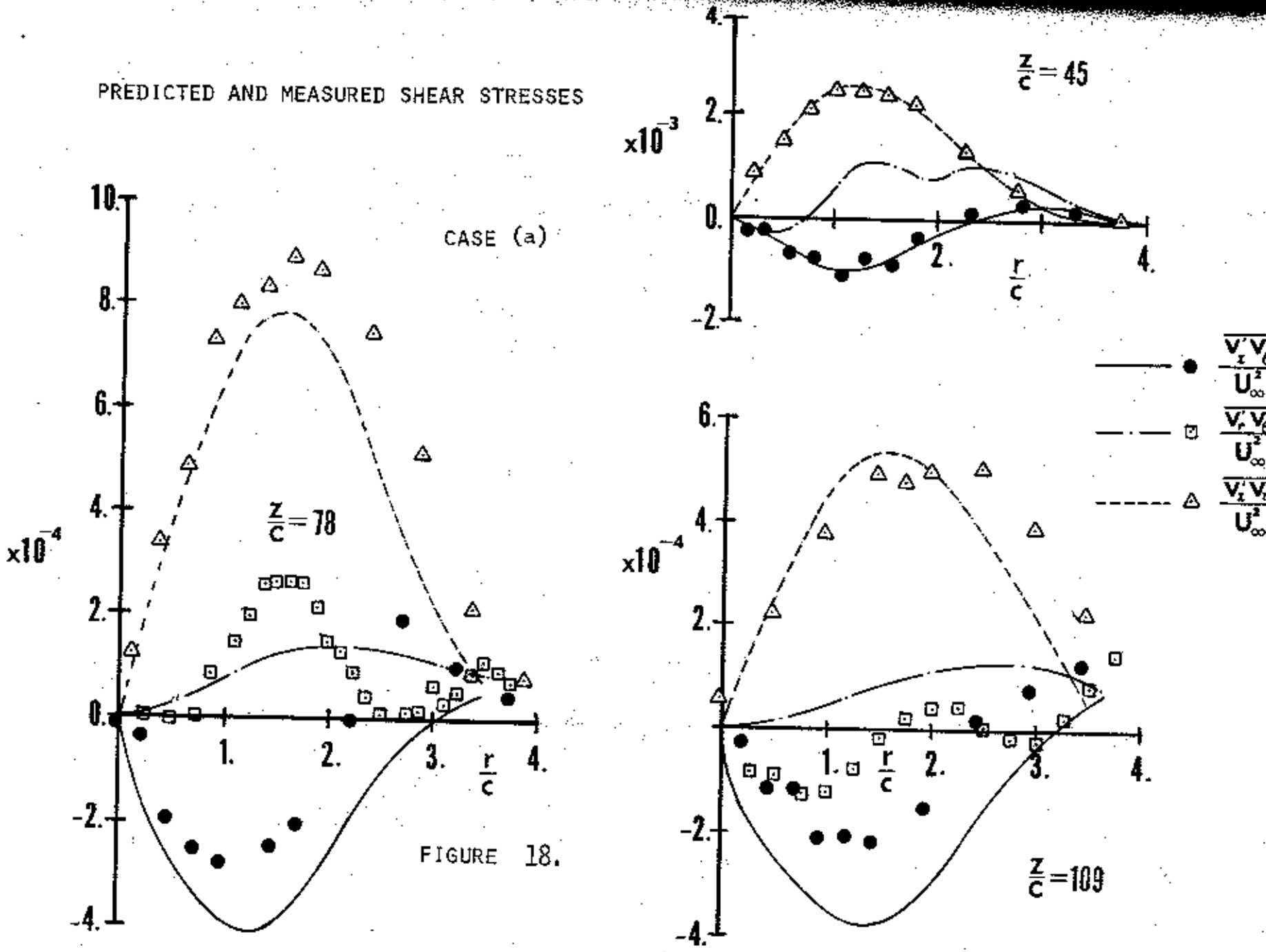

FIGURE 18.

PREDICTED AND MEASURED TURBULENCE LEVELS, CASE(e) FIGURE. 19.

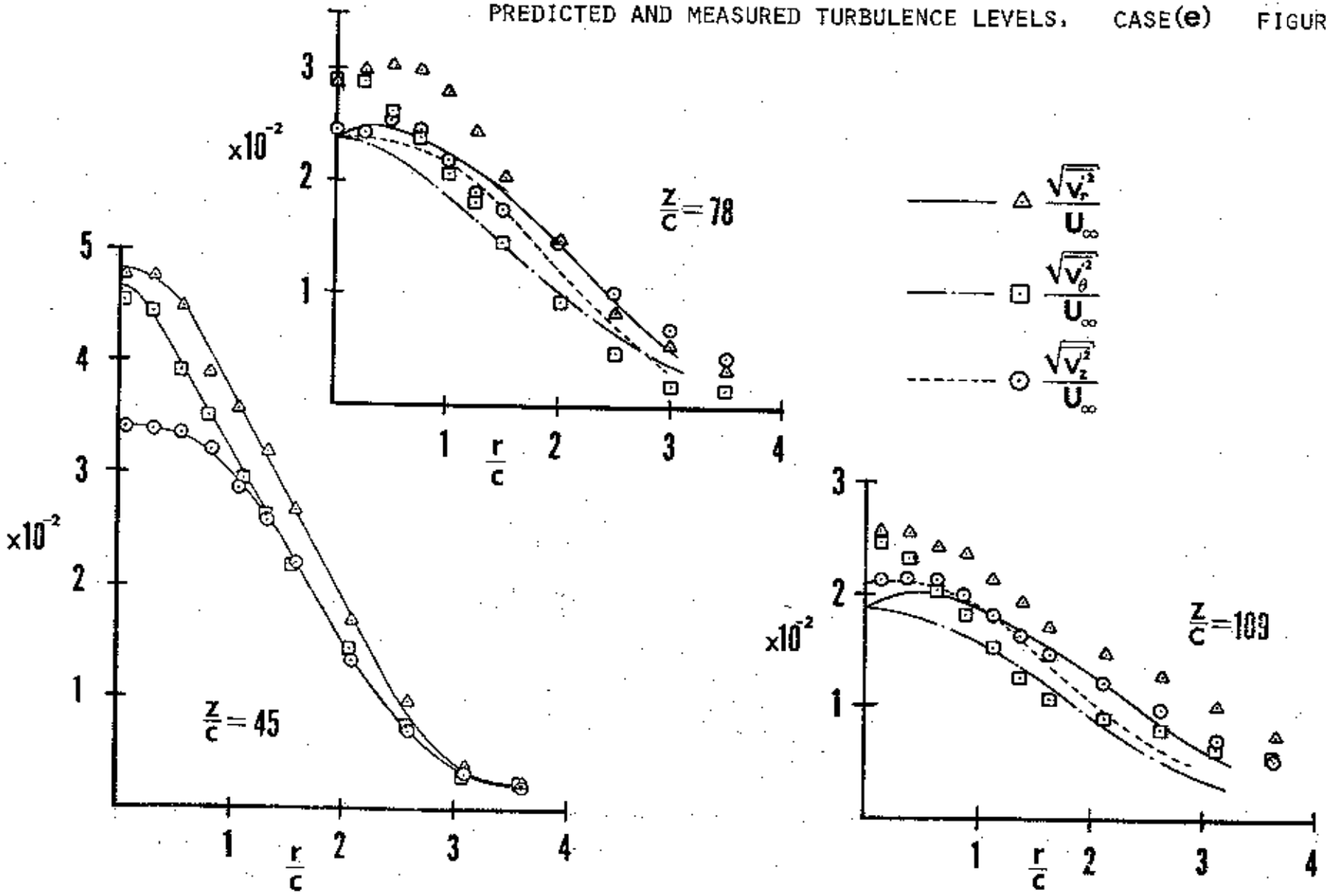

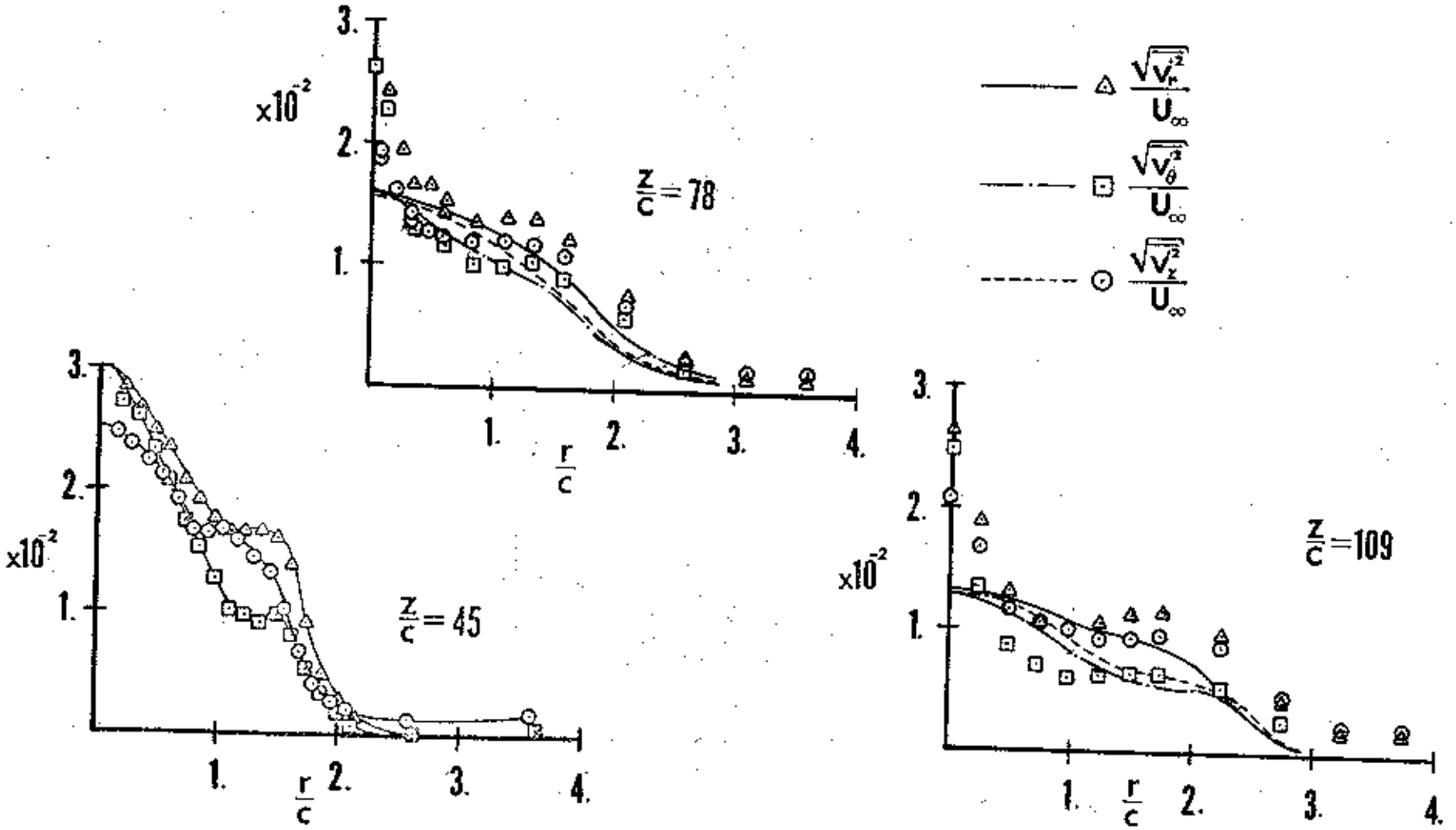

PREDICTED AND MEASURED TURBULENCE LEVELS. CASE(d) FIGURE. 20.

PREDICTED AND MEASURED TURBULENCE LEVELS. CASE(b)

FIGURE. 21.

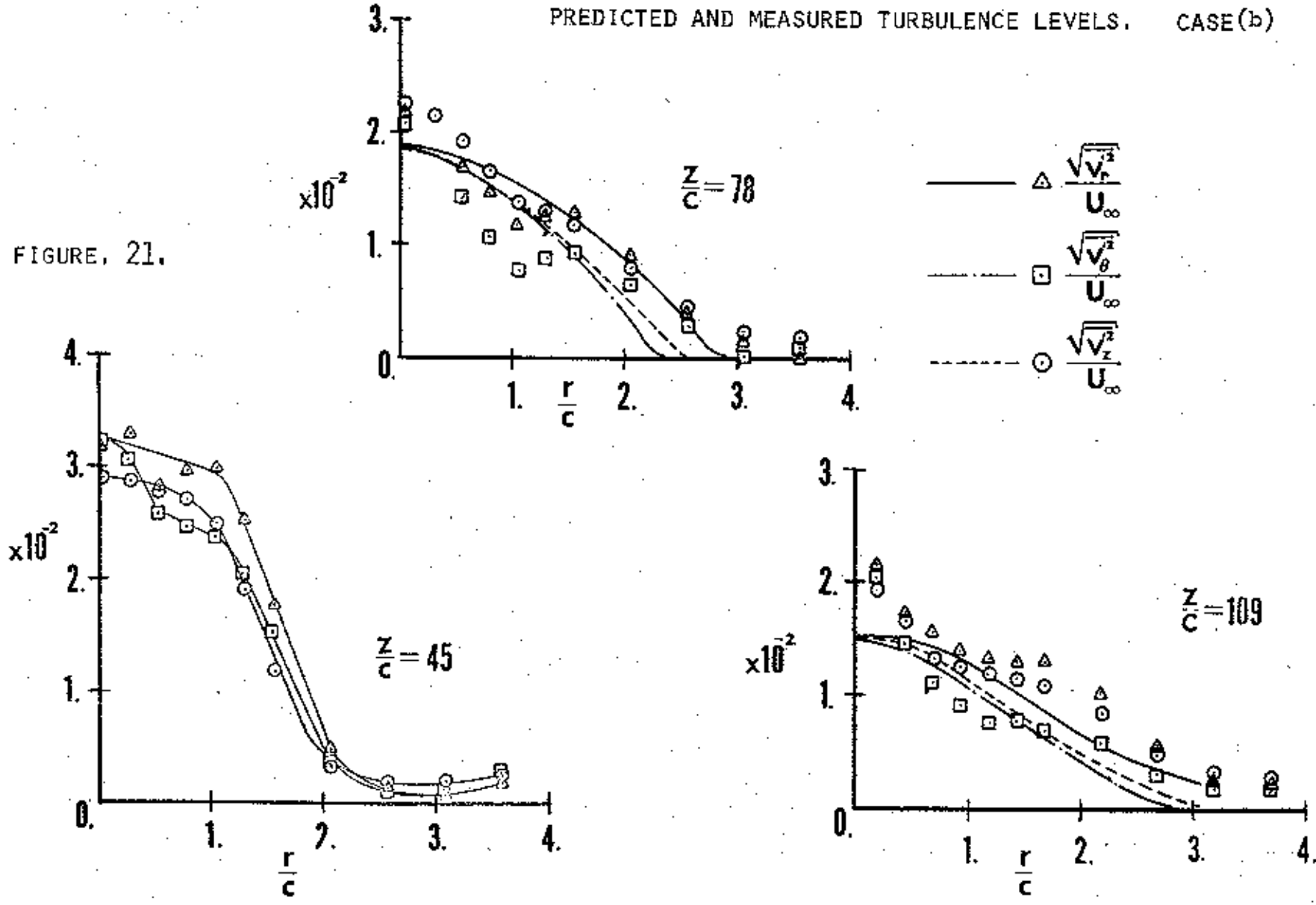

PREDICTED AND MEASURED TURBULENCE LEVELS,

CASE(a) FIGURE. 22.

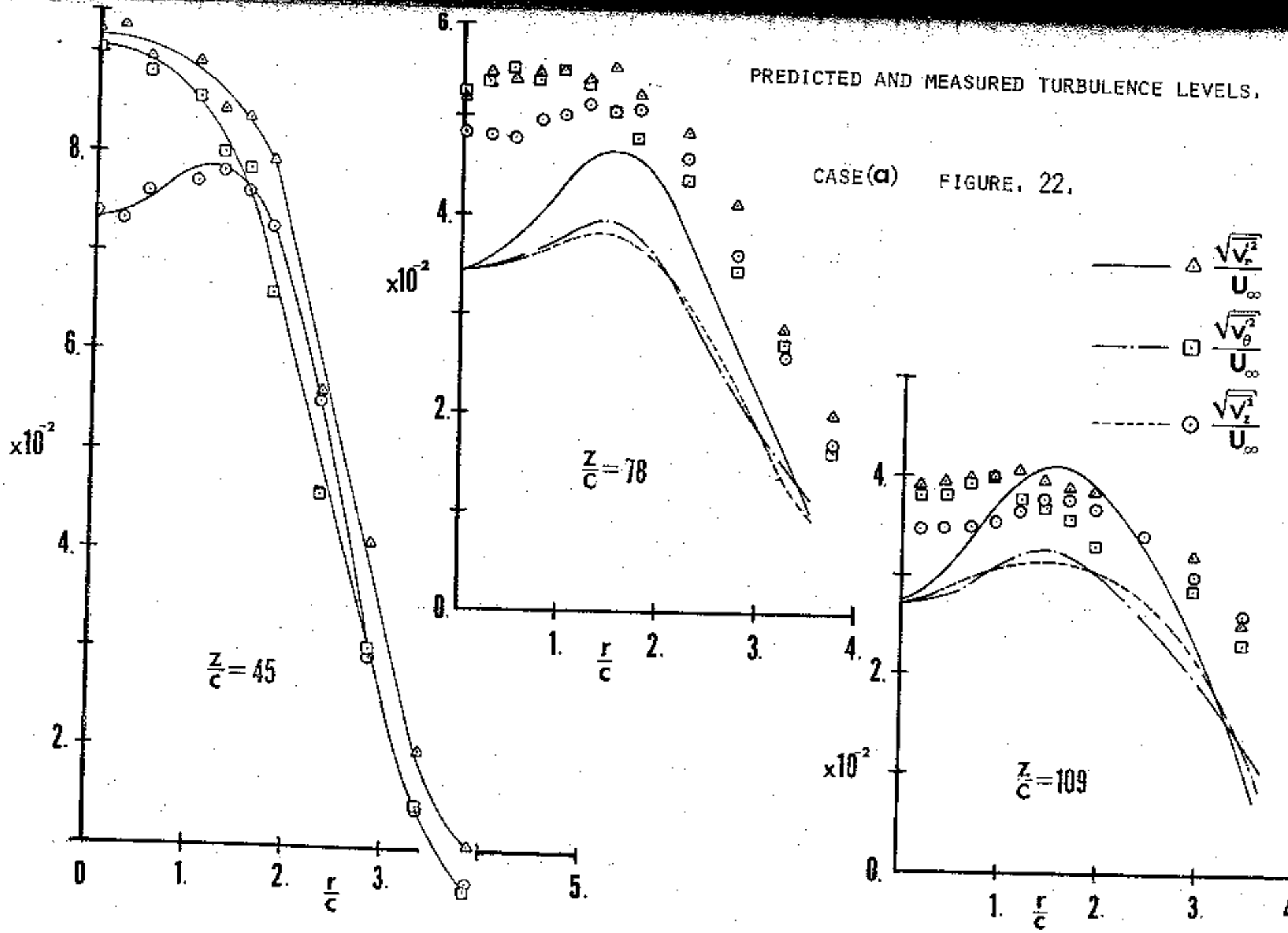

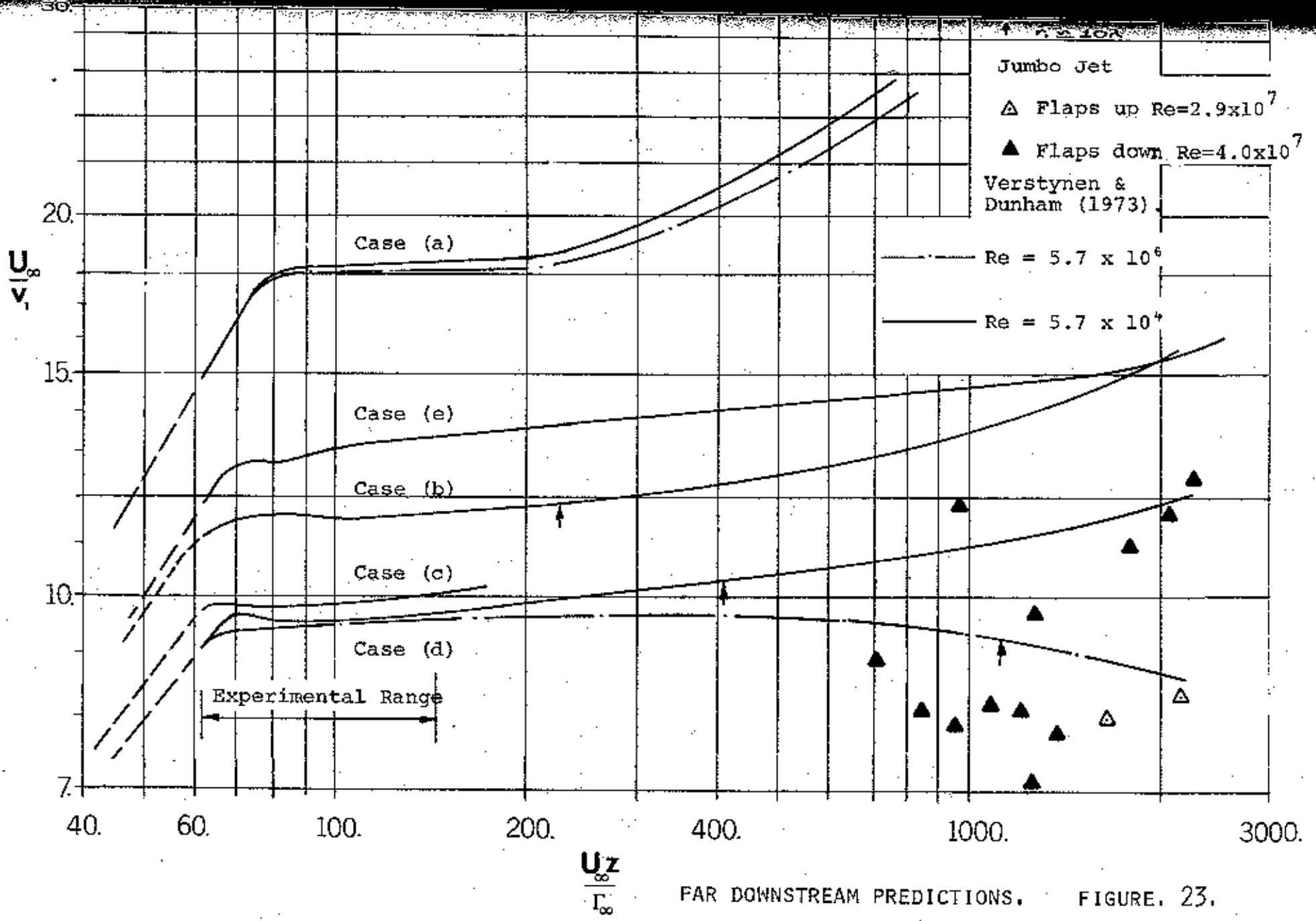

FAR DOWNSTREAM PREDICTIONS. FIGURE. 23.

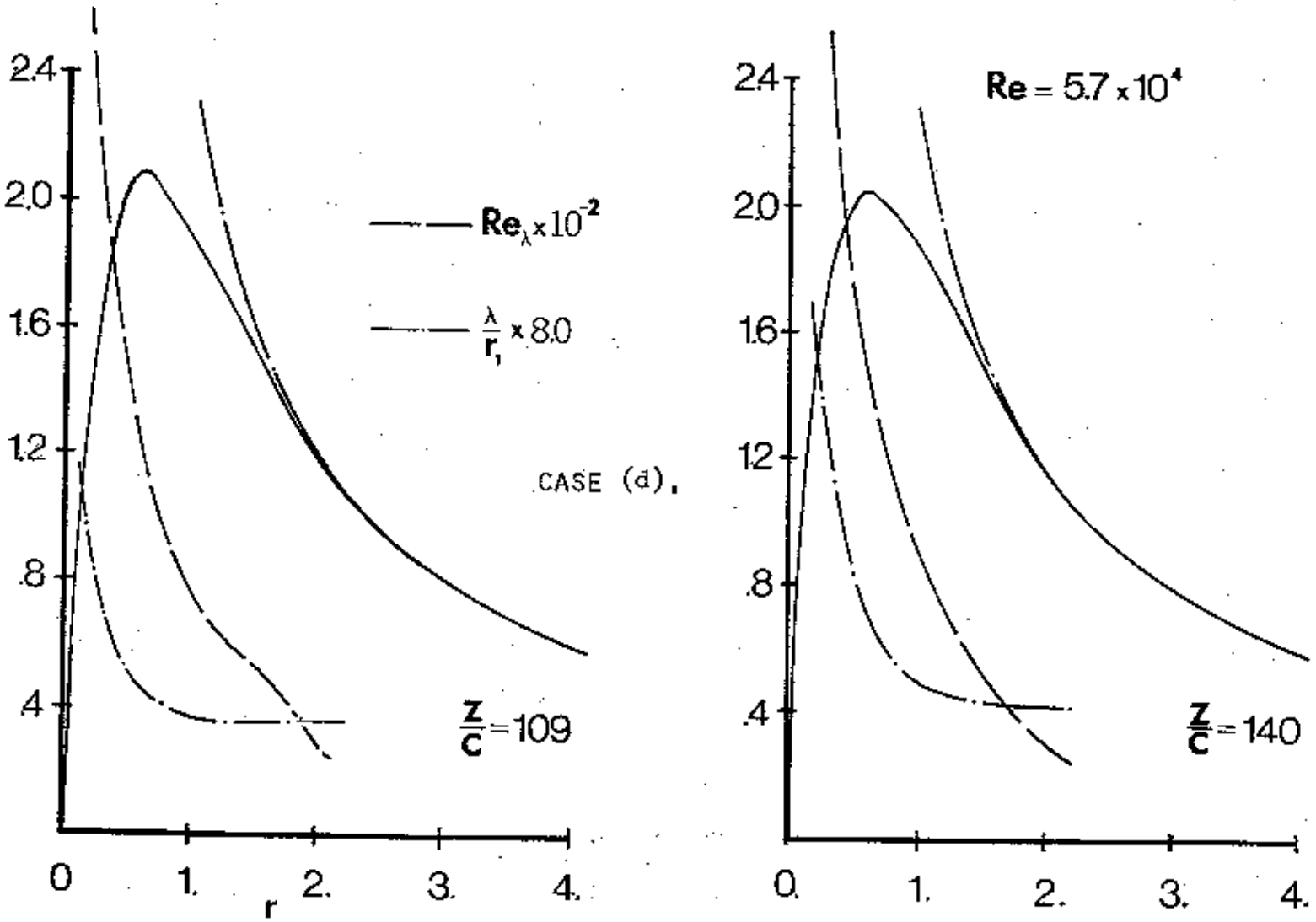

PREDICTED MICROSCALE AND TURBULENCE REYNOLDS NUMBERS. FIGURE. 24.

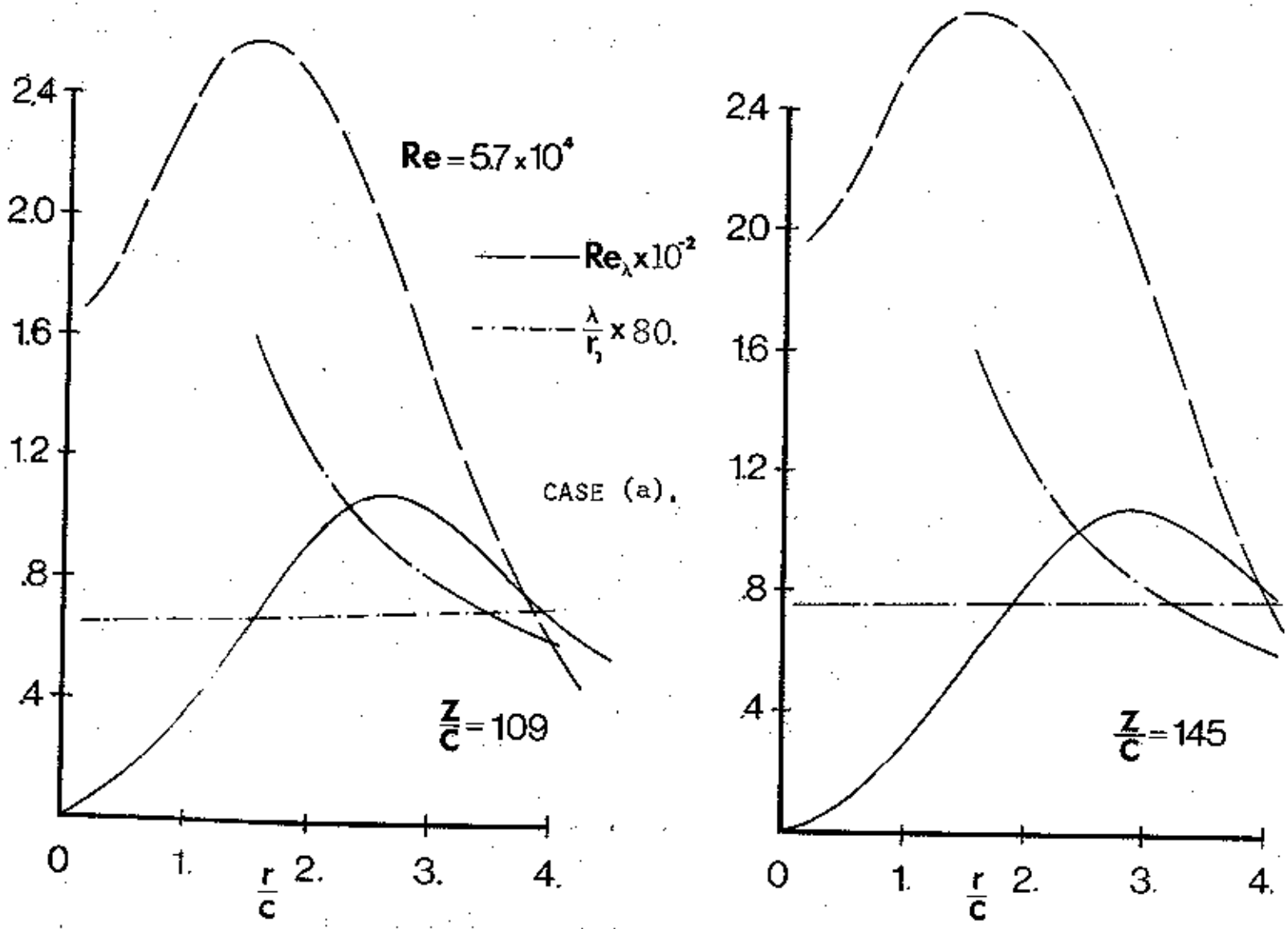

PREDICTED MICROSCALE AND TURBULENCE REYNOLDS NUMBERS. FIGURE. 25.

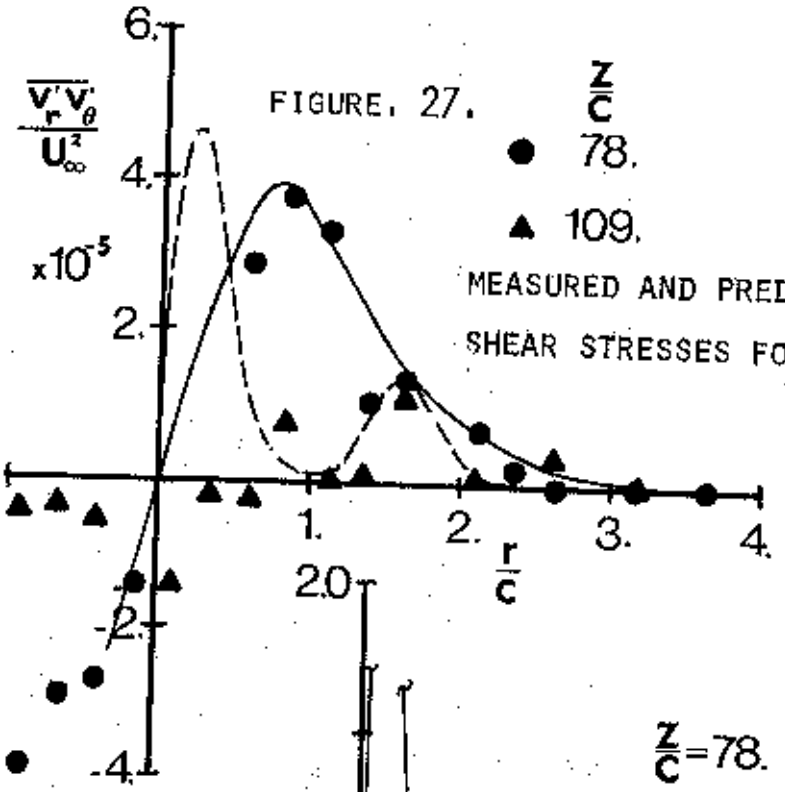

FIGURE. 27.

$\frac{z}{c}$

● 78.

▲ 109.

MEASURED AND PREDICTED SHEAR STRESSES FOR CASE (d)

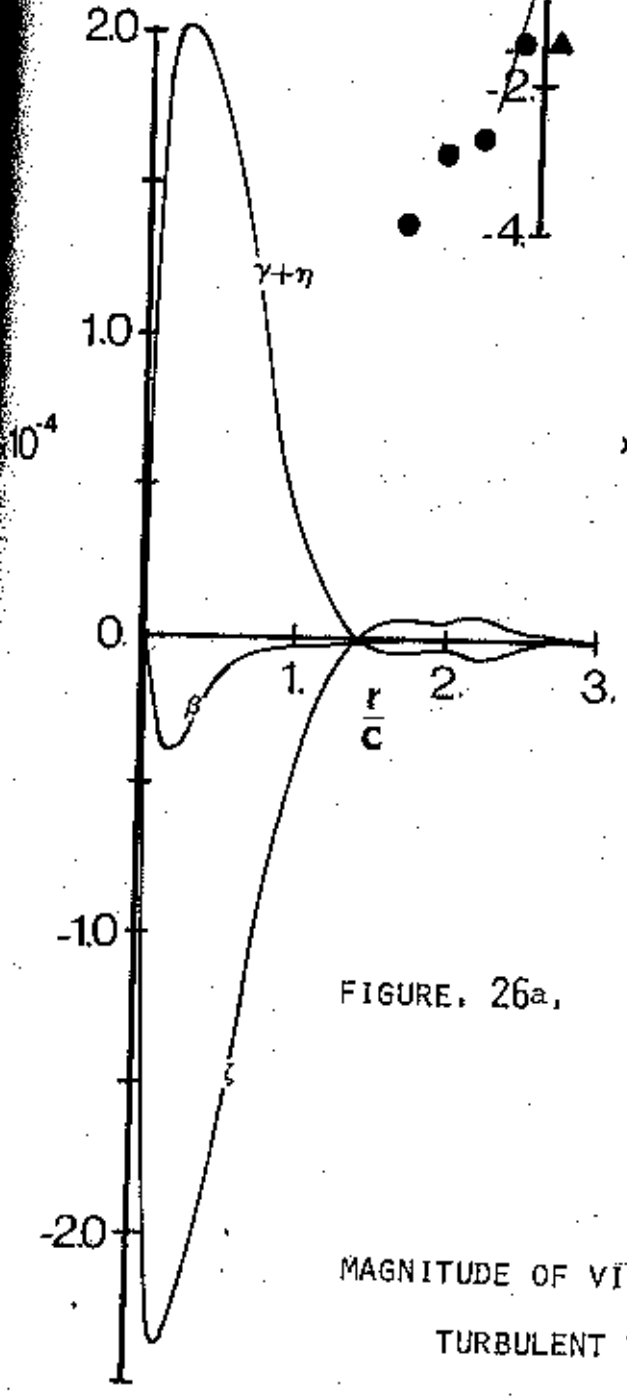

FIGURE. 26a.

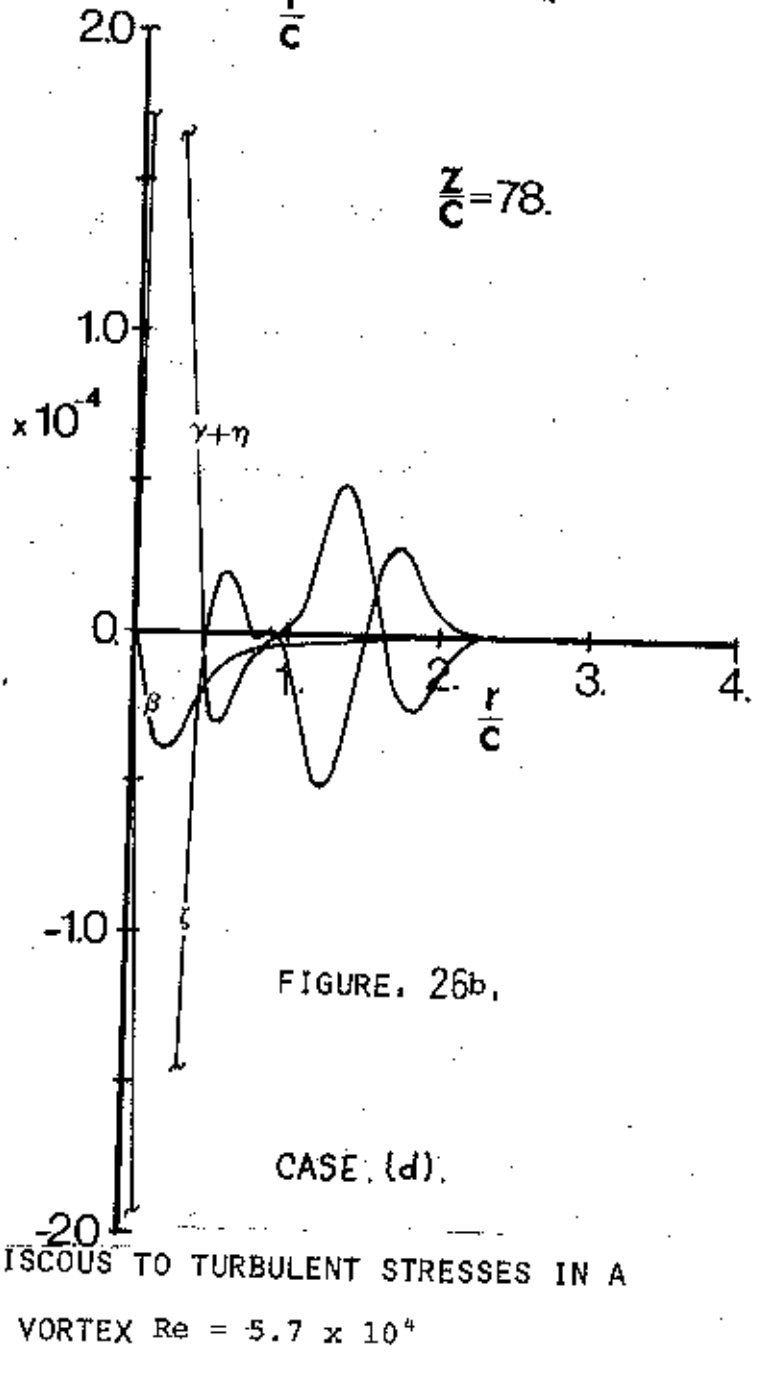

FIGURE. 26b.

CASE (d).

MAGNITUDE OF VISCOUS TO TURBULENT STRESSES IN A TURBULENT VORTEX Re = 5.7×10^4

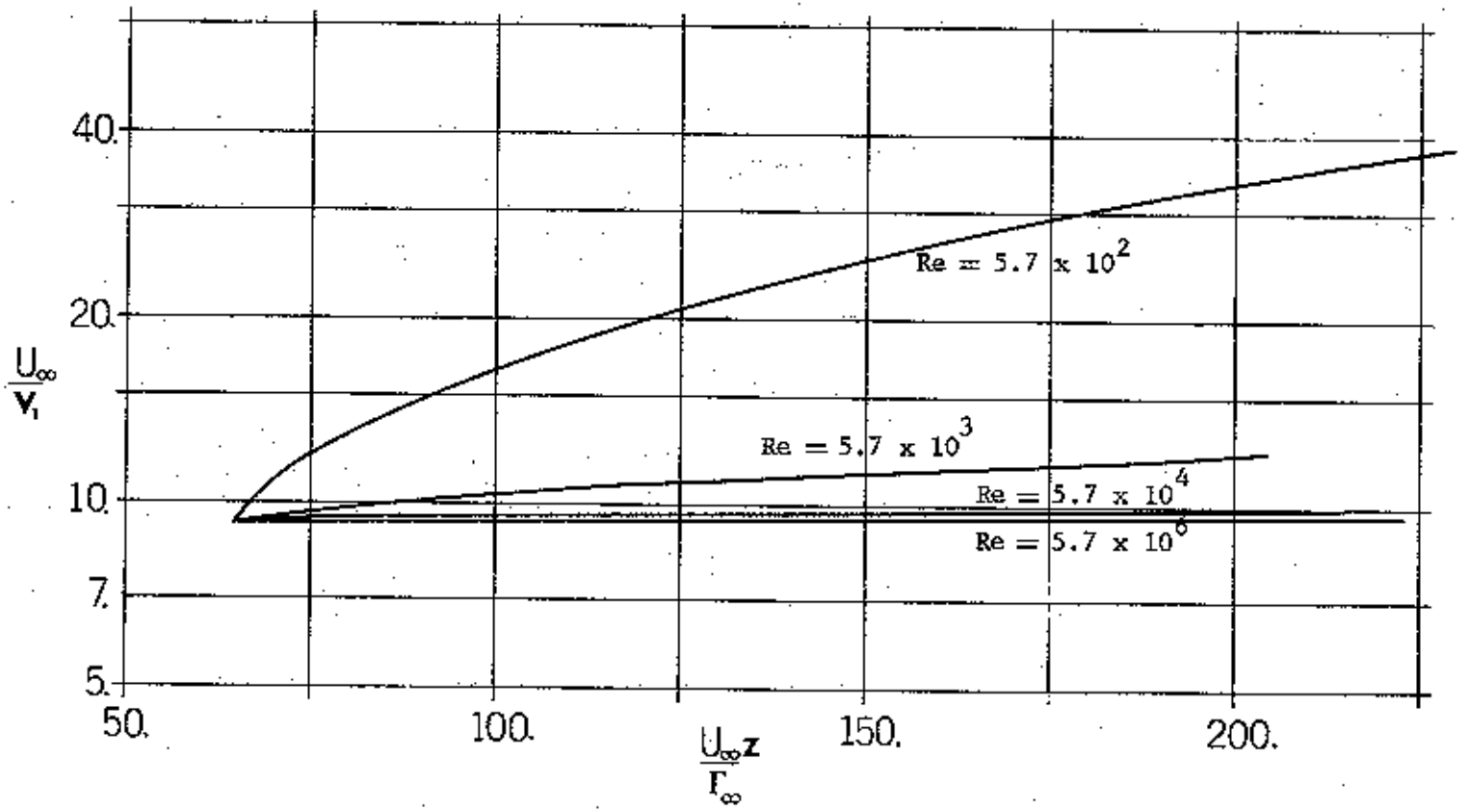

FIGURE. 28.

EFFECT OF REYNOLDS NUMBER ON THE DECAY OF A TURBULENT VORTEX CASE: (d).

DOWNSTREAM CHANGE IN $\overline{v'_r v'_\theta}$ SHEAR STRESS, CASE(d).

FIGURE. 29.

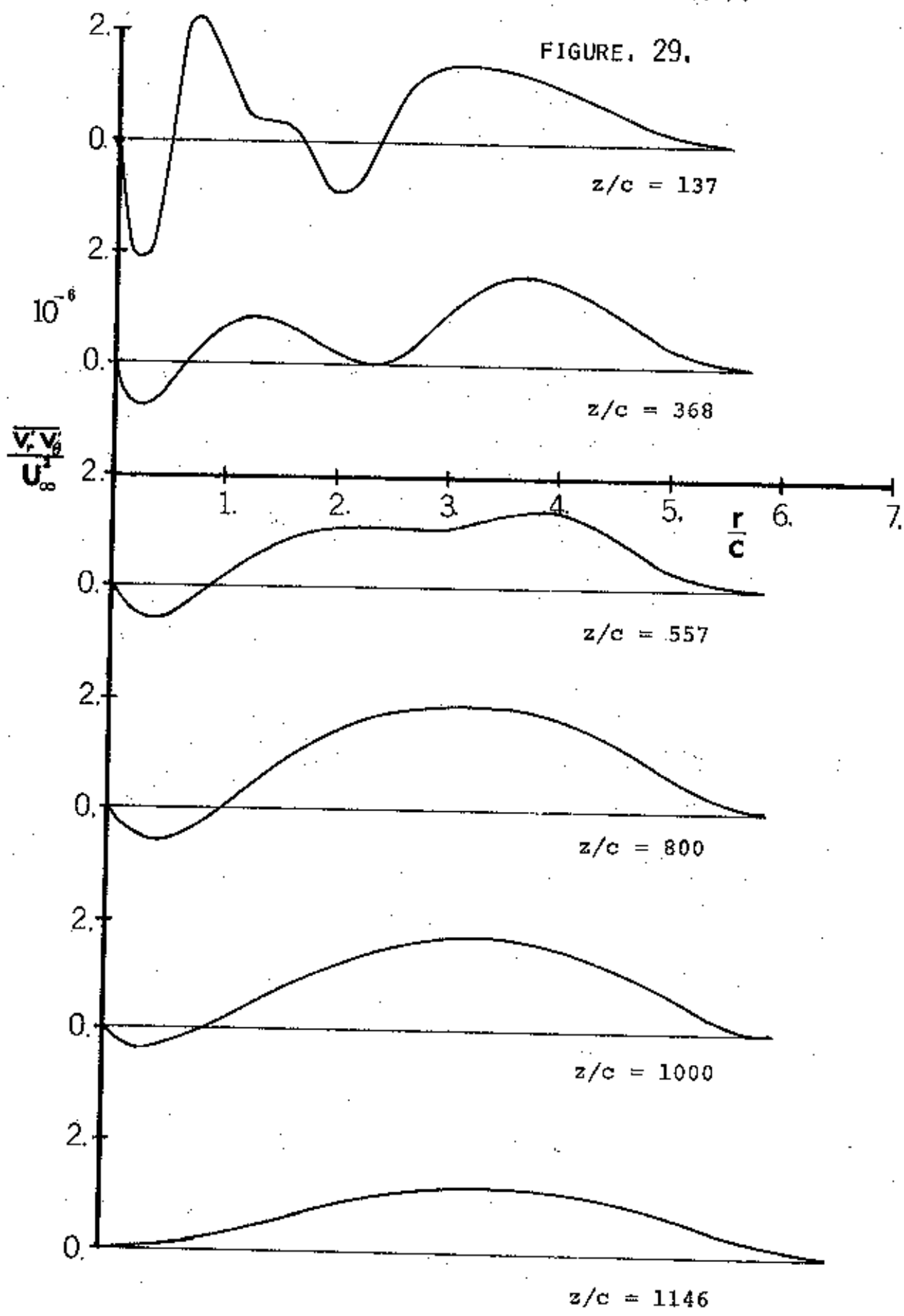

HOT WIRE ANALYSIS. APPENDIX A

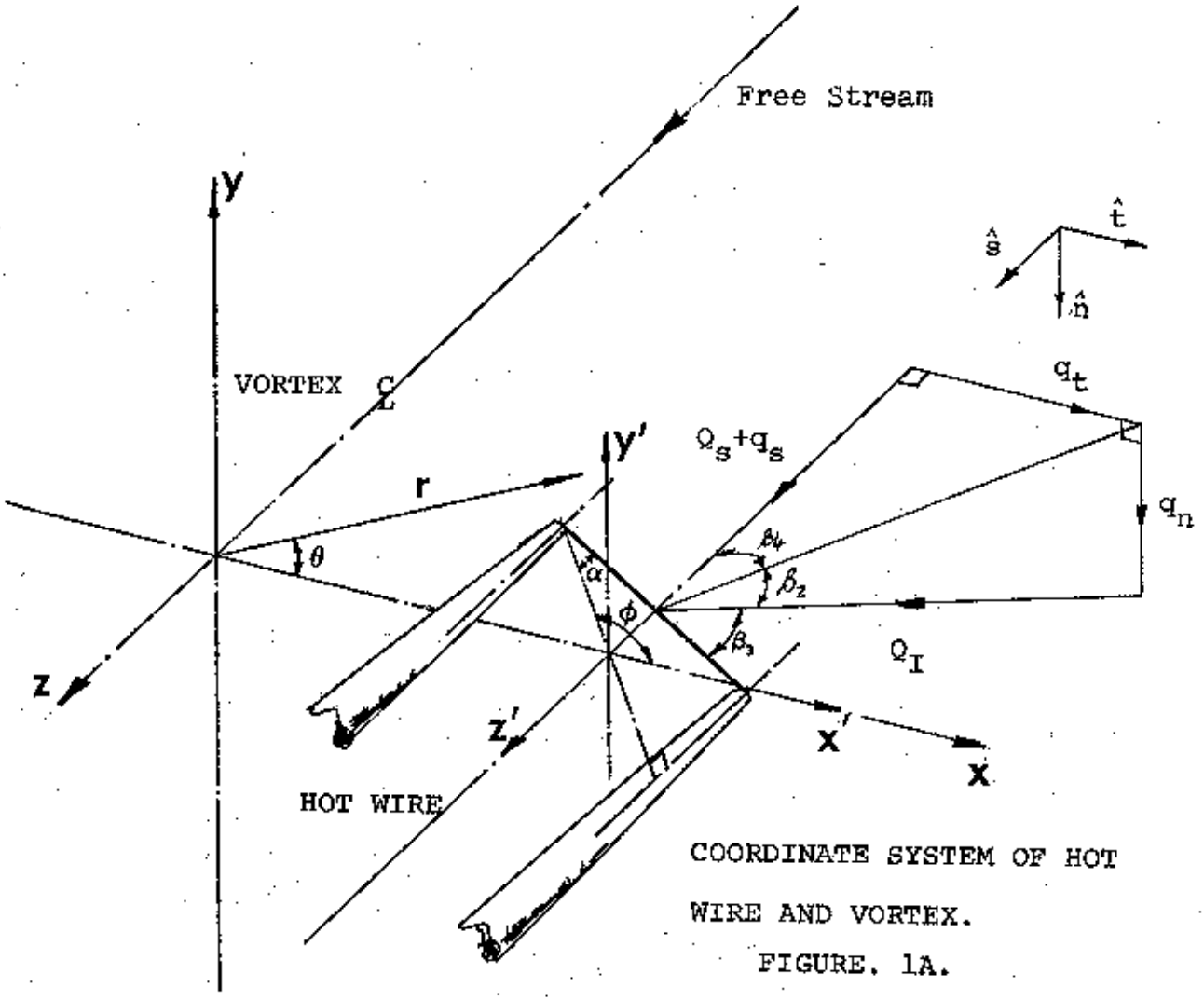

COORDINATE SYSTEM OF HOT WIRE AND VORTEX.

FIGURE. 1A.

The equations 1A - 9A of this analysis are identical to those of Champagne and Sleicher (1967) and are included for completeness. In equation 9A this analysis retains all third order terms rather than discarding some as was done in the above analysis. The present analysis also includes corrections for blockage and pitch as well as the previously included yaw.

From fig.1A it can be shown by the cosine rule that the sine of the angle β_3 between the instantaneous velocity vector Q_I and the hot wire is;

$$-\mathrm{Sin}\beta_3 = \left[\mathrm{Cos}^2\alpha + \frac{2\mathrm{Sin}\alpha\mathrm{Cos}\alpha\mathrm{Tan}\beta_3}{\mathrm{Cos}\beta_4} + \frac{\mathrm{Sin}^2\alpha\,\mathrm{Tan}^2\beta_2}{\mathrm{Cos}^2\beta_4} + \mathrm{Sin}^2\alpha\mathrm{Tan}^2\beta_4 - 1 - \frac{\mathrm{Sin}^2\alpha}{\mathrm{Cos}^2\beta_2\mathrm{Cos}^2\beta_4}\right]\frac{\mathrm{Cos}\beta_2\mathrm{Cos}\beta_4}{2\mathrm{Sin}\alpha} \qquad 1A$$

and similarly that; (where Q_s is the free stream velocity)

$$\mathrm{Sin}\beta_2 = q_n\left[(Q_s + q_s)^2 + q_t^2 + q_n^2\right]^{-\frac{1}{2}} \qquad 2A$$

$$\mathrm{Sin}\beta_4 = q_t\left[(Q_s + q_s)^2 + q_t^2\right]^{-\frac{1}{2}} \qquad 3A$$

$$\mathrm{Cos}\beta_2 = \left[(Q_s+q_s)^2 + q_t^2\right]^{\frac{1}{2}}\left[(Q_s+q_s)^2 + q_t^2 + q_n^2\right]^{-\frac{1}{2}} \qquad 4A$$

$$\mathrm{Cos}\beta_4 = (Q_s + q_s)\left[(Q_s + q_s)^2 + q_t^2\right]^{-\frac{1}{2}} \qquad 5A$$

If these are substituted into equation 1A and rearranged then,

$$-\mathrm{Sin}\beta_3 = (Q_s+q_s)(-\mathrm{Sin}\alpha+q_n\mathrm{Cos}\alpha(Q_s+q_s)^{-1})((Q_s+q_s)^2+q_t^2+q_n^2)^{-\frac{1}{2}} \qquad 6A$$

and squaring gives;

$$\mathrm{Sin}^2\beta_3 = \left[(1+q_s/Q_s)^2 + (q_t^2+q_n^2)/Q_s^2\right]^{-1}\left[\mathrm{Sin}^2\alpha(1+q_s/Q_s)^2 + q_n^2/Q_s^2\mathrm{Cos}^2\alpha - 2\mathrm{Sin}\alpha q_n/Q_s\mathrm{Cos}\alpha(1 + q_s/Q_s)\right] \qquad 7A$$

If the denominator is expanded into a Taylor series firstly in terms of q_s and then q_t and finally q_n

$$\left[(1+q_s/Q_s)^2 + (q_t^2+q_n^2)/Q_s^2\right]^{-1} = 1 - 2q_s/Q_s + 3q_s^2/Q_s^2 - (q_t^2+q_n^2)/Q_s^2 - 4q_s^3/Q_s^3 + 4(q_sq_t^2 + q_sq_n^2)/Q_s^3 + \text{etc.} \qquad 8A$$

Substituting back into equation 7A gives;

$$\text{Sin}^2\beta_3 = \left[-(q_t^2 + q_n^2)/Q_s^2 + 2q_s(q_t^2+q_n^2)/Q_s^3 - 4q_s^3/Q_s^3 - 4q_s^2/Q_s^2\right] \text{Sin}^2\alpha$$

$$+ \text{Sin}^2\alpha + \left[q_n^2/Q_s^2 - 2q_s q_n^2/Q_s^3\right] \text{Cos}^2\alpha$$

$$-2\text{Sin}\alpha\text{Cos}\alpha\left[q_n/Q_s - q_n q_s/Q_s^2 - q_n q_t^2/Q_s^3 - 3q_n q_s^2/Q_s^3 - q_n^3/Q_s^3\right] \quad 9A$$

where only fourth and higher order terms are neglected.
By using the trigonometric equation $\text{Cos}^2\theta + \text{Sin}^2\theta = 1$, it is easily shown that;

$$\text{Cos}^2\beta_3 + k_3^2\text{Sin}^2\beta_3 = \text{Cos}^2\alpha\left\{1 + k_3^2\text{Tan}^2\alpha + (k_3^2-1)\left[\frac{\text{Sin}^2\beta_3}{\text{Cos}^2\alpha} - \text{Tan}^2\alpha\right]\right\} \quad 10A$$

Now the instantaneous velocity vector Q_I is;

$$Q_I^2 = Q_s^2\left[1 + (q_s^2+q_n^2+q_t^2)/Q_s^2 + 2q_s/Q_s\right] \quad 11A$$

And the instantaneous effective cooling velocity Q_E is

$$Q_E^2 = Q_I^2\left[\text{Cos}^2\beta_3 + k_3^2\text{Sin}^2\beta_3\right] \quad 12A$$

Hence $Q_E^2 = Q_s^2\text{Cos}^2\alpha\left\{k_1^2\left(1 + 2q_s/Q_s + (q_s^2-q_n^2)/Q_s^2\right)\right.$

$$+ k_2^2/\text{Cos}^2\alpha\left\{(q_t^2+q_n^2)/Q_s^2 + 12q_s^3/Q_s^3 + 4q_s^2/Q_s^2\right\}$$

$$+2k_1^2\text{Tan}\alpha\left\{q_n/Q_s + q_n q_s/Q_s^2 - 4q_n q_s^2/Q_s^3\right\} + k_3^2\left[k_1^2(q_t^2+2q_n^2)/Q_s^2\right.$$

$$- k_2^2/\text{Cos}^2\alpha\left\{(q_t^2+q_n^2)/Q_s^2 + 12q_s^3/Q_s^3 + 4q_s^2/Q_s^2\right\}$$

$$-2k_1^2\text{Tan}\alpha\left\{q_n/Q_s + q_n q_s/Q_s^2 - 4q_n q_s^2/Q_s^3\right\}$$

$$\left.\left. + k_1^2\text{Tan}^2\alpha\left\{1 + (q_s^2 + q_n^2 + q_t^2)/Q_s^2 + 2q_s/Q_s\right\}\right]\right\} \quad 13A$$

where k_1, k_2, and k_3 are corrections for blockage, pitch and yaw respectively. They were ta ken to be 1.0, 0.985 and 0.17 respectively and were found from the calibration diagrams.

As Q_E is required, an approximation to the square root of equation 13A must be sought. This can be achieved by expanding into a Taylor series; firstly in terms of q_s, then q_n and finally q_t. Before doing this however, it is convienient to regroup the t erms in equation 13A viz;

$$Q_E^2 = Q_s^2\left[A + q_s/Q_s B + q_s^2/Q_s^2 C + q_s^3/Q_s^3 D + q_n/Q_s E + q_n^2/Q_s^2 F + q_t^2/Q_s^2 G + q_n q_s/Q_s^2 H + q_n q_s^2/Q_s^3 I\right] \cos^2\alpha \qquad 14A$$

where,

$$\left.\begin{aligned}
A &= k_1^2 + k_1^2 k_3^2 \tan^2\alpha \\
B &= 2k_1^2 + 2k_1^2 k_3^2 \tan^2\alpha \\
C &= k_1^2 + 4k_2^2 \sec^2\alpha + k_1^2 k_3^2 \tan^2\alpha - 4k_2^2 k_3^2 \sec^2\alpha \\
D &= (1 - k_3^2)\, 12k_2^2 \sec^2\alpha \\
E &= 2k_1^2 \tan\alpha\,(1 - k_3^2) \\
F &= -k_1^2 + k_2^2 \sec^2\alpha + 2k_1^2 k_3^2 - k_2^2 k_3^2 \sec^2\alpha + k_1^2 k_3^2 \tan^2\alpha \\
G &= k_2^2 \sec^2\alpha + k_1^2 k_3^2 + k_1^2 k_3^2 \tan^2\alpha - k_2^2 k_3^2 \sec^2\alpha \\
H &= 2k_1^2 \tan\alpha\,(1 - k_3^2)
\end{aligned}\right\} \qquad 15A$$

$$Q_E = K_1 Q_s \cos\alpha\left[1 + q_s/Q_s\beta + q_n/Q_s\gamma + q_t^2/Q_s^2\xi + q_s^2/Q_s^2\Omega + q_n^2/Q_s^2\Lambda\right.$$
$$+ q_s^3/Q_s^3\theta' + q_n^3/Q_s^3\phi + q_s q_n/Q_s^2\nu + q_s q_n^2/Q_s^3\epsilon + q_n q_s^2/Q_s^3\lambda$$
$$\left. + q_s q_t^2/Q_s^3\kappa + q_n q_t^2/Q_s^3\varsigma\right] \qquad 16A$$

where,

$$\left.\begin{aligned}
K_1 &= A^{\frac{1}{2}} \\
\beta &= \tfrac{1}{2}BA^{-1} \\
\gamma &= \tfrac{1}{2}EA^{-1} \\
\xi &= \tfrac{1}{2}GA^{-1} \\
\Omega &= \tfrac{1}{2}CA^{-1} - B^2/8\,A^{-5/2} \\
\Lambda &= -E^2A^{-5/2}/8 + \tfrac{1}{2}FA^{-1} \\
\theta' &= 0 \\
\phi &= 1/16\,EA^{-7/2} - \tfrac{1}{4}EFA^{-5/2} \\
\nu &= -\tfrac{1}{4}EBA^{-5/2} + \tfrac{1}{2}HA^{-1} \\
\epsilon &= 3/16\,BE^2A^{-7/2} - \tfrac{1}{4}BA^{-5/2} + \tfrac{1}{4}HEA^{-5/2} \\
\lambda &= -\tfrac{1}{4}CEA^{-5/2} + \tfrac{1}{2}IA^{-1} + 3/16EB^2A^{-7/2} - \tfrac{1}{4}BHA^{-5/2} \\
\kappa &= -\tfrac{1}{4}GBA^{-5/2} \\
\varsigma &= -\tfrac{1}{4}EGA^{-5/2}
\end{aligned}\right\} \quad 17A$$

At this stage all third order terms are dropped from this equation. Now if the above terms are expressed as mean and fluctuating components, then;

$$\begin{aligned}
Q_E &= \bar{q} + q \\
Q_s &= U_0 \\
q_s &= \bar{u} + u \\
q_n &= (\bar{w} + w)\cos\theta + (\bar{v} + v)\sin\theta \\
q_t &= (\bar{v} + v)\cos\theta - (\bar{w} + w)\sin\theta
\end{aligned} \qquad 18A$$

Substituting 18A into 16A and separating Q_E into mean and fluctuating components yields;

$$\bar{q} = K_1 U_0 \cos\alpha\left[1 + \beta\bar{u}/U_0 + \gamma(\bar{v}\sin\theta + \bar{w}\cos\theta)/U_0 + \right.$$
$$+ \xi\left[(\bar{w}\sin\theta - \bar{v}\cos\theta)^2 + \overline{(w\sin\theta - v\cos\theta)^2}\right]/U_0^2 + \Omega(\bar{u}^2 + \overline{u^2})/U_0^2$$
$$+ \Lambda\left[(\bar{v}\sin\theta + \bar{w}\cos\theta)^2 + \overline{(v\sin\theta + w\cos\theta)^2}\right]/U_0^2$$
$$\left. + \nu\left[(\bar{u}\bar{v}\sin\theta + \bar{u}\bar{v}\cos\theta) + (\overline{uv}\sin\theta + \overline{uv}\cos\theta)\right]/U_0^2\right] \qquad 19A$$

and,

$$q = k_1 U_0 \cos\alpha \Big\{ \beta u/U_0 + \gamma(v\sin\theta + w\cos\theta)/U_0 + 2\Lambda u\bar{u}/U_0^2$$
$$+ \xi\left[2w\bar{w}/U_0^2\sin^2\theta + 2v\bar{v}/U_0^2\cos^2\theta - 2(\bar{v}w + v\bar{w})\sin\theta\cos\theta/U_0^2\right]$$
$$+ \Lambda(2v\bar{v}\sin^2\theta + 2w\bar{w}\cos^2\theta + 2(\bar{v}w + v\bar{w})\sin\theta\cos\theta)/U_0^2$$
$$+ \nu\left[\sin\theta(\bar{u}v + u\bar{v}) + \cos\theta(\bar{u}w + u\bar{w})\right]/U_0^2 \Big\} \qquad 20A$$

Now it is possible to obtain the velocity components $\bar{u}, \bar{v}$, and $\bar{w}$ from equation 19A but it will not yield the coupled velocity components $u_i u_j$, these are found from the square of equation 20A.

$$q^2 = K_1^2 U_0^2 \cos^2\alpha \Big\{ u^2/U_0^2\beta^2 + \gamma^2(v^2\sin^2\theta + w^2\cos^2\theta + 2vw\sin\theta\cos\theta)/U_0^2$$
$$+ 4\Lambda^2\bar{u}^2u^2/U_0^4 + 2\beta\gamma\left[uv\sin\theta + uw\cos\theta\right)/U_0^2 + 4\beta\Lambda u^2\bar{u}/U_0^3$$
$$+ 4\xi\beta\left[uw\bar{w}\sin^2\theta + uv\bar{v}\cos^2\theta - (u\bar{v}w + uv\bar{w})\sin\theta\cos\theta\right]/U_0^3$$
$$+ 4\Lambda\beta\left[uv\bar{v}\sin^2\theta + uw\bar{w}\cos^2\theta + (u\bar{v}w + uv\bar{w})\sin\theta\cos\theta\right]/U_0^3$$
$$+ 2\nu\beta\left[(\bar{u}uv + u^2\bar{v})\sin\theta + (\bar{u}uw + uv\bar{w})\cos\theta\right]/U_0^3$$
$$+ 4\gamma\xi\left[vw\bar{w}\sin^3\theta + v^2\bar{v}\sin\theta\cos^2\theta - (\bar{v}vw + v^2\bar{w})\sin^2\theta\cos\theta\right.$$
$$\left. + w^2\bar{w}\sin^2\theta\cos\theta + \bar{v}vw\cos^3\theta - (\bar{v}w^2 + vw\bar{w})\sin\theta\cos^2\theta\right]/U_0^3$$
$$+ 4\alpha\gamma\left[\bar{u}uv\sin\theta + \bar{u}uw\cos\theta\right]/U_0^3$$
$$+ 4\Lambda\gamma\left[v^2\bar{v}\sin^3\theta + vw\bar{w}\sin\theta\cos^2\theta + (\bar{v}vw + v^2\bar{w})\sin^2\theta\cos\theta\right.$$
$$\left. + \bar{v}vw\cos\theta\sin^2\theta + w^2\bar{w}\cos^3\theta + (w^2\bar{v} + vw\bar{w})\sin\theta\cos^2\theta\right]/U_0^3$$
$$+ 2\gamma\nu\left[(v^2\bar{u} + uv\bar{v})\sin^2\theta + (\bar{u}vw + v^2\bar{w})\sin\theta\cos\theta\right.$$
$$\left. + (\bar{u}w^2 + vw\bar{w})\cos^2\theta + (\bar{u}vw + u\bar{v}w)\sin\theta\cos\theta\right]/U_0^3 \Big\} \qquad 21A$$

where all fourth order terms (with the exception of $u^2\bar{u}^2$) have been dropped. This may appear inconsistent with equation 20A where only second order and lower terms were retained, in fact it is not because the same expression for equation 21A results whether the third order terms in 20A are retained or not, simply because during the squared expansion their order is increased by at least one.

EVALUATION OF VELOCITY TERMS.

The three velocity components can all be obtained from a single inclined hot wire, each via two readings taken 180° apart. From equation 19A then,

$$\bar{u}/U_o = \left[2\beta K_1 U_o \cos\alpha\right]^{-1}\left[(\bar{q}_0 + \bar{q}_{180}) - 2K_1 U_o \cos\alpha\left\{1 + \xi(\bar{v}^2 + \overline{v^2})/U_o^2 + \Omega(\bar{u}^2 + \overline{u^2})/U_o^2 + \Lambda(\bar{w}^2 + \overline{w^2})/U_o^2\right\}\right] \quad 22A$$

$$\bar{v}/U_o = \left[2\gamma K_1 U_o \cos\alpha\right]^{-1}\left[(\bar{q}_{90} - \bar{q}_{270}) - 2\nu K_1 \cos\alpha\,(\bar{u}\bar{v} + \overline{uv})/U_o\right] \quad 23A$$

$$\bar{w}/U_o = \left[2\gamma K_1 U_o \cos\alpha\right]^{-1}\left[(\bar{q}_0 - \bar{q}_{180}) - 2\nu K_1 \cos\alpha(\bar{u}\bar{w} + \overline{uw})/U_o\right] \quad 24A$$

The axial velocity component $\bar{u}/U_o$ can also be evaluated from a single normal hot wire reading viz

The Reynolds stress terms are found by difference between two readings from inclined hot wires, for $\overline{uv}$ and $\overline{uw}$ the readings are 180° apart, for $\overline{vw}$, they are 90° apart. Hence from equation 21A;

$$\overline{uv}/U_o^2 = \left[4\gamma\beta + 4\nu\beta\bar{u}/U_o + 8\alpha\gamma\bar{u}/U_o\right]^{-1}\left[A_1^2(\overline{e_{90}^2} - \overline{e_{270}^2})/(U_o^2\cos^2\alpha)\right.$$
$$\left. - \overline{vw}/U_o^2 . 8\gamma\xi\bar{w}/U_o - \overline{u^2}/U_o^2 . 4\nu\beta\bar{v}/U_o - \overline{v^2}/U_o^2 . 8\lambda\gamma\bar{v}/U_o\right] \qquad 29A$$

$$\overline{uw}/U_o^2 = \left[4\gamma\beta + 4\nu\beta\bar{u}/U_o + 8\alpha\gamma\bar{u}/U_o\right]^{-1}\left[A_1^2(\overline{e_o^2} - \overline{e_{180}^2})/(U_o^2\cos^2\alpha)\right.$$
$$\left. - \overline{uv}/U_o^2 . 4\nu\beta\bar{w}/U_o - \overline{vw}/U_o^2 . 8\gamma\xi\bar{v}/U_o - \overline{w^2}/U_o^2 . 8\lambda\gamma\bar{w}/U_o\right] \qquad 30A$$

$$\overline{vw}/U_o^2 = \left[2\gamma^2 + 4\sqrt{2}\lambda\gamma\bar{v}/U_o + 4\gamma\nu\bar{u}/U_o\right]^{-1}\left[A_1^2(\overline{e_{45}^2} - \overline{e_{135}^2})/(U_o^2\cos^2\alpha)\right.$$
$$- \overline{uw}/U_o^2(2\sqrt{2}\beta\gamma - 4\xi\beta\bar{v}/U_o + 4\lambda\beta\bar{v}/U_o + 2\sqrt{2}\nu\beta\bar{u}/U_o +$$
$$4\sqrt{2}\alpha\gamma\bar{u}/U_o + 2\gamma\nu\bar{v}/U_o)$$
$$- \overline{uv}/U_o^2(-4\xi\beta\bar{w}/U_o + 4\lambda\beta\bar{w}/U_o + 2\sqrt{2}\nu\beta\bar{w}/U_o)$$
$$- \overline{v^2}/U_o^2(-2\sqrt{2}\gamma\xi + 2\sqrt{2}\lambda\gamma + 2\gamma\nu).\bar{w}/U_o$$
$$\left. - \overline{w^2}/U_o^2(2\sqrt{2}\gamma\xi + 2\sqrt{2}\lambda\gamma).\bar{w}/U_o\right] \qquad 31A$$

SOLUTION OF EQUATIONS 22A - 31A.

Due to the form of these equations it is not possible to solve them exactly. They are solved therefore by a simple iteration technique. To ensure convergence, damping is applied to $\bar{u}/U_o$ in the form of $\bar{u}/U_o|_n$ being replaced by

$$\tfrac{1}{2}(\bar{u}/U_o|_n + \bar{u}/U_o|_{n-1}) + \tfrac{1}{4}(\bar{u}/U_o|_n - \bar{u}/U_o|_{n-1})$$

About five iterations were generally required for convergence.

EVALUATION OF CALIBRATION CONSTANTS.

Before equations 22A - 31A can be evaluated , a relationship between the measured voltages $\bar{e}$ and $\overline{e^2}$ and $\bar{q}$ and $\overline{q^2}$ must be found. It was noted in equation 12A that,

$$Q_E^2 = Q_I^2 \cos^2\beta_3 (1 + k_3^2 \tan^2\beta_3)$$

$$\text{so, } Q_E \simeq Q_I \cos\beta_3 (1 + \tfrac{1}{2} k_3^2 \tan^2\beta_3) \qquad 1B$$

During calibration the wire is placed in a region of the tunnel where both $\bar{v}/U_o$ and $\bar{w}/U_o$ are very small ($<.05\%$) and hence $\beta_3 \simeq \alpha$; therefore,

$$Q_I \simeq Q_E/(A\cos\alpha) \qquad 2B$$

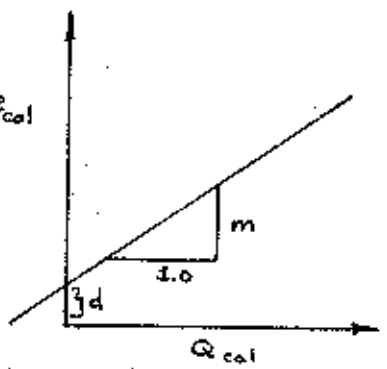

The calibrated linearized signal is

$$e_{cal} = mQ_{cal} + d \qquad 3B$$

hence,

$$Q_{cal} \cdot Q_E/Q_I = (e_{cal} - d)/m \cdot Q_E/Q_I \qquad 4B$$

$$= A_o + A_1 e_{cal} \qquad 5B$$

therefore,

$$A_o = -d\,A\cos\alpha/m \qquad 6B$$

$$A_1 = A\cos\alpha/m \qquad 7B$$

In general then,

$$A_o + A_1(e + \bar{e}) = q + \bar{q} \qquad 8B$$

Taking the mean of equation 8B yields.

$$A_o + A_1\bar{e} = \bar{q} \qquad 9B$$

which may then be used in equations 22A - 25A to find the velocity terms. Squaring 8B and taking the mean gives.

$$A_o^2 + 2A_1A_o\bar{e} + A_1^2(\overline{e^2} + \bar{e}^2) = \overline{q^2} + \bar{q}^2 \qquad 10B$$

This can now be used in equations 26A - 31A to find the coupled velocity terms.

COVARIANT DERIVATIVES. APPENDIX B

In a cylindrical coordinate system, the physical components are $x^1 = z$; $x^2 = r$; $x^3 = \theta$; hence

$$y^1 = x^1 \; ; \; y^2 = x^2 \mathrm{Cos} x^3 \; ; \; y^3 = x^2 \mathrm{Sin} x^3$$

and so the metric tensors are,

$$g^{11} = g_{11} = g^{22} = g_{22} = 1$$

$$g^{33} = 1/r^2, \; g_{33} = r^2$$

$$g_{ij} = g^{ij} = 0 \quad i \neq j$$

hence the scale factors are,

$$h_1 = h_2 = 1 \quad ; \quad h_3 = r$$

The non zero Christoffel symbols then are

$$\left\{ {3 \atop 3\,2} \right\} = 1/r \quad ; \quad \left\{ {2 \atop 3\,3} \right\} = -1/r \quad ; \quad \left\{ {3 \atop 2\,3} \right\} = 1/r \; .$$

Now the covariant derivatives of first and second order tensor quantities are

$$A^j\big|_i = A^j_{,i} + \left\{ {j \atop i\,k} \right\} A^k$$

and

$$\overline{A^i A^j}\big|_k = \overline{A^i A^j}_{,k} + \left\{ {i \atop k\,n} \right\} \overline{A^n A^j} + \left\{ {j \atop k\,n} \right\} \overline{A^i A^n}$$

which in physical components lead to,

$$U^j\big|_i = \begin{bmatrix} \dfrac{\partial v_z}{\partial z} & \dfrac{\partial v_z}{\partial r} & \dfrac{\partial v_z}{r\partial\theta} \\ \dfrac{\partial v_r}{\partial z} & \dfrac{\partial v_r}{\partial r} & \dfrac{\partial v_r}{r\partial\theta} - \dfrac{v_\theta}{r} \\ \dfrac{\partial v_\theta}{\partial z} & \dfrac{\partial v_\theta}{\partial r} & \dfrac{\partial v_\theta}{r\partial\theta} + \dfrac{v_r}{r} \end{bmatrix}$$

and

$$\overline{u^i u^j}\Big|_k =$$

$$\begin{array}{lll}
\dfrac{\partial \overline{v_z'^2}}{\partial z} & \dfrac{\partial \overline{v_z' v_r'}}{\partial z} & \dfrac{\partial \overline{v_z' v_\theta'}}{\partial z} \\
 & \dfrac{\partial \overline{v_r'^2}}{\partial z} & \dfrac{\partial \overline{v_r' v_\theta'}}{\partial z} \\
\text{Symmetrical} & & \partial \overline{v_\theta'^2} / \partial z
\end{array} \qquad k = 1$$

$$\begin{array}{lll}
\dfrac{\partial \overline{v_z'^2}}{\partial r} & \dfrac{\partial \overline{v_z' v_r'}}{\partial r} & \dfrac{\partial \overline{v_z' v_\theta'}}{\partial r} \\
 & \dfrac{\partial \overline{v_r'^2}}{\partial r} & \dfrac{\partial \overline{v_r' v_\theta'}}{\partial r} \\
\text{Symmetrical} & & \partial \overline{v_\theta'^2} / \partial r
\end{array} \qquad k = 2$$

$$\begin{array}{lll}
\dfrac{\partial \overline{v_z'^2}}{r\partial\theta} & \dfrac{\partial \overline{v_z' v_r'}}{r\partial\theta} - \dfrac{\overline{v_z' v_\theta'}}{r} & \dfrac{\partial \overline{v_z' v_\theta'}}{r\partial\theta} + \dfrac{\overline{v_z' v_r'}}{r} \\
 & \dfrac{\partial \overline{v_r'^2}}{r\partial\theta} - \dfrac{2\overline{v_r' v_\theta'}}{r} & \dfrac{\partial \overline{v_r' v_\theta'}}{r\partial\theta} + \dfrac{\overline{v_r'^2} - \overline{v_\theta'^2}}{r} \\
\text{Symmetrical} & & \dfrac{\partial \overline{v_\theta'^2}}{r\partial\theta} + \dfrac{2\overline{v_r' v_\theta'}}{r}
\end{array} \qquad k = 3$$

List of constants;

$$a_1 = 1.5$$
$$a_2 = 0.4$$
$$a_3 = 0.15$$
$$a_4 = 1.45$$
$$a_5 = 1.9$$
$$a_6 = 0.11$$
$$a_7 = -(2.0 + 3.0a_2)/11.0$$
$$a_8 = -(50.0a_2 + 4.0)/55.0$$
$$a_9 = (20a_2 + 6.0)/55.0$$
$$a_{10} = (4.0a_2 + 10.0)/11.0$$

Diffusion constants;

$$\alpha^{ij} = a_6 \begin{bmatrix} 1 & 2 & 1 \\ 2 & 3 & 2 \\ 1 & 2 & 1 \end{bmatrix}$$

The numerical procedure used was the finite difference scheme proposed by Spalding and Patankar (1967). In this procedure all equations are forced into the form;

$$\frac{\partial \phi}{\partial z} + (a+b\omega)\frac{\partial \phi}{\partial \omega} = \frac{\partial}{\partial \omega}\left(c\frac{\partial \phi}{\partial \omega}\right) + d$$

and hence all of the coupled and most of the nonlinear terms

The radial momentum equation (2.4.4);

$$\frac{p_o}{\rho} = \frac{p_r}{\rho} - \int_o^r \frac{v_\theta^2}{r}\,dr$$

is differentiated with respect to z , thus giving the downstream pressure gradient which is required in the axial momentum equation. The radial velocity is then obtained from the continuity equation; viz

$$v_r = \frac{-\int_o^R r\frac{\partial v}{\partial z}z\,dr}{R}$$

The program is in four segments and follows the approach suggested by Spalding and Patankar . Routine MAIN is the main calling program in which the initial data is read in and the boundary conditions are defined. It also determines the non dimensional radial grid step size, calculates the entrainment rate and finally prints out the required information.

Subroutine AUX calculates the parameters required for the turbulence model, sets up δ^{ij}, α^{ij}, $U^j|_i$ and S^{ij} and then calculates the source terms. This routine calls subroutine CHOU in which C^{mnij}, ϕ_1^{ij} and ϕ_2^{ij} are calculated. Subroutine STRIDE is principally Irwin's (1974) version of the subroutine originally written by Spalding and Patankar contracted to account for axisymmetric conditions only. It consists of three main parts; STRIDE I where the radial coordinate spacing is calculated; STRIDE II where the boundary

conditions are put into the form required by STRIDE III where the equations listed earlier are solved. For specific details of the solution procedure the reader is referred to Spalding and Patankar (1967).

The program requires about 30000_8 words of core storage and takes about 60-80 seconds of central processor time (IBM-360) to predict from z/c = 45 station to the z/c = 109 station. The downstream step size is controlled by the factor FRA in MAIN and is equal to FRA*Y(NP3) where Y(NP3) is the maximum non dimensional radial ordinate. This product must not exceed 1.0; which was found to be the largest value that could be used before the program departed into a world of wistful (but what appears on the surface reasonable) fantasy.

MAIN

```
      COMMON/GENRAL/ AJE(9),AJI(9),CSALFA,DPDX(40),DX,
     1   FS(9,40),H, IFIN,INDE(9),INDI(9),ISTEP,ITEST,IUTRAP,KEX,KIN,KRAD,
     2   N,NEQ,NPH,NP1,NP2,NP3,OM(40),PEI,PR(9),PSIE,PSII,
     3 R(40),RME,RMI,RU(40),XD,XU,YE,YI,UT,UTE,CU ,TACT
      COMMON/TED/Y(40),U(40),RHO(40),EMU(40),KHL
      COMMON/RENY/F(9,40),PREF(9,40),SU(9,40),SD(9,40),VR(40),VO(40)
      COMMON/BITS/P156,P218,TEL
      LRUN=1
      DO 22 IRUN = 1,LRUN
      XS  = P90
      CU = .00001
      CORD = 2.0
      ALEN = 1.0/CORD
      LASTEP = 3000
      OMPO2P=1.
      N = 32
      NP1=N+1
      NP2=N+2
      NP3=N+3
      KHL = NP2
      XU = 45.
      XD = XU
      XULAST = 3000.
      ISTEP=0
      FRA = .15
      CSALFA=1.
      NEQ = 9
      NPH=NEQ-1
      DO 1 I = 1, NP3
    1 RHO(I) = 1.0
      RHOL = 1.0
      PII = 3.1415
      READ(5,3    )(Y(I),U(I),VR(I),VO(I),F(1,I),F(2,I),F(3,I),F(4,I),
     1 F(5,I),F(6,I), I = 2,NP2)
      EMUL = 2.0E-5
    3 FORMAT(10F8.3)
      DO4 I = 2,NP2
      VR(I) = VR(I)*.01
      VO(I) = VO(I)*.01
      F(1,I) = F(1,I)*.01
      F(2,I) = F(2,I)*.01
      F(3,I) = F(3,I)*.01
      F(4,I) = F(4,I)*.0001
      F(5,I) = F(5,I)*.0001
      F(6,I) = F(6,I)*.0001
      Y(I) = Y(I)/CORD
      DO 4 J = 1,3
      F(J,I)=F(J,I)*F(J,I)
    4 F(7,I) = ((F(1,I)+F(2,I)+F(3,I))*.5)**1.5/ALEN
      Y(1)=0.0
```

CONSTANTS

STARTING VALUE FOR ϵ

```
      Y(2) = 1./3.*Y(3)
      U(1) = U(2)
      Y(NP3)=Y(NP2)
      U(NP3)=U(NP2)
      VR(1) = VR(2)
      VO(1) = VO(2)
      YR2 = (Y(2)-Y(1))/(Y(3)-Y(1))
      VR(2) = VR(1)+YR2*(VR(3)-VR(1))
      VO(2) = VO(1)+YR2*(VO(3)-VO(1))
      VR(NP3) = VR(NP2)
      VO(NP3) = VO(NP2)
      DO 5 J = 1,7
      F(J,1) = F(J,2)
    5 F(J,NP3) = 0.0
      DO 6 J = 1,7
      F(J,NP2) = 0.0
    6 F(J,2) = F(J,1)+(Y(2)-Y(1))/(Y(3)-Y(1))*(F(J,3)-F(J,1))
      OM(1)=0.0
      OM(2)=0.0
      OM(3)=(Y(3)-Y(1))*(U(3)*Y(3)+U(1)*Y(1))*RHO(1)/2.0
      DO 7 I = 4,NP3
    7 OM(I)=(Y(I)-Y(I-1))*(U(I)*Y(I)+U(I-1)*Y(I-1))*RHO(I-1)/2.0 +OM(I-1
     1  )
      PSII=0.0
      PSIE=OM(NP3)
      PEI=PSIE-PSII
      DO 8 I = 1,NP3
    8 OM(I)=OM(I)/OM(NP3)
      DO 9 J = 1,NPH
      INDI(J)=1
    9 INDE(J)=1
      DO 10 I = 1,NP3
      FS(1,I) = 0.0
      DO 10 J = 1,NPH
      SU(J,I)=0.0
      CALL STRIDE(1)
      DO 12 I = 2,NP1
      F(8,I) = VO(I)*Y(I)
      EMU(I) = EMUL/(Y(I+1)-Y(I))
   12 EMU(I) = EMU(I)*.5*(R(I)+R(I+1))
      F(8,1) = 0.0
      F(8,NP2) = VO(NP3)*Y(NP3)
      F(8,NP3) = F(8,NP2)
      DX=FRA*(Y(NP3)-Y(1))
      XD = XU + DX
      IF(XD.GE.77..AND.XD.LE.79.) P156 = XD
      IF(XD.GE.109..AND.XU.LE.111.) P218 = XD
      DP=0.0
      DO 14 I = 1,NP3
   14 DPDX(I)=-DP
```

Boundary Conditions.

Radial Grid Spacing in ω coordinates.

```
      UFR=.1
      UMAX=0.0
      DO 15 I = 1,NP3
      IF(U(I).LT.UMAX)GO TO 15
      YMAX=Y(I)
      UMAX=U(I)
      IMAX=I
15    CONTINUE
      UMAXST=UMAX
      IF(U(NP3).GT.0.1*UMAX)UMAX=U(NP3)
      IF(U(NP3).GT.0.1*UMAX)UFR=.02
      DO 16 I = 1,N
      J=NP3-I
      IF(ABS(U(NP3)-U(J))/UMAX    .GT.UFR )GO TO 17
16    CONTINUE
 17   IF((U(J+1)-U(J)).LE.1.0E-10) GOTO27
      OMP02=OM(J)+ABS((OM(J+1)-OM(J))/(U(J+1)-U(J)))*(ABS(U(NP3)-U(J))-
     1UFR*UMAX)
      IF(ISTEP.EQ.0)OMP02I=OMP02
      IF(OMP02.EQ.1.0)GOTO27
      RME=-PEI*((2.0*OMP02-OMP02P)/OMP02I-1.0)/DX
      OMP02P=OMP02
      IF(RME.GT.0.0)RME=0.0
27    RMI = 0.0
      UMAX=UMAXST
      CALL AUX
      CALL STRIDE(2)
      IF(XS.EQ.P90.OR.XD.EQ.P156.OR.XD.EQ.P218) GOTO18
      GOTO 19
18    WRITE(6,25)
      WRITE(6,23)(Y(I),U(I),VR(I),VO(I),F(1,I),F(2,I),F(3,I),I=1,NP3)
      XL = XD*CORD
      WRITE(6,26) XL
      WRITE(6,24)(Y(I),F(4,I),F(5,I),F(6,I),F(7,I),I=1,NP3)
      XS = 1.0
      TEL = 0.0
      IF(XD.EQ.P218) GOTO22
19    IF(IFIN.EQ.1)GO TO 22
      IF(ISTEP.LT.LASTEP.AND.XL.LT.XULAST)GO TO 20
      IFIN=1
20    CONTINUE
      CALL STRIDE(3)
      DO 21 I = 1, NP3
      IF (F(7,I).LE.0.0) F(7,I) = 1.E-9
      DO 21 J = 1,3
      IF(F(J,I).LT.0.)F(J,I)=CU*U(NP3)*U(NP3)
21    CONTINUE
      GOTO 11
22    CONTINUE
23    FORMAT(7E15.4)
24    FORMAT(5E15.4)
25    FORMAT(1H1,10X,1HY,15X,1HU,15X,2HVR,14X,2HVO,12X,3HU2B,11X,4HVR2B,
     111X,4HVO2B//)
26    FORMAT(1H1,10X,1HY,15X,4HUVRB,10X,5HVRVOB,11X,4HUVOB,12X,3HDIS,
     1 10X,8HXDIST = ,F7.1//)
      STOP
      END
```

ENTRAINMENT

OUTPUT

```
      SUBROUTINE AUX
      DIMENSION SI(9),EXT(9),REDI(6),PROD(6),DIFS(6)
      COMMON/TUB/PHI(3,3,2),DUDX(3,3),D(3,3),ALPHA,BETA,ETA,UPS
      COMMON/RENY/F(9,40),PREF(9,40),SU(9,40),SD(9,40),VR(40),VO(40)
      COMMON/TED/Y(40),U(40),RHO(40),EMU(40) ,NP2
      COMMON/BITS/P156,P218,TEL
      C1 = 1.5
      C2 = .40
      CS = .11
      CE = .15
      CE1 = 1.45
      CE2 = 1.9
      ALPHA = (4.0*C2+10.0)/11.
      BETA = -(2.0+3.0*C2)/11.
      ETA = -(50.0*C2+4.0)/55.
      UPS = (20.0*C2+6.0)/55.
      DO1 I=1,3
      DO1 J=1,3
      D(I,J) = 0.0
1     DUDX(I,J) = 0.0
      D(1,1) = 1.0
      D(2,2) = 1.0
      D(3,3) = 1.0
      DO4 I = 2,NP2
      AKE = .5*(F(1,I) + F(2,I) + F(3,I))
      DIS = (F(7,I+1)+F(7,I-1))*.5
      DIS2 = (F(7,I)+F(7,I+1))/2.0
      IF(DIS.LE.0.0) GOTO5
      IF((Y(I)-Y(I+1)).EQ.0.0) GOTO8
      CFTP = CS*AKE*(Y(I)+Y(I+1))/2.0*(F(2,I)+F(2,I+1))/(2.0*DIS2*
     1 (Y(I+1)-Y(I)))
      PREF(8,I) = EMU(I)*(Y(I)+Y(I+1))/(2.*(Y(I+1)-Y(I)))
      GOTO6
5     SI(7) = 0.0
8     CFTP = 0.0
      PREF(8,I) = 0.0
6     PREF(1,I) = CFTP
      PREF(2,I) = 3.* CFTP
      PREF(3,I) = CFTP
      PREF(4,I) = 2.0* CFTP
      PREF(5,I) = 2.0*CFTP
      PREF(6,I) = CFTP
      PREF(7,I) = CFTP*CE/CS
      DY =(Y(I+1) - Y(I-1))*.5
      DIS23 = 2.0/3.0*DIS  *DY
      DRVR =(Y(I+1)*VR(I+1) - Y(I-1)*VR(I-1))  *.5
      DUDR =(U(I+1) - U(I-1))*.5
      DVRDR =(VR(I+1) - VR(I-1))*.5
      DVODR =(VO(I+1) - VO(I-1))*.5
      U2B = .5*(F(1,I+1)+F(1,I-1))
      VR2B = .5*(F(2,I+1)+F(2,I-1))
      VO2B = .5*(F(3,I+1)+F(3,I-1))
      UVRB = .5*(F(4,I+1)+F(4,I-1))
      VRVOB = .5*(F(5,I+1)+F(5,I-1))
      UVOB = .5*(F(6,I+1)+F(6,I-1))
```

CONSTANTS $a_1 - a_{10}$ APPENDIX B.

δ^{ij}

α^{ij}

$\frac{\partial r v_r}{\partial r}$ $\partial v_\theta/\partial r$ $\partial v_r/\partial r$ $\partial v_\theta/\partial r$ $\overline{v_\theta^2}$ $\overline{v_r^2}$ $\overline{v_\theta^2}$ $\overline{v_r v_r}$ $\overline{v_r v_\theta}$ $\overline{v_r v_\theta}$

```
      Y(2) = .5*Y(3)
      IF(I.LE.3) VOR = VO(3)/Y(3)
      IF(I.LE.3) VRR = VR(3)/Y(3)
      IF(I.LE.3) GOTO9
      VRR = .5*(VR(I+1)/Y(I+1)+VR(I-1)/Y(I-1))
      VOR = .5*(VO(I+1)/Y(I+1)+VO(I-1)/Y(I-1))
9     DUDX(1,1) = -1.0/Y(I)*DRVR
      DUDX(1,2) = DUDR
      DUDX(2,2) = DVRDR
      DUDX(2,3) = -VOR*DY
      DUDX(3,2) = DVODR
      DUDX(3,3) = VRR*DY
      CALL CHOU (3,C1,C2,AKE,DIS,I,DY)
      DO 10 J = 1,7
      EXT(J) = 0.0
10    CONTINUE
11    SI(1)=-DIS23+PHI(1,1,1)+PHI(1,1,2)+2.0*U2B/Y(I)*DRVR-2.0*UVRB*DUDR
     1 -EXT(1)
      SI(2) = -DIS23+PHI(2,2,1)+PHI(2,2,2)-2.0*VR2B*DVRDR+4.0*VOR*VRVOB*
     1 DY - EXT(2)*3.0
      SI(3) = -DIS23+PHI(3,3,1)+PHI(3,3,2)-2.0*VRVOB*DVODR-2.0*VOR*VRVOB
     1 *DY - 2.0*VRR*VO2B*DY - EXT(3)
      SI(4) = PHI(1,2,1)+PHI(1,2,2)-VR2B*DUDR+2.0*VOR*UVOB*DY
     1  - EXT(4)*2.0    +UVRB*VRR*DY
      SI(5) = PHI(2,3,1)+PHI(2,3,2)-VR2B*DVODR+VOR*(2.0*VO2B -VR2B)*DY
     1- EXT(5)*2.0 - VRVOB*DRVR/Y(I)
      SI(6) = PHI(1,3,1)+PHI(1,3,2)-VRVOB*DUDR-UVRB*DVODR-VOR*UVRB*DY
     1  -EXT(6) + UVOB*DVRDR
      SI(8) = -2.0*EMU(I)*(VOR*DY+DVODR)-2.0*VRVOB*DY-Y(I)*(F(5,I+1)-F(5
     1 ,I-1))
      IF(DIS.LE.0.0) GOTO7
      IF(AKE.LE.0.0) SI(7) = 0.0
      IF(AKE.LE.0.0) GOTO7
      SI(7) = -CE1*DIS/AKE*(-U2B*DRVR/Y(I)+UVRB*DUDR+VRVOB*DVODR
     1  -VOR*VRVOB*DY
     1  + VRR*VO2B*DY) - CE2*DIS**2/AKE*DY - EXT(7)
      Y(2) = YH2
7     DO2 K = 1,8
2     SU(K,I) = SI(K) * RHO(I) * Y(I)
      DO3 K=4,8
3     SD(K,I) = 0.0
4     CONTINUE
      RETURN
      END
```

$U^j|_i$ Appendix B.

S^{ij} eqns 2-4-12 to 2-4-18.

Source terms

```
      SUBROUTINE CHOU(N,C1,C2,AKE,DIS,NK,DY)
      DIMENSION U(3,3),A(3,3,3,3)
      COMMON/RENY/F(9,40),PREF(9,40),SU(9,40),SD(9,40),VR(40),VD(40)
      COMMON/TUD/PHI(3,3,2),DUDX(3,3),D(3,3),ALPHA,BETA,ETA,UPS
      U(1,1) = F(1,NK)
      U(1,2) = F(4,NK)
      U(1,3) = F(6,NK)
      U(2,1) = F(4,NK)
      U(2,2) = F(2,NK)
      U(2,3) = F(5,NK)
      U(3,1) = F(6,NK)
      U(3,2) = F(5,NK)
      U(3,3) = F(3,NK)
      DO 1 I=1,N
      DO 1 J = 1,N
      IF(DIS.LE.0.0) PHI(I,J,1) = 0.0
      IF(DIS.LE.0.0) GOTO2
      IF(AKE.LE.0.0) PHI(I,J,1) = 0.0
      IF(AKE.LE.0.0) GOTO2
      PHI(I,J,1) = -C1*DIS/AKE*(U(I,J)-2.0/3.0*D(I,J)*AKE) *DY
    2 DO1 M = 1,N
      DO 1 L=1,N
      A(I,J,M,L) = ALPHA*D(L,J)*U(M,I)
     1  + BETA*(D(M,L)*U(I,J) +D(M,J)*U(I,L)
     1    + D(I,L)*U(M,J) + D(I,J) * U(M,L))
     1    + C2*D(M,I)*U(L,J)
     1    +AKE * (ETA*D(M,I)*D(L,J)
     1    + UPS*(D(M,L)*D(I,J) + D(M,J)*D(I,L)))
    1 CONTINUE
      DO3 I = 1,N
      DO3 J=1,N
      SUM = 0.0
      DO3 M=1,N
      DO3L=1,N
      SUM= DUDX(L,M)*(A(I,J,M,L)+A(J,I,M,L)) + SUM
      PHI(I,J,2) = SUM
    3 CONTINUE
      RETURN
```

$\overline{u^i u^j}$

ϕ_1^{ij} EQN 2.3.3

C^{mnij} EQN 2.3.5.

ϕ_2^{ij} EQN 2.3.4.

STRIDE

```
      SUBROUTINE STRIDE(ISW)
      DIMENSION A(9,83),AU(83),B(9,83),BU(83),C(9,83),CU(83),FDIFE(9),
     1  FDIFI(9),GE(9),GI(9),TTPF(9) ,VOL(40) ,UOL(40) ,UZBX(40)
      COMMON/GENRAL/ AJE(9),AJI(9),CSALFA,DPDX(40),DX,
     1  FS(9,40),H,IFIN,INDE(9),INDI(9),ISTEP,ITEST,IUTRAP,KEX,KIN,KRAD,
     2  N,NEQ,NPH,NP1,NP2,NP3,OM(40),PEI,PR(9),PSIE,PSII,
     3 R(40),RNE,RMI,RU(40),XD,XU,YE,YI,UT,UTE,CUS,TACT
      COMMON/RENY/F(9,40),FREF(9,40),SU(9,40),SD(9,40),VR(40),VU(40)
      COMMON/TED/Y(40),U(40),RHO(40),EMU(40)  ,KZML3
      GO TO (1000,2000,3000), ISW
C
C**************************************  S T R I D E 1  ***************
 1000 IF(ISTEP.GT.0) GO TO 1100
      OM(1)=0.
      OM(2)=0.
      OM(NP2)=1.
      OM(NP3)=1.
      OMI=.5*OM(3)
      OME=.5*(1.-OM(NP1))
      BPE=1.
      BPI=1.
      Y(1)=0.
      R(1) = 0.0
C-------------------------------  CALCULATION OF RHO*U 'S  ----------------
 1100 DO 1101 I=1,NP3
 1101 RU(I)=RHO(I)*U(I)
      RU3=RU(3)
      RUN1=RU(NP1)
      DO 1102 I=2,NP1
      RU(I)=.5*(RU(I)+RU(I+1))
      IF(RU(I).GT.0.)GO TO 1102
      IF(ITEST.EQ.0) WRITE(6,1200)
 1200 FORMAT(26HOAN RU IS ZERO OR NEGATIVE)
      ITEST=1
      IFIN=1
 1102  CONTINUE
C-------------------------------  CALCULATION OF Y 'S AND R 'S  -----------
C  ---------------------------------------------  Y'S FOR PLANE GEOMETRY
      YI=PEI*OMI/(BPI*RU(2))
      Y(3)=YI+PEI*OM(3)/(RU(2)+RU3)
      Y(2)=Y(3)-PEI*OM(3)/RU(2)
      DO 1103 I=4,NP2
 1103 Y(I)=Y(I-1)+PEI*(OM(I)-OM(I-1))/RU(I-1)
      YN15=Y(NP1)+PEI*(1.-OM(NP1))/(RU(NP1)+RUN1)
      YE=PEI*OME/(BPE*RU(NP1))
      Y(NP3)=YN15+YE
C  ----------------------  Y'S AND R'S FOR AXISYMMETRICAL GEOMETRY
C  ---------------------------------------------  CSALFA NE ZERO
```

```
      COSD2=.5*CSALFA
C-------------------------------------------------  R(1)=0.
      DO 1106 I=2,NP3
      Y(I)=SQRT(ABS(Y(I)/COSD2))
 1106 R(I)=Y(I)*CSALFA
      YI=SQRT(ABS(YI/COSD2))
      YN15=SQRT(ABS(YN15/COSD2))
      R25 = R(1)+YI*CSALFA
      RN15=R(1)+YN15*CSALFA
      YE=Y(NP3)-YN15
      RETURN
C  ---------------------------------------------  CSALFA EQ ZERO
C**************************************  S T R I D E 2  ****************
C  ------------------------------  PRELIMINARIES FOR COEFFICIENTS
 2000 PX=PEI/DX
      PLA = 12.
           G=RMI-RME
           PD8=.125*PX
      PD4=.25*PX
           PG=PX+G
           PGD8=.125*PG
      PGD4=PGD8+PGD8
           RMID2=.5*RMI
           GD4=.25*G
           DOMP=OM(3)-OM(2)
      PGOMP=PGD4*DOMP
      P4OMP=PD4*DOMP
C  ---------------------------------------------  GRID POINT 2
      T1 = 0.0
      IF(TACT.EQ.2.) U2BX(3) = F(1,3)
      AJUI = -RHO(3)*F(4,3)*R25     -(F(1,3)-U2BX(3))/DX*R25 *YI *2.0
C  ----------------------  BOUNDARY COEFFICIENTS FOR VELOCITY
      BPI = (R(1)*(.5*RU(1)+RU(2))+3.*R25*
     1    (RU(1)+RU(2)))/6./(R(1)+R25)/RU(2)
 2002 HLP=RMID2-GD4*(OM(2)+OM(3))
           AHLP=ABS(HLP)
      THLP=HLP+HLP
           TP=EM U(2)
      TTP=TP+AHLP+ABS(TP-AHLP)
      AD=TTP-THLP-T1-PGOMP
      BD=2.*(T1+RMI)
      FS(2,2) = -DPDX(2)*(R(1)+R25)*YI+AJUI
      CD=P4OMP*(3.*U(2)+U(3))+FS(2,2)
      DU=AD+BD+PX*DOMP
      IF(PLA.EQ.12.) GOTO4
      AU(2)=AD/DU
      BU(2)=BD/DU
      CU(2)=CD/DU
C  ---------------------------------  BOUNDARY COEFFICIENTS FOR F'S
 4    IF(NEQ.EQ.1) GOTO2304
```

```
      DO 2300 J=1,NPH
      TPF2=PREF(J,2)
      TTPF(J)=TPF2+AHLP+ABS(TPF2-AHLP)
      T1F = 0.0
      FDIFI(J)=0.
C  ------------------------------------------  COEFFICIENTS
 2302 ADF=TTPF(J)-THLP-T1F-PGDMP+.5*SD(J,2)
      BDF=2.*(T1F+RMI)
      DF=ADF+BDF+PX*DOMP-2.*SD(J,2)
      T=-T1F*FDIFI(J)
      GO TO 2305
 2303 ADF=TTPF(J)-THLP-PGDMP+.5*SD(J,2)
      BDF=0.
      DF=ADF+PX*DOMP-2.*SD(J,2)+RMI*2.
      T=RMI*F(J,1)+AJI(J)*R(1)
 2305 TT=3.*F(J,2)+F(J,3)
      CDF=P4DMP*TT+2.*(T+SU(J,2))
      IF(J.GE.4.AND.J.LE.6) GOTO22302
      A(J,2)=ADF/DF
      B(J,2)=BDF/DF
      C(J,2)=CDF/DF
      GO TO 2300
22302 A(J,2)=0.0
     * B(J,2)=0.0
      C(J,2) = 0.0
 2300 CONTINUE
C  ------------------------------------------  GRID POINT NP2
C------------------------------------------  TAUE, BPE, TNP3
 2304  TNP3 = 0.0
      IF(TACT.EQ.2.0) U2BX(NP1) = F(1,NP1)
      AJUI=RHO(NP1)*   F(4,NP1)
      BPE = (R(NP3)*(5.*RU(NP3)+RU(NP1))+3.*RN15*
     1     (RU(NP3)+RU(NP1)))/6./(R(NP3)+RN15)/RU(NP1)
C  ----------------------  BOUNDARY COEFFICIENTS FOR VELOCITY
 2310 BOMM=OM(NP2)-OM(NP1)
      HLM=RMID2-GD4*(OM(NP1)+OM(NP2))
      AHLM=ABS(HLM)
      THLM=HLM+HLM
      TM=EM U(NP1)
      TTM=TM+AHLM+ABS(TM-AHLM)
      PGDMM=PGD4*BOMM
      P4DMM=PD4*BOMM
      AD=2.*(TNP3-RME)
      BD=TTM+THLM-TNP3-PGDMM
      DEXT =     (RN15+R(NP3))*(F(1,NP1)-U2BX(NP1))/DX*YE
      FS(2,NP2)=-DPDX(NP2)*(RN15+R(NP3))*YE-AJUI*(RN15+R(NP3))  -DEXT
      CD=P4DMM*(3.*U(NP2)+U(NP1))+FS(2,NP2)
      DU=AD+BD+PX*BOMM
      IF(PLA.EQ.12.) GOTO3
      AU(NP2)=AD/DU
```

```
      DU2DX = (F(1,I)-U2DX(I))/DX
      U2DX = DU2DX*.5*(R(I-1)+R(I+1))*    (R(I+1)-R(I-1))
      IF(TACT.EQ.2.) U2DX = 0.0
      FS(2,I)=-DPDX(I)*R(I)*(Y(I+1)-Y(I-1))     +RHO(I)*FPM -U2DX
      CD=PD4*(BOMT3*U(I)+BOMP*U(I+1)+BOMM*U(I-1))+FS(2,I)
            DU=AD+BD+PBOM
            AU(I)=AD/DU
            BU(I)=BD/DU
 3045 CU(I)=CD/DU
      TACT = 3.0
      U(NP3) = U(NP3)-DPDX(NP3)*DX/RU(NP3)
C------------------------------    SOLVE FOR DOWNSTREAM U'S  ------------
 3047 BU(2)=BU(2)*U(1)+CU(2)
      DO 3048 I=3,NP2
      T=1./(1.-BU(I)*AU(I-1))
      AU(I)=AU(I)*T
 3048 BU(I)=(BU(I)*BU(I-1)+CU(I))*T
      DO 3050 IDASH=2,NP2
      I=N+4-IDASH
      U2DX(I) = F(1,I)
      UOL(I) = U(I)
      U(I)=AU(I)*U(I+1)+BU(I)
C  TEST FOR NEGATIVE VELOCITY
C      IUTRAP=0 NO ACTION,  =1 SET U'S TO ZERO, =2 PRINT AND STOP
      IF(IUTRAP.EQ.0) GO TO 3050
      IF(U(I).GE.0.0)GO TO 3050
      IF(IUTRAP.EQ.1) GO TO 3051
      IFIN=1
      ITEST=1
      WRITE(6,3120)
3120  FORMAT(10X,33HAT LEAST ONE VELOCITY IS NEGATIVE)
      RETURN
 3051 U(I)=1.E-30
 3050 CONTINUE
      U(1) = .5*(U(2)+U(3))
   72 IF(NEQ.EQ.1) GO TO 3060
      IF(ITEST.EQ.1)WRITE(6,3610)(U(I),I=1,NP3)
 3610 FORMAT(3HOU'S     ,11E11.4)
C
C     CALCULATION OF F'S
C
      BOMP=OM(3)-OM(2)
      PBOMP=PB04*BOMP
      HLP=RMID2-GD4*(OM(3)+OM(2))
      THLP=HLP+HLP
      AHLP=ABS(HLP)
      DO 3710 J=1,NPH
      TPF=PREF(J,2)
 3710 TTPF(J)=TPF+AHLP+ABS(TPF-AHLP)
      DO 3005 I=3,NP1
```

```
      BOMM=BOMP
      BOMP=OM(I+1)-OM(I)
      BOM=BOMM+BOMP
      BOMT3=BOM*3
      PGOMM=PGOMP
      PGOMP=PGD4*BOMP
      PBOM=PX*BOM
      THLM=THLP
      HLP=RMID2-GD4*(OM(I+1)+OM(I))
      THLP=HLP+HLP
      AHLP=ABS(HLP)
            DO 3004 J=1,NPH
 3002 TTMF=TTPF(J)
 3003 TPF=PREF(J,I)
      TTPF(J)=TPF+AHLP+ABS(TPF-AHLP)
      AD=TTPF(J)-THLP-PGOMP
      BD=TTMF+THLM-PGOMM
      CD=PD4*(BOMT3*F(J,I)+BOMP*F(J,I+1)+BOMM*F(J,I-1))
      CD=CD+2.*SU(J,I)
      DF=AD+BD+PBOM-2.*SD(J,I)
            A(J,I)=AD/DF
            B(J,I)=BD/DF
 3004       C(J,I)=CD/DF
 3005 CONTINUE
 9013 CONTINUE
C-------------------------------                                  ----------------
      DO 3320 J=1,NPH
C-------------------------------    SOLVE FOR DOWNSTREAM F 'S  ---------------
      B(J,2)=B(J,2)*F(J,1)+C(J,2)
      DO 3148 I=3,NP2
      T=1./(1.-B(J,I)*A(J,I-1))
      A(J,I)=A(J,I)*T
 3148 B(J,I)=(B(J,I)*D(J,I-1)+C(J,I))*T
      DO 3150 IDASH=2,NP2
      I=N+4-IDASH
 3150 F(J,I)=A(J,I)*F(J,I+1)+B(J,I)
C-------------------------------  ADJUST F(J,1) AND F(J,NP3)  ---------------
      F(J,1) = .5*(F(J,2)+F(J,3))
 3320 CONTINUE
      F(2,1) = .5*(F(2,1)+F(3,1))
      F(3,1) = F(2,1)
      DO1 I=2,NP2
      VOL(I) = VO(I)
 1    VO(I) = F(8,I)/Y(I)
      VO(2) = 1.0/3.0*VO(3)
      VO(NP1) = .032*3.5/Y(NP1)
      VO(NP3) = .032*3.5/Y(NP3)
      VO(NP2) = VO(NP3)
      F(8,NP2) = VO(NP2)*Y(NP2)
      F(8,2) = VO(2)*Y(2)
```

```
      BU(NP2)=BD/DU
      CU(NP2)=CD/DU
      IF(NEQ. EQ. 1) RETURN
C  ---------------------  BOUNDARY COEFFICIENTS FOR F'S
 3    DO2320 J = 1, NPH
      TMF=PREF(J, NP1)
      TTMF=TMF+AHLM+ABS(TMF-AHLM)
      TNP3F = 0. 0
      FDIFE(J)=0.
C  ---------------------------------------------  COEFFICIENTS
 2312 ADF=2. *(TNP3F-RME)
      BDF=TTMF+THLM-TNP3F-PGOMM+. 5*SD(J, NP2)
      DF=ADF+BDF+PX*BOMM-2. *SD(J, NP2)
      T=-TNP3F*FDIFE(J)
      GO TO 2315
2313  ADF=0.
      BDF=TTMF+THLM-PGOMM+. 5*SD(J, NP2)
      DF=BDF+PX*BOMM-2. *SD(J, NP2)-RME*2.
      T=-RME*F(J, NP3)-AJE(J)*R(NP3)
 2315 TT=3. *F(J, NP2)+F(J, NP1)
      CDF=P4OMM*TT+2. *(T+SU(J, NP2))
      A(J, NP2) = 0. 0
      B(J, NP2)=0. 0
      CW=CUS
      IF(J. GE. 4. AND. J. LE. 7) CW = 0. 0
      C(J, NP2)=CW*U(NP3)*U(NP3)
2320  CONTINUE
      C(3, NP2) = . 0314*3. 5
      RETURN
*****************************************  S T R I D E 3  ****************
3000  IF(PLA. EQ. 12. ) GOTO3050
      DO3045 I = 3, NP1
             BOMM=BOMP
             BOMP=OM(I+1)-OM(I)
             BOM=BOMM+BOMP
             BOMT3=BOM*3.
             PGOMM=PGOMP
      PGOMP=PGD4*BOMP
      PBOM=PX*BOM
      THLM=THLP
             HLP=RMID2-GD4*(OM(I+1)+OM(I))
      THLP=HLP+HLP
             AHLP=ABS(HLP)
      TTM=TTP
             TP=EM U(I)
      TTP=TP+AHLP+ABS(TP-AHLP)
      AD=TTP-THLP-PGOMP
      BD=TTM+THLM-PGOMM
      F4P = . 5*(F(4, I+1)+F(4, I))
      F4M = . 5*(F(4, I-1)+F(4, I))
      FPM=(-F4P*(R(I)+R(I+1))+F4M*(R(I)+R(I-1)))
```

```
      Y2H = Y(2)
      VOH = VO(2)
      TOL = 0.0
      Y(2) = 0.0
      VO(2) = 0.0
      VOL(2) = 0.0
      VUM = 0.0
      DO2 K = 3,NP1
      DUODX = (U(K) - UOL(K))/DX
      IF(PLA.EQ.12.) DUODX = 0.0
      VUM = DUODX*.25*(Y(K+1)+Y(K-1))*(Y(K+1)-Y(K-1)) + VUM
      VR(K) = -VUM/Y(K)
      I = NP3 -K+1
      TOL = ((.5*(VO(I-1)+VO(I+1)))**2 - (.5*(VOL(I-1)+VOL(I+1)))**2)
     1  /(.5*(Y(I-1)+Y(I+1)))*(Y(I+1)-Y(I-1))*.5 + TOL
 2    DPDX(I) = TOL/DX
      VO(2) = VOH
      Y(2) = Y2H
      DPDX(2) = DPDX(3)
      VR(2) = 1.0/3.0*VR(3)
3060  XU=XD
      PSII=PSII-RMI*DX
      PSIE=PSIE-RME*DX
      PEI=PSIE-PSII
      ISTEP=ISTEP+1
      RETURN
      END
```